Volume 43 Number 5/6 May 1987

PHILIPS TECHNICAL REVIEW

Layered semiconductor structures

(special issue)

PHILIPS

Philips Technical Review (ISSN 0031-7926) is published by Philips Research Laboratories, Eindhoven, the Netherlands, and deals with the investigations, processes and products of the laboratories and other establishments that form part of or are associated with the Philips group of companies. In the articles the associated technical problems are treated along with their physical or chemical background. The Review covers a wide range of subjects, each article being intended not only for the specialist in the subject but also for the non-specialist reader with a general technical or scientific training.

The Review appears in English and Dutch editions; both are identical in contents. There are twelve numbers per volume, each of about 32 pages. An index is included with each volume and indexes covering ten volumes are published (the latest one was included in Volume 40, 1982).

PHILIPS TECHNICAL REVIEW

Volume 43, No. 5/6, May 1987

Layered semiconductor structures

Special issue

Contents

PHILIPS

PHILIPS TECHNICAL REVIEW

Volume 43, No. 5/6, May 1987

Layered semiconductor structures

In research on materials for the electronics industry we have recently seen a growing interest in layered epitaxial structures. If the layers are very thin, these structures often have very different physical properties from the individual materials, and different kinds of applications. Typical examples are the combinations of the III-V semiconductors GaAs and $Al_xGa_{1-x}As$ in field-effect transistors with a high electron mobility and in semiconductor lasers with a short emission wavelength.

Although these new structures do not seem to be compatible with the laws of ordinary chemical thermodynamics, they can be fabricated if careful attention is paid to the facilities for preparation. The layers or films are deposited on a substrate by evaporation in ultra-high vacuum (molecular beam epitaxy, or MBE) or by deposition from a gas mixture containing metal-organic compounds (metal-organic vapour-phase epitaxy, or MO-VPE). When these technologies are combined with sophisticated methods of characterization and analysis, monolayers of atoms or molecules can be applied, a layer at a time, and abrupt transitions can be introduced into the composition.

The main centre for the Philips activities in the MBE of III-V semiconductors is the Research Laboratories at Redhill, in Britain. The leading position of these Laboratories can be judged by the record established there for electron mobility in semiconductor structures. Work on the MBE of II-VI semiconductors has recently been started at the Research Laboratories at Briarcliff, in the U.S.A., while the MBE of silicon and combinations of metals is being investigated at the Research Laboratories in Eindhoven.

The MO-VPE technology has perhaps won greater industrial acceptance than MBE. Contributions from our Laboratories at Limeil-Brévannes (France) and Eindhoven have helped to bring this technology to a high degree of perfection in recent years.

Combinations of very different materials, such as silicon on GaAs (or GaP), GaAs on silicon, semiconductors on oxide substrates or combinations of metals and semiconductors also receive attention. There are good prospects for the discovery of new physical effects and unusual properties of materials that can be used in new applications.

The time was clearly ripe for a special issue of Philips Technical Review on these structures. We now present a general survey of the subject and four articles that describe some of the activities of Philips Research on layered semiconductor structures. However, our special issue can really give no more than a glimpse of a field still forging strongly ahead.

A. R. Miedema

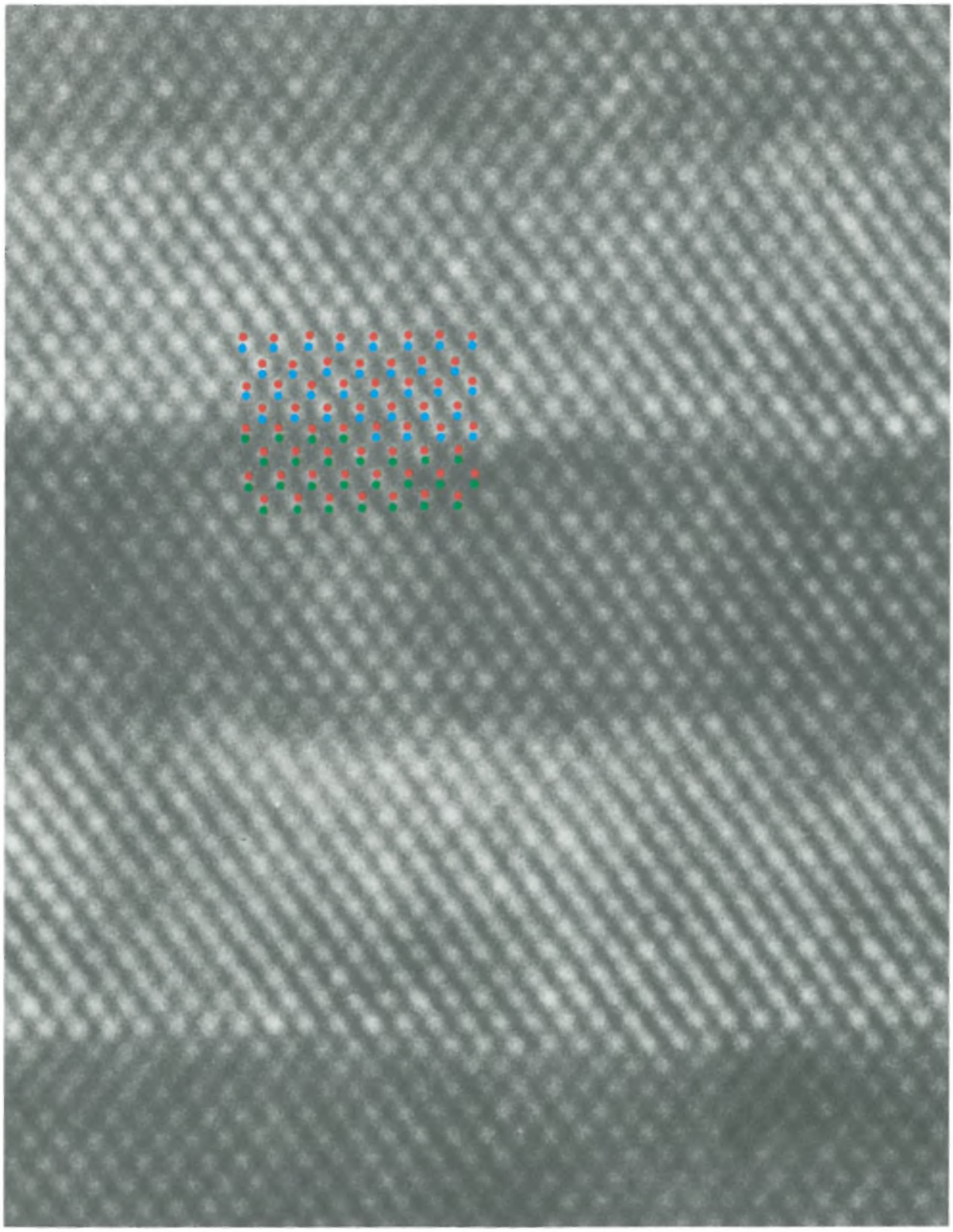

The crystal perfection that can be achieved in layered semiconductor structures can be seen from images made by transmission electron microscopy of the crystal lattice. This image shows alternate 3.5-nm layers of GaAs (dark) and AlAs (light); the arrangement of the atoms is indicated by blue for Al, green for Ga and red for As. Changes in composition are completed within a thickness of about one monolayer.

Research on layered semiconductor structures

J. Wolter

Introduction

The special properties of semiconductor single crystals have regularly led to the introduction of devices based on new principles of application. This has resulted for example in silicon integrated circuits with high packing densities and complex functions, and in optoelectronic devices based on III-V compounds such as gallium arsenide (GaAs). Materials scientists have contributed extensively to these developments by making it possible to grow high-purity crystals free from lattice defects.

Most semiconductor devices manufactured today contain only one basic material. We now see the emergence of a completely new class of devices with structures consisting of 'stacked' thin layers of dissimilar semiconductors. In these 'heterostructures' the electric potential in the direction perpendicular to the layers can be modified to produce interesting physical effects, sometimes with novel applications.

During the last ten years or so, research on these structures has expanded rapidly. Their physical background is now much more clearly understood and various discoveries have been evaluated for practical application. This has only been possible through the interplay of ideas, potential device applications and advanced growth techniques, with multi-disciplinary contributions from large numbers of workers in industrial and university laboratories. Efforts in this field are expected to intensify in the years ahead.

Among the structures investigated, probably the most fascinating are the 'superlattices'. These are built up from alternate ultra-thin layers, typically 1 nm thick, of two dissimilar semiconductor materials. Then there is the 'quantum-well structure', consisting of a semiconductor layer less than 30 nm thick between two layers of another semiconductor with a larger band gap. This also has peculiarly interesting properties. And even a simple heterojunction between two dissimilar semiconductors offers interesting potential applications.

This article gives a brief review of the research on these multilayer structures. It includes a general discussion of some of the physical aspects and practical implications. An indication is also given of the methods of preparation and the semiconductor materials. Finally there is a summary of the Philips activities in this field.

Superlattices

The basic idea of the formation of superlattices was put forward in about 1970 by L. Esaki and R. Tsu [1]. They considered an array of alternating ultra-thin layers of two dissimilar semiconductors with different band gaps; see *fig. 1*. The alternation gives a periodic modification of the electric potential perpendicular to the interfaces. Extra potential wells are therefore created for the electrons, in addition to the 'ordinary' potential wells around each atom in the crystal lattice. When the periodicity of the superlattice becomes less than about 10 nm, there is a marked change in the energy-level diagram for the electrons: the valence and conduction bands are split into 'minibands' and new forbidden zones ('minigaps') are created. A similar modification applies to the energy of the quantized lattice vibrations (phonons) as a function of their wave number; this has already been demonstrated experimentally by Raman spectroscopy [2].

A curious effect can occur when an electric field is applied to a superlattice [1]. The presence of minigaps gives rise to 'Bloch oscillations' and to a negative dif-

Prof. Dr J. Wolter, Professor in Semiconductor Physics at Eindhoven University of Technology, was formerly with Philips Research Laboratories, Eindhoven.

[1] L. Esaki and R. Tsu, Superlattice and negative differential conductivity in semiconductors, IBM J. Res. & Dev. 14, 61-65, 1970.

[2] J. L. Merz, A. S. Barker, Jr., and A. C. Gossard, Raman scattering and zone-folding effects for alternating monolayers of GaAs-AlAs, Appl. Phys. Lett. 31, 117-119, 1977.

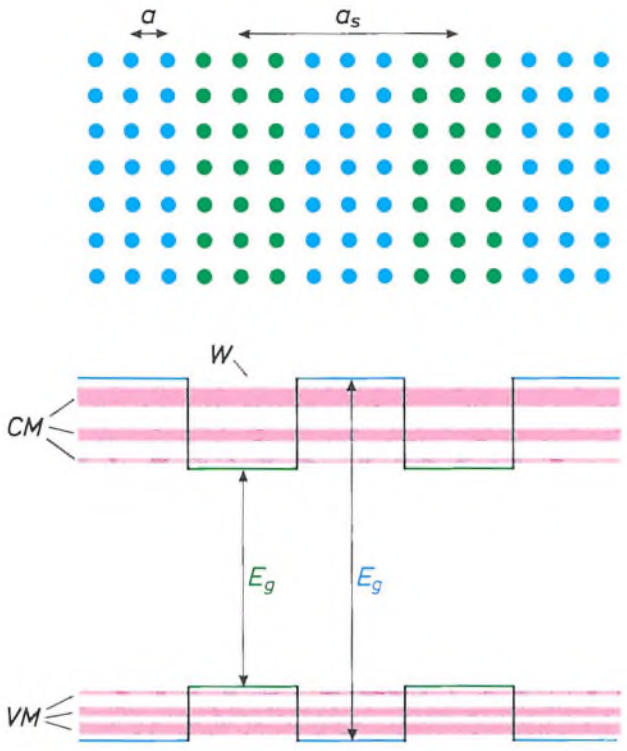

Fig. 1. Atomic arrangement and energy-band diagram of a superlattice consisting of alternate ultra-thin layers of two semiconductors with different band gaps E_g. In addition to the normal lattice period a, there is also a superlattice period a_s. At the interfaces the band-gap difference creates potential wells W, which split the valence and conduction bands into valence minibands VM and conduction minibands CM.

ferential conductivity, as illustrated in *fig. 2*. The energy bands are tilted and the resulting slope is proportional to the voltage. Electrons are driven towards the upper edge of the conduction band, but in a conventional semiconductor they never arrive there, since the distance they have to travel is much farther than the mean distance between two phonon emissions. In a superlattice, however, the minibands may be so narrow that the electrons do have a good chance of reaching the upper edge. Once they arrive there, they turn back towards the bottom edge because they cannot pass the forbidden zone. The electrons therefore oscillate between the two edges many times before emitting a phonon. The average electron position is shifted by a phonon emission, and the shift decreases as the angle of tilt becomes larger. A higher voltage therefore gives a lower current.

Another type of superlattice has also been proposed and investigated [3]. This consists of layers of the same semiconductor with alternate p-type and n-type doping. The donor atoms in the n-type layers deliver electrons and the acceptor atoms in the p-type layers deliver holes. The resulting charge distribution creates a new set of potential wells, again producing energy-band structures with minibands and minigaps. Important features of these superlattices are the nearly perfect lattice matching and the spatial separation of electrons and holes, which can increase the recombination lifetimes. The effective band gap can also be changed by applying an external voltage.

Superlattices have unusual physical properties, which can be varied in a controlled way by modifying the band structure via the composition, the doping or

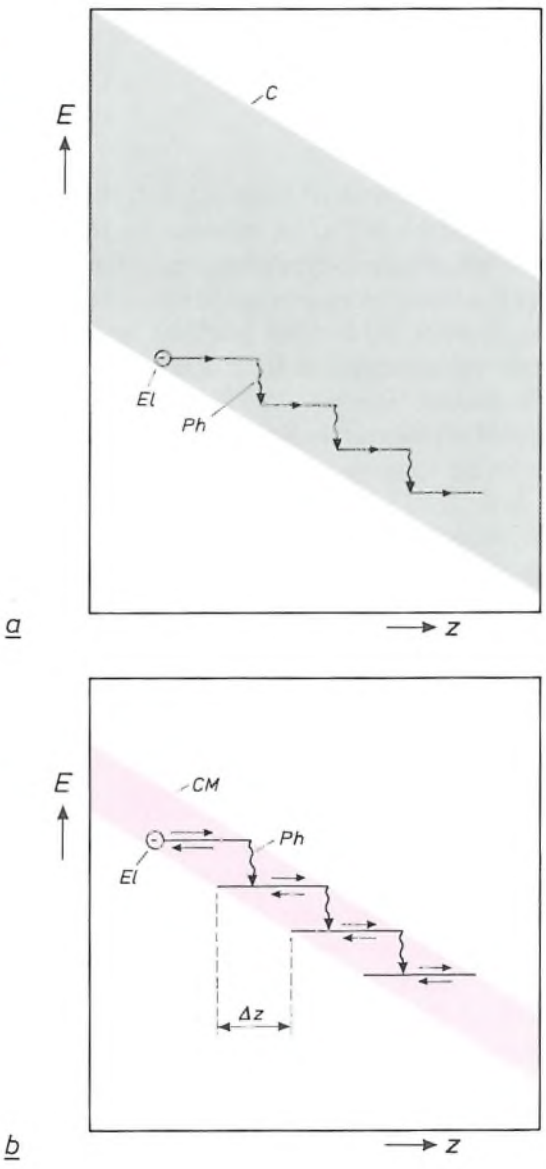

Fig. 2. The occurrence of Bloch oscillations and a negative differential conductivity in a superlattice in an electric field [3]. The energy diagrams (energy E as a function of position z) are shown for the conduction electrons in a conventional semiconductor (*a*) and in a superlattice (*b*). In a conventional semiconductor the emission of phonons *Ph* prevents electrons *El* from reaching the upper edge of the conduction band *C*. In a superlattice the miniband *CM* is so narrow that electrons do have a chance of arriving at the upper edge. They are reflected there, and may oscillate repeatedly between the band edges before emitting a phonon. The shift Δz in the mean position of the electrons at a phonon emission decreases as the slope of the tilted band increases. This means that the current through the lattice decreases with increasing voltage.

the layer thickness. A practical example of this 'band-gap engineering' is the 'staircase' modification of the energy-band structure for an avalanche photodiode [4]. Here the band gap is increased in steps in such a way that the band-edge discontinuities provide the entire ionization energy; see *fig. 3*. The multiplication of electrons then only occurs at the well-defined steps. The statistical fluctuations in the internal gain will therefore be much smaller than in conventional avalanche photodiodes, resulting in a better noise performance.

Another example is a superlattice of two semiconductors with an indirect band gap. In the separate materials the minimum of the conduction band does not correspond to the same wave number as the maximum of the valence band, and therefore the coupling to a phonon is required for an electron-hole recombination. Consequently the recombination probability is much smaller (e.g. by a factor of 1000) than in a direct-gap semiconductor. In a superlattice, however, the band structure can be tailored in such a way that a material with a direct band gap is obtained [5].

This principle might be applied to gallium phosphide (GaP) and aluminium phosphide (AlP), which have nearly the same lattice constant and have band-gap transitions in the green and the blue, respectively. If these two indirect-gap semiconductors could be used to form a superlattice with a direct band gap, a blue-emitting laser material could perhaps be obtained. It might even be possible to obtain light emission from a superlattice of silicon and germanium. This would be a revolutionary development in optoelectronics, and the idea of growing these structures and studying them experimentally and theoretically presents a challenge.

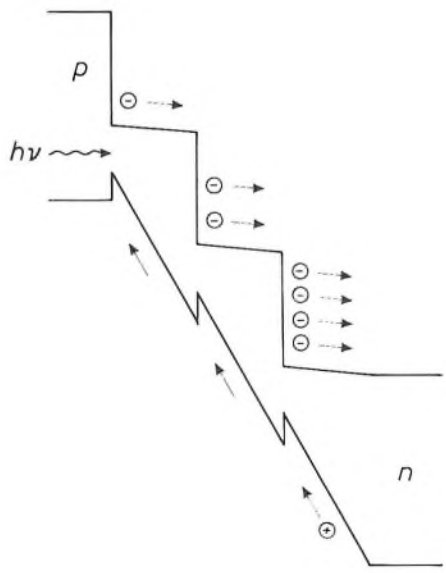

Fig. 3. Energy-band diagram of a 'staircase' superlattice for an avalanche photodiode [4]. The electrons generated by the incident photons can only ionize the atoms in the crystal at the steps in the conduction band. The creation of new electrons therefore occurs at well-defined positions in the lattice. This reduces the statistical fluctuations in the electron multiplication.

Quantum-well structures

A semiconductor layer sandwiched between two other semiconductor layers with a larger band gap is called a quantum well when it is so thin (< 30 nm) that the states for electrons and holes moving perpendicular to the interfaces are quantized. The confinement of charge carriers then gives rise to discrete energy levels; see *fig. 4*. The energies corresponding to movements parallel to the interfaces have to be added to these levels. The difference between the lowest conduction level and the highest valence level is greater than in the bulk material. Luminescence due to electron-hole recombinations will therefore occur at shorter wavelengths. The changes in the densities of states associated with quantization [6] also help to increase the probability of recombination.

In recent years quantum wells consisting of III-V semiconductors have been studied in many research laboratories. Most attention is given to structures of

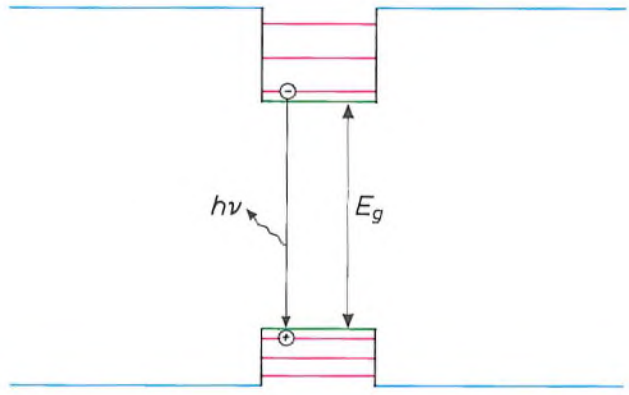

Fig. 4. Band diagram for a quantum well consisting of a semiconductor layer (green) sandwiched between two other layers of semiconductors with a larger band gap (blue). Only the discrete levels (red) are shown that correspond to states in which the electrons and holes only move at right angles to the interfaces. The difference in energy between the lowest conduction level and the highest valence level is larger than the band gap E_g in the bulk material, so that the luminescence due to electron-hole recombinations occurs at shorter wavelengths.

[3] G. H. Döhler, Electron states in crystals with 'nipi-superstructure', Phys. Stat. Sol. B **52**, 79-92, 1972. This author also gives a clear description of superlattices in: Sci. Am. **249**, No. 5 (November), 118-126, 1983.

[4] F. Capasso, W. T. Tsang and G. F. Williams, Staircase solid-state photomultipliers and avalanche photodiodes with enhanced ionization rates ratio, IEEE Trans. **ED-30**, 381-390, 1983.

[5] U. Gnutzmann and K. Clausecker, Theory of direct optical transitions in an optical indirect semiconductor with a superlattice structure, Appl. Phys. **3**, 9-14, 1974.

[6] R. Dingle, Confined carrier quantum states in ultrathin semiconductor heterostructures, Festkörperprobleme **15**, 21-48, 1975.

GaAs sandwiched between $Al_xGa_{1-x}As$, two materials that have nearly the same lattice constant. Similar structures, but with a thicker active layer with no quantization effects, are applied in semiconductor lasers [7], e.g. for Compact Disc players [8] and digital optical recording [9]. With a quantum-well version of this laser [10] the wavelength of the laser emission can be reduced by making the well thinner. Similar wavelength tuning can of course be applied in other devices such as light-emitting diodes and photodetectors.

In addition to the wavelength tuning, quantum-well devices have other attractive features, such as a high luminescence efficiency and a lower and less temperature-dependent threshold current for laser operation [11]. They may also offer stability and long life. Recognition of these features has already led to an industrial application.

High electron mobilities

It is well known that III-V semiconductors have good transport properties. Electrons in GaAs, for instance, have a smaller effective mass and therefore a higher mobility than in silicon. The electron mobility is generally limited, however, by a number of scattering processes, especially at built-in impurities. Collisions between electrons and their donor atoms are often unavoidable because they are present in the same medium. These processes, which are more important at low temperatures (< 77 K) than the interactions with phonons, were until recently the obstacles in the race to achieve higher electron mobilities by improving methods for growing crystals.

The introduction of modulation doping in heterostructures containing GaAs and $Al_xGa_{1-x}As$ provided a breakthrough [12]. The principle, based on ideas put forward earlier by Esaki and Tsu [1], is simple and ingenious: only the $Al_xGa_{1-x}As$ is doped, e.g. by the incorporation of donor atoms (n-type doping). Because of the band-gap discontinuity the electrons move from the donor atoms to the undoped GaAs. This results in a spatial separation between the donor atoms and the electrons, thus increasing the mobility by several orders of magnitude [13]. A further increase can be obtained by introducing a thin spacer layer of undoped $Al_xGa_{1-x}As$, which increases the distance between the donor atoms and the electrons still further. The increase in mobility is particularly large at low temperatures. At the Philips laboratories at Redhill in England a value of 3.1×10^6 $cm^2V^{-1}s^{-1}$ has recently been measured [14].

This principle can be applied in super-fast transistors and integrated circuits. Most of them are based on a structure of the MOSFET type (metal-oxide-semiconductor field-effect transistor). This consists of a p-type silicon layer with connections to source and drain, an insulating SiO_2 layer and a metal layer connected to the gate; see *fig. 5a*. When a negative voltage is applied to the gate the conduction electrons are pushed away from the interface between semiconductor and insulator and no current can flow between source and drain. When a positive voltage is applied to the gate the conduction electrons are attracted to the interface, forming a very thin inversion layer with a 'two-dimensional electron gas'. The electrons can now only move freely in the directions parallel to the interface. Partly because of their good switching characteristics MOSFETs are widely used in computers today.

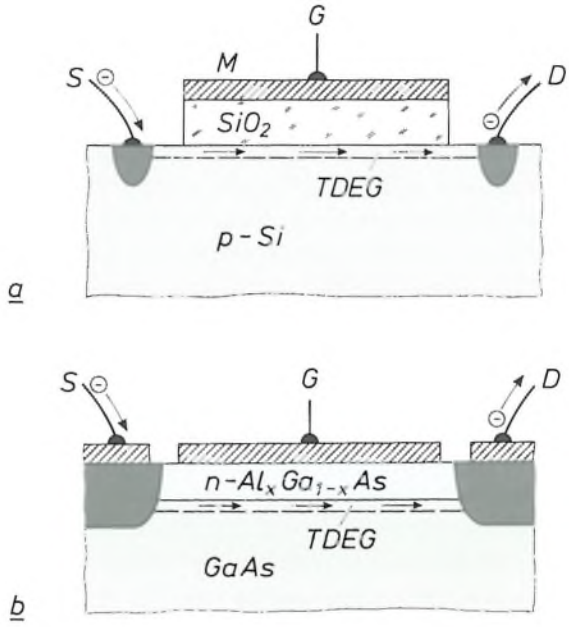

Fig. 5. *a*) Schematic cross-section of a MOSFET (metal-oxide-semiconductor field-effect transistor). The metal layer *M* is connected to the gate *G* and is separated from the p-type silicon by an insulating layer of SiO_2. Contact regions connect the silicon to the source *S* and the drain *D*. At a positive gate voltage the electrons flow from *S* to *D* in a very thin inversion layer containing a two-dimensional electron gas (*TDEG*) near the interface with the SiO_2 layer. *b*) Schematic cross-section of a field-effect transistor with a modulation-doped heterojunction. The donor atoms of the n-$Al_xGa_{1-x}As$ layer deliver electrons to the undoped GaAs layer. Near the interface a two-dimensional electron gas is formed at a positive gate voltage. Owing to the spatial separation from the parent donor atoms, the electrons here have a very high mobility.

If the p-type silicon layer is replaced by GaAs and the SiO_2 layer is replaced by n-type $Al_xGa_{1-x}As$ (fig. 5*b*), structures with higher electron mobility can be produced. The two-dimensional electron gas is then formed in the undoped GaAs layer near the interface with the n-$Al_xGa_{1-x}As$ layer. Since this layer is fully depleted, it behaves as an insulator. Whereas a MOSFET contains amorphous SiO_2, the heterojunction here is formed by single-crystal semiconductors

with nearly perfect lattice matching. The absence of dislocations and asperities at the interface gives a further reduction in electron scattering.

This type of field-effect transistor is commonly referred to as a HEMT (high-electron-mobility transistor) [15]. Nowadays many industrial laboratories are fabricating and studying HEMTs. Integrated circuits containing these transistors have already been made. An important feature of HEMTs is the high speed at which they can process signals. Considerable amounts of charge are rapidly accepted and released, with relatively little energy dissipation [16]. Switching times of the order of 10^{-11} s have already been observed, which makes them faster, for the same energy dissipation, than any other semiconductor device. It seems highly likely that they will be widely used in advanced applications such as high-frequency amplifiers, supercomputers and super-fast signal-processing systems.

Modulation doping is also applicable to superlattices and quantum wells, of course. The combination with the minibands in superlattices offers much scope for speculation, but we shall leave the matter here.

Quantized Hall effect

In a measurement of the Hall effect the quantity determined is the voltage induced in the y-direction (for example) of a sample by the combination of a current in the x-direction and a magnetic field in the z-direction: see *fig. 6a*. The ratio of this voltage to the current is called the Hall coefficient (or Hall resistance). The structures described here, with a two-dimensional electron gas, can exhibit an intriguing effect, the quantized Hall effect, which was first observed in a silicon MOSFET [17]. At very low temperatures and strong magnetic fields there are plateaus in the curve of the Hall coefficient as a function of the magnetic field. The conductivity at these plateaus is independent of the experimental parameters and is given very accurately by h/ne^2, where h is Planck's constant, n is an integer and e is the electronic charge. Klaus von Klitzing received the Nobel Prize for Physics in 1985 for his discovery of this effect.

There is as yet no full explanation of this effect. It is however generally accepted that it is related to the properties of the two-dimensional electron gas, whose energy levels for the motion perpendicular to the

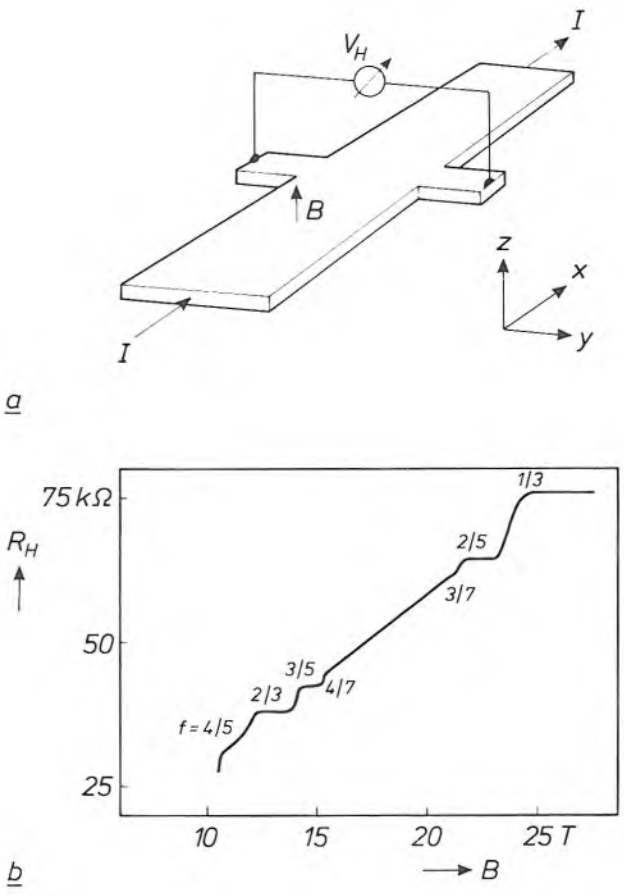

Fig. 6. *a*) Arrangement for Hall-coefficient measurements. I current in the x-direction. B magnetic flux density in the z-direction. V_H induced Hall voltage in the y-direction. The Hall coefficient (or Hall resistance) R_H is given by V_H/I. *b*) The fractional quantized Hall effect measured for a heterojunction of GaAs and $Al_xGa_{1-x}As$ at a very low temperature and a very strong magnetic field [20]. The Hall-coefficient curve has plateaus with a value of h/fe^2, where h/e^2 is equal to 25813 Ω and f is a fraction of 1.

[7] J. C. J. Finck, H. J. M. van der Laak and J. T. Schrama, A semiconductor laser for information read-out, Philips Tech. Rev. **39**, 37-47, 1980.

[8] Special issue 'Compact Disc Digital Audio', Philips Tech. Rev. **40**, 149-180, 1982.

[9] K. Bulthuis, M. G. Carasso, J. P. J. Heemskerk, P. J. Kivits, W. J. Kleuters and P. Zalm, Ten billion bits on a disk, IEEE Spectrum **16**, No. 8 (August), 26-33, 1979.

[10] N. Holonyak, Jr., R. M. Kolbas, R. D. Dupuis and P. D. Dapkus, Quantum-well heterostructure lasers, IEEE J. **QE-16**, 170-186, 1980.

[11] W. T. Tsang, Extremely low threshold (AlGa)As modified multiquantum well heterostructure lasers grown by molecular-beam epitaxy, Appl. Phys. Lett. **39**, 786-788, 1981.

[12] R. Dingle, H. L. Störmer, A. C. Gossard and W. Wiegmann, Electron mobilities in modulation-doped semiconductor heterojunction superlattices, Appl. Phys. Lett. **33**, 665-667, 1978.

[13] A concise survey of the electron mobilities in modulation-doped heterostructures of GaAs and $Al_xGa_{1-x}As$ is given in: H. L. Störmer, Surf. Sci. **132**, 519-526, 1983.

[14] Measurement by C. T. Foxon and J. J. Harris, to be published shortly.

[15] T. Mimura, S. Hiyamizu, T. Fujii and K. Nanbu, A new field-effect transistor with selectively doped GaAs/n-$Al_xGa_{1-x}As$ heterojunctions, Jap. J. Appl. Phys. **19**, L225-L227, 1980.

[16] T. Mimura, Why HEMT are necessary and how they are made, J. Electron. Eng. **20**, No. 200, 60-62, 1983;
H. Morkoc and P. M. Solomon, The HEMT: a superfast transistor, IEEE Spectrum **21**, No. 2 (February), 28-35, 1984.

[17] K. von Klitzing, G. Dorda and M. Pepper, New method for high-accuracy determination of the fine-structure constant based on quantized Hall resistance, Phys. Rev. Lett. **45**, 494-497, 1980.

interface are quantized. Because of the magnetic field, quantization also occurs parallel to the interface, giving rise to the formation of 'Landau levels'. These levels are successively depleted as the magnetic field is increased. Whenever a level becomes fully depleted, there is a plateau in the curve of the Hall coefficient. To explain this it is generally assumed that between the Landau levels there are localized energy states in which the electrons do not contribute to the conductivity. It may also be significant that the electrons are not homogeneously distributed throughout the sample [18].

Soon after the discovery of the quantized Hall effect, it was also found in heterostructures of GaAs and $Al_xGa_{1-x}As$ [19]. Further investigations of these structures revealed another unexpected effect, the fractional quantized Hall effect [20]. It was found that plateaus also occur where the Hall coefficient is given by h/fe^2, with $f = \frac{1}{3}, \frac{2}{3}, \frac{2}{5}, \ldots$; see fig. 6*b*. This means that plateaus must also occur when the Landau levels are only partially occupied. This effect cannot be explained from the single-electron model. This provides further motivation for much more theoretical and experimental investigation of these structures.

The observation of the quantized Hall effect also has practical consequences in view of the high accuracy with which the Hall coefficient at the plateaus can be experimentally determined. Attempts are being made in various standards institutions to use this effect for creating a new reference resistance with an accuracy better than 1 in 10^8.

Growth technologies

The progress made in research on the structures described here has only been possible because of the development of advanced methods for the epitaxial growth of thin-film semiconductor layers. The potential applications that have emerged have provided a tremendous stimulus. At the same time the growth technologies have greatly stimulated the development of sophisticated semiconductor devices.

Two growth technologies are pre-eminent for the ability to control compositions and layer thicknesses and for obtaining virtually defect-free surfaces and interfaces. One of them is metal-organic vapour-phase epitaxy (MO-VPE). In this technology layers of a material such as $Al_xGa_{1-x}As$ are deposited on a heated GaAs substrate from a reactive gas mixture containing AsH_3 and metal-organic compounds of aluminium and gallium [21] [22]. The other technology is molecular beam epitaxy (MBE), which is essentially a special form of evaporation in ultra-high vacuum [23] [24]. Here the layers are deposited by the reaction of molecular (or atomic) beams incident on the heated substrate.

The success of these technologies is largely due to the facilities available for controlling the growth and analysing the structures. They include the use of photoluminescence, transmission electron microscopy and various methods of surface analysis [25]. With these technologies structures can be made that are virtually defect-free, with transitions that are abrupt on an atomic scale.

Materials

The materials that have received most attention are GaAs and $Al_xGa_{1-x}As$. They have very similar lattice constants, which means that epitaxial structures on a GaAs substrate are nearly free of stress. These structures have proved suitable for testing new ideas and for practical evaluation. Some work has also been done with other materials, mainly III-V semiconductors. However, the considerable scope offered by modification of the band structure discussed here will be a considerable stimulus to the use of other materials.

Many materials cannot easily be combined because their lattice constants are too different. This inhibits perfect epitaxial growth and induces undesired dislocations at the interface. Some lattice mismatch can nevertheless be accommodated by an elastic strain in the crystal lattice, without the generation of misfit dislocations at the interface. Interesting combinations of semiconductors that have very different properties can be made in this way.

An example of such a combination is silicon on GaAs [24], with a 4% difference between the lattice constants. With such a structure integrated circuits in silicon could be combined with optoelectronic

[18] R. Woltjer, R. Eppenga, J. Mooren, C. E. Timmering and J. P. André, A new approach to the quantum Hall effect, Europhys. Lett. **2**, 149-155, 1986.
[19] D. C. Tsui and A. C. Gossard, Resistance standard using quantization of the Hall resistance of GaAs-$Al_xGa_{1-x}As$ heterostructures, Appl. Phys. Lett. **38**, 550-552, 1981.
[20] D. C. Tsui, H. L. Störmer and A. C. Gossard, Two-dimensional magnetotransport in the extreme quantum limit, Phys. Rev. Lett. **48**, 1559-1562, 1982.
A survey of the fractional quantized Hall effect is given by H. L. Störmer in: Festkörperprobleme **24**, 25-44, 1984.
[21] P. M. Frijlink, J. P. André and M. Erman, this issue, pp. 118-132.
[22] M. R. Leys, M. P. A. Viegers and G. W. 't Hooft, this issue, pp. 133-142.
[23] B. A. Joyce and C. T. Foxon, this issue, pp. 143-153.
[24] P. C. Zalm, C. W. T. Bulle-Lieuwma and P. M. J. Marée, this issue, pp. 154-165.
[25] See the other articles in this issue. A general description of various methods of surface analysis is given in: H. H. Brongersma, F. Meijer and H. W. Werner, Philips Tech. Rev. **34**, 357-369, 1974.
[26] J. C. Bean, J. C. Feldman, A. T. Fiory, S. Nakahara and I. K. Robinson, Ge_xSi_{1-x}/Si strained-layer superlattice grown by molecular beam epitaxy, J. Vac. Sci. & Technol. A **2**, 436-440, 1984.

components, such as lasers and photodiodes, in GaAs, on the same wafer. Another example is a strained-layer structure of silicon and SiGe. It has been demonstrated that dislocation-free SiGe layers as thick as 75 nm can be grown on silicon [26]. The ideas of modulation doping and band-structure modification can also be applied in this way for silicon. In layer structures that have an elastic strain degeneracies in the conduction band can also be eliminated, so that higher electron mobilities are possible in principle.

Structures of materials with a moderate lattice mismatch are now being widely studied by many materials scientists. It is hard to say whether this will lead to novel devices. The only certainty is that there will be many problems to overcome in the fabrication.

Research at Philips

In recent years Philips have done a great deal of work on thin-film epitaxial semiconductor structures. The study of MO-VPE and MBE processes has resulted in a continuous improvement in the control of the growth of multilayer structures. A variety of interesting structures have been fabricated and their properties have been investigated, with particular attention to the fundamental physics of the structures. Potential device applications, such as the quantum-well laser and the HEMT, are also topics of research.

There is work on MO-VPE growth at the research laboratories in Limeil-Brévannes, in France, and in Eindhoven. Structures of various III-V semiconductors are being investigated, but the emphasis is on combinations of GaAs and $Al_xGa_{1-x}As$. The same applies to the work on MBE at the Redhill laboratories, in England. Another MBE activity has been the growth of silicon layers on GaP and GaAs, a joint project undertaken by the FOM Institute for Atomic and Molecular Physics in Amsterdam and the Philips Research Laboratories in Eindhoven. At the Briarcliff laboratories, in the U.S.A., work has recently started on MBE of II-VI semiconductors. MBE of silicon and silicon-germanium structures is also being studied at the Eindhoven laboratories.

Some of these activities are reviewed in the following articles in this special issue. The first two deal with various aspects of the growth of GaAs and $Al_xGa_{1-x}As$ structures by MO-VPE. The growth of similar structures by MBE is then discussed. The final article deals with MBE of silicon films on GaP and GaAs.

Summary. Research on layered epitaxial structures of semiconductor materials is a field of rapidly growing significance. Structures of special interest are the superlattice consisting of alternate ultra-thin layers of two dissimilar semiconductors, the quantum well formed by a thin semiconductor layer sandwiched between two semiconductor layers with a larger band gap, and the modulation-doped heterojunction. The controlled modification ('tailoring') of the energy-band structure gives some fascinating physical effects. There are also potential new applications, such as quantum-well lasers and high-electron-mobility transistors. Suitable growth technologies are metal-organic vapour-phase epitaxy (MO-VPE) and molecular beam epitaxy (MBE). Various aspects of fundamental physics, growth procedures and device applications are topics of research at several Philips laboratories.

Philips Tech. Rev. 43, No. 5/6, 118-132, May 1987

Metal-organic vapour-phase epitaxy of multilayer structures with III-V semiconductors

P. M. Frijlink, J. P. André and M. Erman

Introduction

Thin single-crystal films of III-V semiconductor materials such as GaAs and $Al_xGa_{1-x}As$ are now widely used in devices such as solid-state lasers [1] and microwave field-effect transistors [2]. The films are obtained by epitaxial growth, in which they adopt the crystal structure of the substrate (usually GaAs). Conventionally, the films are grown by deposition from a melt or a solution (liquid-phase epitaxy, LPE) or from a reactive gas mixture (vapour-phase epitaxy, VPE). In recent years the control over these growth processes has been improved considerably to reduce the dimensions of the semiconductor devices and circuits. There is however only a limited capability for growing multilayer structures with very abrupt interfaces, required for particular applications as mentioned in the opening article [3].

In the last ten years or so two growth techniques have been developed which can meet the special requirements for interface abruptness. One is a modified version of VPE, in which the reactive gas mixture contains metal-organic compounds (metal-organic vapour-phase epitaxy, MO-VPE), the other is molecular beam epitaxy (MBE), which will be discussed later in this issue [4]. An important feature of these techniques is that the chemical composition near the growing surface can be changed in a time interval an order of magnitude smaller than the time necessary for growing a single atomic layer. This has made it possible to grow multilayer structures with sharp interfaces on the scale of one atomic monolayer. Consequently, new devices requiring such abrupt interfaces can now be made. An example of such a device is the $Al_xGa_{1-x}As/GaAs$ quantum-well laser: a semiconductor laser with a very thin active GaAs layer between $Al_xGa_{1-x}As$ barriers, which gives a narrow emission peak at a relatively short wavelength with a low threshold current [5]. Another example is the high-electron-mobility transistor (HEMT): a microwave field-effect transistor with an $Al_xGa_{1-x}As/GaAs$ heterojunction, which has an excellent high-frequency performance [6].

At LEP the MO-VPE growth of III-V layer structures has been extensively investigated [7]. Several aspects have been considered, such as the development of a suitable growth-reactor system and the assessment of the relevant growth parameters for obtaining multilayer structures with the required properties. The layers and their interfaces have been characterized by spectroscopic ellipsometry and photoluminescence measurements. In addition, the applicability of various structures for practical devices has been studied.

It has been found that MO-VPE is a reliable and versatile method for growing a large variety of device-quality III-V semiconductor materials and multilayer structures. It has proved possible to grow successive layers with precise control of composition and lattice match to the substrate, giving high electrical and optical quality. Precise compositional control is possible not only with ternary materials such as $Al_xGa_{1-x}As$ but also with quaternary materials such as $In_xGa_{1-x}P_yAs_{1-y}$. Doping profiles are controlled with a resolution of less than 10 nm. MO-VPE growth is particularly successful for the preparation of quantum-well lasers and HEMT devices based on GaAs and $Al_xGa_{1-x}As$.

A large number of results have shown that MO-VPE and the characterization methods have great potential, and that practical devices can be made.

Ir P. M. Frijlink, Dr J. P. André and Dr M. Erman are with Laboratoires d'Electronique et de Physique Appliquée (LEP), Limeil-Brévannes, France.

Some examples are:

- The photoluminescence of a quantum well in which the active layer is only about 0.6 nm thick.
- A strong visible luminescence of a quantum well with $Al_{0.2}Ga_{0.8}As$ in the active layer.
- A quantum-well laser emitting at 775 nm with a maximum power of 230 mW per facet in continuous-wave (CW) operation at 300 K and a CW threshold current density of 660 A/cm^2.
- A two-dimensional electron gas at the interface of a GaAs/$Al_xGa_{1-x}As$ heterojunction giving an electron Hall mobility of 7.5×10^3 cm^{2}V^{-1}s^{-1} at 300 K and of 2.7×10^5 cm^{2}V^{-1}s^{-1} at 4 K, yielding field-effect transistors with a transconductance as high as 250 S/m for a gate length of 1 μm.

In this article, the discussion of our MO-VPE investigations will be restricted to multilayer structures of GaAs and $Al_xGa_{1-x}As$, the most widely investigated of the III-V structures and the most promising for immediate practical application. After a general description of the MO-VPE method, it will be shown how structures with abrupt interfaces can be obtained. It will be demonstrated that spectroscopic ellipsometry can be a useful tool for depth profiling and interface characterization. Next, the composition and luminescence properties of quantum wells will be dealt with, as well as the application in quantum-well lasers. Finally, modulation-doped heterostructures will be discussed, with emphasis on the special properties related to the formation of a two-dimensional electron gas.

Preparation of multilayer structures with abrupt interfaces

A suitable reactor system for the MO-VPE growth of $Al_xGa_{1-x}As$ is shown in *fig. 1*. A heated GaAs substrate is exposed to a gaseous mixture containing

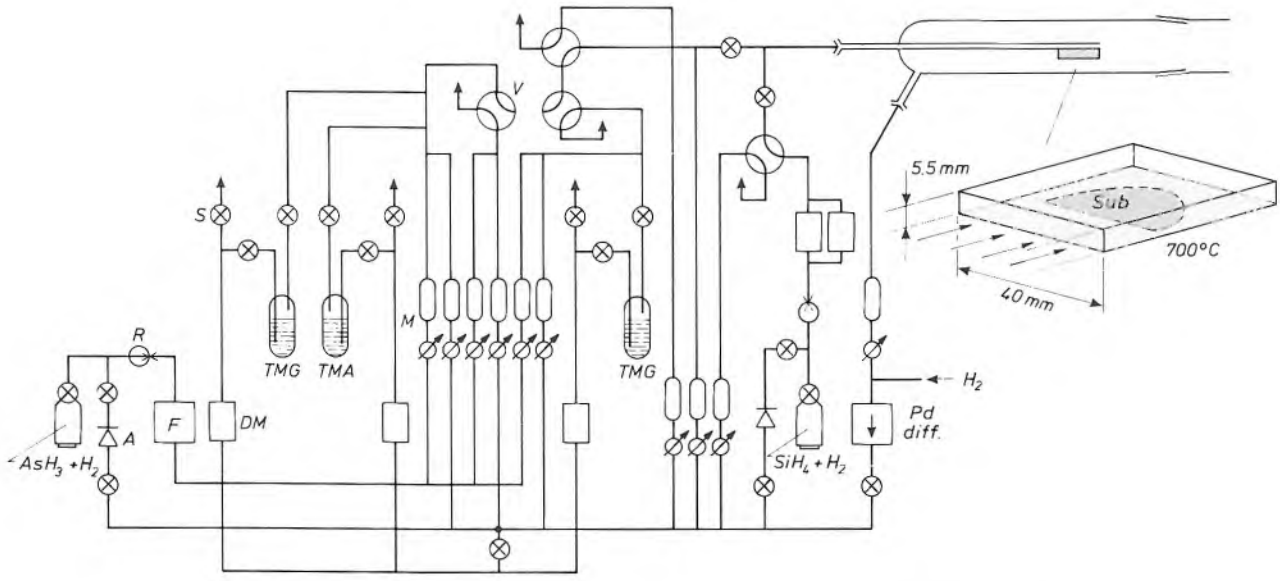

Fig. 1. Schematic diagram of the MO-VPE equipment used for growing $Al_xGa_{1-x}As$ multilayer structures. In a quartz reactor layers are deposited from the gas phase on to a GaAs substrate *Sub*. This is kept at a temperature of about 700 °C by inductive r.f. heating of the substrate holder. The gas phase contains hydrogen (used as the carrier gas) and the reactive components trimethyl aluminium (*TMA*), trimethyl gallium (*TMG*) and arsine (AsH_3), supplemented by doping reactants, e.g. silane (SiH_4) for n-doping. The hydrogen is purified by diffusion through a membrane of palladium (*Pd diff.*). The supply of the several gases can be controlled and mixed in such a way that any desired gas composition can be obtained very rapidly. *S* standard valve; *R* pressure regulator; *M* flow meter with regulating valve; *DM* mass-flow meter; *F* filter for gas purification; *A* non-return valve; *V* four-way valve.

[1] See for example J. C. J. Finck, H. J. M. van der Laak and J. T. Schrama, A semiconductor laser for information read-out, Philips Tech. Rev. **39**, 37-47, 1980.

[2] See for example P. Baudet, M. Binet and D. Boccon-Gibod, Low-noise microwave GaAs field-effect transistor, Philips Tech. Rev. **39**, 269-276, 1980.

[3] J. Wolter, Research on layered semiconductor structures, this issue, pp. 111-117.

[4] B. A. Joyce and C. T. Foxon, Molecular beam epitaxy of multilayer structures with GaAs and $Al_xGa_{1-x}As$, this issue, pp. 143-153.

[6] One of the first descriptions of a quantum-well laser, operating at room temperature, has been given by R. D. Dupuis, P. D. Dapkus, N. Holonyak, Jr., E. A. Rezek and R. Chin, Appl. Phys. Lett. **31**, 295-297, 1978.

[6] Successful fabrication of a HEMT device was reported for the first time by T. Mimura, S. Hiyamizu, T. Fujii and K. Nanbu, Jap. J. Appl. Phys. **19**, L225-L227, 1980.

[7] Many of our colleagues at LEP contributed to the investigations described here. The MO-VPE growth of $Al_xGa_{1-x}As$ multilayer structures has also been investigated at the Philips Research Laboratories in Eindhoven, see M. R. Leys, M. P. A. Viegers and G. W. 't Hooft, this issue, pp. 133-142.

the metal-organic compounds trimethyl aluminium ($Al_2(CH_3)_6$) and trimethyl gallium ($Ga(CH_3)_3$) with arsine (AsH_3) and hydrogen (H_2), which is used as carrier gas. The pyrolysis of the reactive compounds at the substrate surface leads to the epitaxial deposition of a single-crystal $Al_xGa_{1-x}As$ layer in the overall reaction:

$$\tfrac{1}{2}x\,Al_2(CH_3)_6(g) + (1-x)\,Ga(CH_3)_3(g) + AsH_3(g) \xrightarrow[600\text{-}750\ ^\circ C]{H_2(g)} Al_xGa_{1-x}As(s) + 3\,CH_4(g).$$

The composition of the deposited layer depends on the partial pressures of $Al_2(CH_3)_6$ and $Ga(CH_3)_3$ in the gas phase. Addition of substances such as silane (SiH_4) or diethyl zinc ($Zn(C_2H_5)_2$) to the gas phase leads to n- or p-doping of the layer.

Compared with the more conventional VPE and LPE methods, the MO-VPE method has some advantages for growing multilayer structures with abrupt interfaces: it is essentially a 'far-from-equilibrium' or 'one-way-deposition' process. Since the growth rate is essentially proportional to the supply of the reactants that provide the group III elements, decreasing the supply of these reactants will in principle make the growth rate arbitrarily small. By changing the gas composition very thin layers with abrupt compositional changes can be obtained. However, for high electrical and optical quality, these layers must be pure. If we assume a constant rate of contamination, e.g. from outgassing of the reactor walls, it is clear that an extremely small growth rate will result in a high contamination level in the solid grown. This means that there are essentially two ways of obtaining very pure heterostructures with very abrupt interfaces: either we use a reactor system in which we make sure that the overall contamination level is very low, and reduce the growth rate sufficiently to avoid transient control problems on changing the gas composition to grow an interface, or we aim for effective control of very rapid changes in the gas composition and use a high growth rate, thus reducing the requirements for contamination control. In view of the present 'state of the art' in MO-VPE reactors, we chose the second option.

In our investigations, the $Al_xGa_{1-x}As$ layers are generally deposited on substrates consisting of chromium-doped semi-insulating GaAs wafers. These wafers are sawn from a single-crystal ingot, grown by the Czochralski method. The mechanically polished substrate surface is disoriented with respect to the (001) crystal plane by a few degrees. The substrate is supported by a graphite susceptor. The appropriate substrate temperature, between 600 and 750 °C, is obtained by inductive r.f. heating of the susceptor. A thermocouple in the susceptor measures the substrate temperature. The carrier gas is purified by diffusion through a palladium membrane. The supply of the various reactive compounds is controlled by mass-flow meters.

As pointed out, the MO-VPE growth of multilayer structures with abrupt interfaces requires an instantaneous and precise control of the partial pressures in the reactor system. In the system of fig. 1 the gas transport is arranged so that the gas composition over the wafer can be changed in a controlled way within 0.1 s, neglecting adsorption and desorption at the reactor walls. At a total gas pressure of 10^5 Pa (1 atm) and a suitably low growth temperature of 650 °C, the growth rate of $Al_xGa_{1-x}As$ layers can be as low as 0.5 nm/s. This means that the time required for changing the chemical composition at the crystal surface is much less than the growth time of one monomolecular layer of $Al_xGa_{1-x}As$. This permits the growth of well-defined multilayer structures, with a reproducible control over composition, thickness and doping profile in the direction of growth on an atomic scale.

As will be discussed later, depth profiling and interface quality can be demonstrated for quantum wells by analysing their luminescence properties and for modulation-doped heterostructures by considering the increase in the electron mobility near the interface. However, we shall first discuss a more general characterization method: spectroscopic ellipsometry. This method has been found to be very useful in investigating the chemical and structural quality of the interfaces.

Depth profiling and interface characterization by spectroscopic ellipsometry

Ellipsometry is an optical technique that makes use of the change in polarization of light at the surface to be investigated [8]. The state of polarization of polarized light can be characterized by the amplitude A and the phase δ of two perpendicular components into which the total electric vector of the light can be resolved. The component parallel to the plane of incidence (E_p) and the component perpendicular to it (E_s) are given by:

$$E_p = A_p \exp j(\delta_p + \omega t), \qquad E_s = A_s \exp j(\delta_s + \omega t), \tag{1}$$

where j is the imaginary unit and ω is the angular frequency of the light wave. At arbitrary values of the amplitudes and phases, the tip of the total electric vector will describe an ellipse; the light is then said to be elliptically polarized. On reflection the change in

the parallel component is different from the change in the perpendicular component, so that the shape of the ellipse will change; see *fig. 2*.

In an ellipsometer the complex ratio ϱ of the reflectances of the parallel and perpendicular omponents is determined; this can be expressed as:

$$\varrho = \frac{(E_p/E_s)_r}{(E_p/E_s)_i}, \qquad (2)$$

where the indices r and i refer to the reflected and incident beams. Substitution from eq. (1) gives the relation with the changes in amplitude and phase on reflection, which can be described by two parameters ψ and Δ:

$$\varrho = \tan\psi \exp j\Delta, \qquad (3)$$

$$\tan\psi = \frac{(A_p/A_s)_r}{(A_p/A_s)_i}, \qquad (4)$$

$$\Delta = (\delta_p - \delta_s)_r - (\delta_p - \delta_s)_i. \qquad (5)$$

For a reflection at a clean substrate, the quantities ψ and Δ can be correlated with its refractive index and absorption coefficient. If the substrate is coated with a thin layer, information about the thickness of the layer and its optical properties can also be obtained.

The layers we have deposited and their interfaces have been investigated by a special form of ellipsometry, in which ϱ is determined as a function of the energy of the incident light (spectroscopic ellipsometry). Since ϱ is directly related to the dielectric function of the reflective material, such measurements enable us to make a detailed structural and chemical analysis of the surface. The spectroscopic ellipsometer used in our experiments has the following optical components: a xenon lamp, a rotating polarizer, the sample, a fixed analyser, a double monochromator and a photomultiplier. The optical range is from 1.6 eV (because of the limited sensitivity at longer wavelengths of the S20 extended-UV photocathodes) to 5.4 eV (because of the use of calcite prisms for the polarizer and analyser). The output signal of the photomultiplier is sampled as a function of the angular position of the polarizer and a Fourier analysis is made by a minicomputer to determine the value of ϱ.

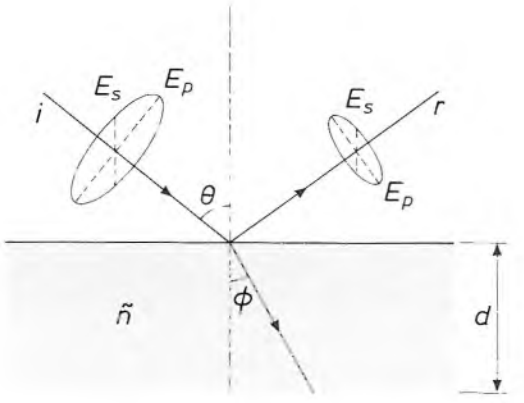

Fig. 2. Schematic representation of the reflection of elliptically polarized light at the surface of a layer. The parallel and perpendicular components E_p and E_s of the electric vector of the reflected light beam (r) differ from those of the incident beam (i). The ratio of the reflectances of the two components depends on the angle of incidence θ, the angle of refraction ϕ and the complex index of refraction $\tilde{n}$ and the thickness d of the layer.

The dielectric function ε can be derived at each energy by using the Fresnel expressions for the reflection coefficients of the parallel and perpendicular components and Snell's law. For a clean wafer ε is given by:

$$\varepsilon = \varepsilon_1 - j\varepsilon_2 = \frac{(1-\varrho)^2}{(1+\varrho)^2} \sin^2\theta \tan^2\theta + \sin^2\theta, \qquad (6)$$

where θ is the angle of incidence. In *fig. 3a* the continuous lines give the dielectric function for a carefully cleaned GaAs wafer under vacuum at room temperature. A characteristic feature is the presence of a double-peak structure in the ε_2 curve, corresponding to different optical transitions (at 2.93 and 3.16 eV) between the valence and conduction bands [9]. The spectrum of the dielectric function of GaAs is very sensitive to crystalline imperfections induced for example by high temperatures (lattice vibrations), doping or Al incorporation. Generally speaking, any type of imperfection tends to reduce the ε_2 peak height and especially the contrast in the double-peak structure. Evaluation of the spectrum obtained can therefore give useful information about the ordering of the GaAs lattice and the doping level or Al incorporation [10].

The dielectric functions of various $Al_xGa_{1-x}As$ alloys have also been measured. As an example, the continuous lines in fig. 3*b* give the spectrum for an undoped $Al_{0.54}Ga_{0.46}As$ sample. Compared with the

[8] See for example D. E. Aspnes, Spectroscopic ellipsometry of solids, in: B. O. Seraphin (ed.), Optical properties of solids, New developments, North-Holland, Amsterdam 1976, pp. 799-846.
Surface analysis by ellipsometry has also been described in this journal: K. H. Beckmann, Optical investigations of semiconductor surfaces, Philips Tech. Rev. **29**, 129-142, 1968;
F. Meijer and G. A. Bootsma, Investigation of the chemical behaviour of clean silicon and germanium surfaces, Philips Tech. Rev. **32**, 131-140, 1971.

[9] A survey of the various valence-conduction band transitions in GaAs has been given by Y. Petroff in: M. Balkanski (ed.), Optical properties of solids, North-Holland, Amsterdam 1980, Chapter 1.

[10] M. Erman, J. B. Theeten, N. Vodjdani and Y. Demay, Chemical and structural analysis of the GaAs/AlGaAs heterojunctions by spectroscopic ellipsometry, J. Vac. Sci. & Technol. B **1**, 328-333, 1983;
M. Erman, J. B. Theeten, P. Frijlink, S. Gaillard, Fan Jia Hia and C. Alibert, Electronic states and thicknesses of GaAs/GaAlAs quantum wells as measured by electroreflectance and spectroscopic ellipsometry, J. Appl. Phys. **56**, 3241-3249, 1984.

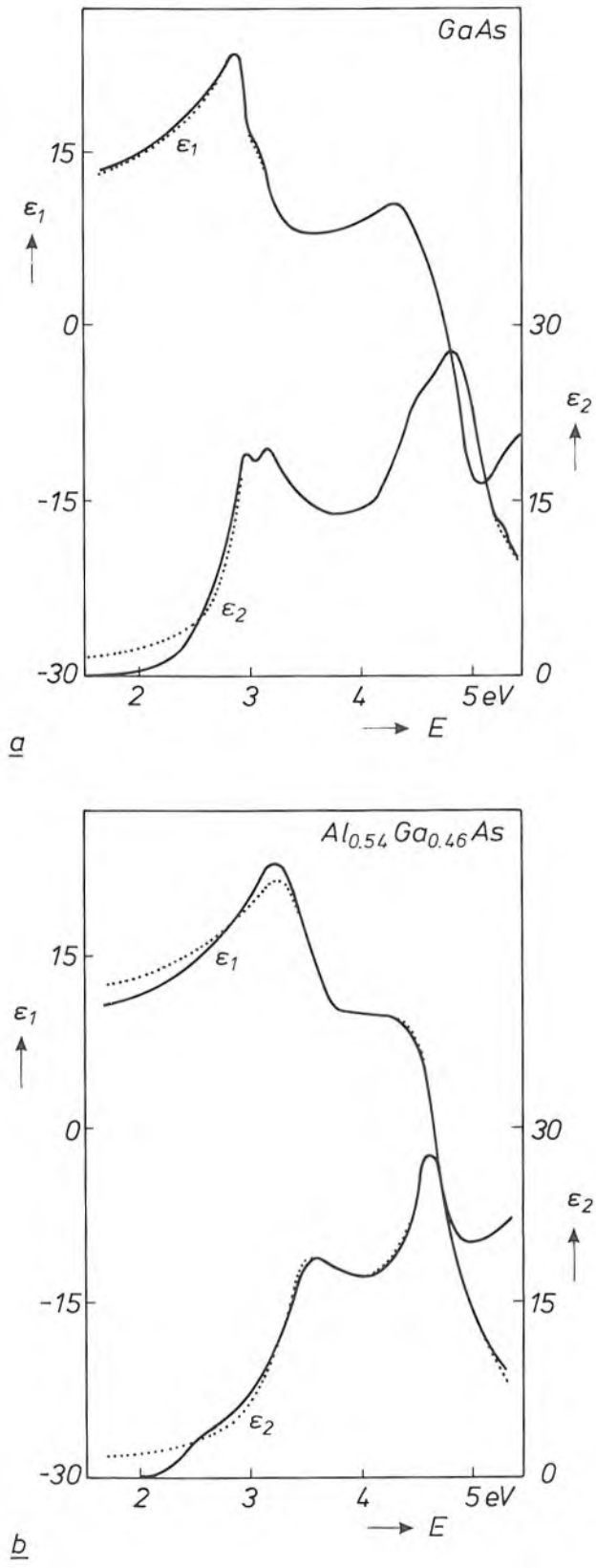

Fig. 3. Real and imaginary parts ε_1 and ε_2 of the dielectric functions of GaAs (*a*) and $Al_{0.54}Ga_{0.46}As$ (*b*), plotted against the energy E of the incident light. The continuous curves were derived from the measured complex ratio ϱ as given by eq. (6). The ε_2 curve for GaAs has a characteristic double-peak structure at about 3 eV. The dotted curves refer to simulations generated by using a set of seven harmonic oscillators (see text). Above 2.5 eV good agreement with the measurements is obtained.

pure GaAs case, the spectrum shows no double-peak structure in the neighbourhood of 3 eV, but otherwise it has the same general features. It has been demonstrated that the spectrum of an arbitrary $Al_xGa_{1-x}As$ alloy can be derived by interpolation. This can be done accurately by describing the variation of ε with the energy E as a sum of harmonic oscillators, each characterized by its amplitude A_i, its centre position E_i and its half-width Γ_i:

$$\varepsilon = \sum_i A_i\{(E_i - E - j\Gamma_i)^{-1} + (E_i + E + j\Gamma_i)^{-1}\}. \quad (7)$$

The GaAs dielectric function can be simulated by a set of seven oscillators as shown in fig. 3*a* by the dotted lines. The description is satisfactory above 2.5 eV. The basic idea for simulating the dielectric function of any $Al_xGa_{1-x}As$ alloy is to use the *same* set of seven oscillators with a simple variation (quadratic in x) of A_i, E_i and Γ_i. The law of variation can be determined from measurements at a few x-values. This simulation method is illustrated by the dotted lines in fig. 3*b* for $Al_{0.54}Ga_{0.46}As$. Good agreement with the measurements is again obtained above 2.5 eV.

The results for pure wafers can be used for simulations on actual samples of $Al_xGa_{1-x}As$ layers deposited on a GaAs substrate. These simulations are based on the 'effective-medium approximation' [11] for thicknesses less than the wavelength of the incident light. This means that the dielectric function ε of a mixture of two materials A and B, with known dielectric functions ε_A and ε_B, can be evaluated from the relation:

$$v(\varepsilon_A - \varepsilon)(\varepsilon_A + 2\varepsilon)^{-1} + (1 - v)(\varepsilon_B - \varepsilon)(\varepsilon_B + 2\varepsilon)^{-1} = 0, \quad (8)$$

where v is the volume fraction of A.

In evaluating and understanding the specific properties of heterojunctions and multilayer structures, an important aspect is the structure, on the atomic scale, of the transition regions between the various layers. In the ideal case of an abrupt heterojunction, the top of the semiconductor substrate A has the same composition and crystalline structure as the bulk of A, while the bottom of the deposited layer of the other semiconductor B has the same composition and structure as the bulk of B. Two types of deviation can occur from this ideal case:

- Interdiffusion of A and B and formation of an alloy with a chemical nature distinct from both materials: this will be referred to as a 'chemical' interface.
- Interpenetration of A and B, without changing their chemical nature, so that their separation is not planar

[11] C. G. Granqvist and O. Hunderi, Optical properties of ultrafine gold particles, Phys. Rev. B 16, 3513-3554, 1977.

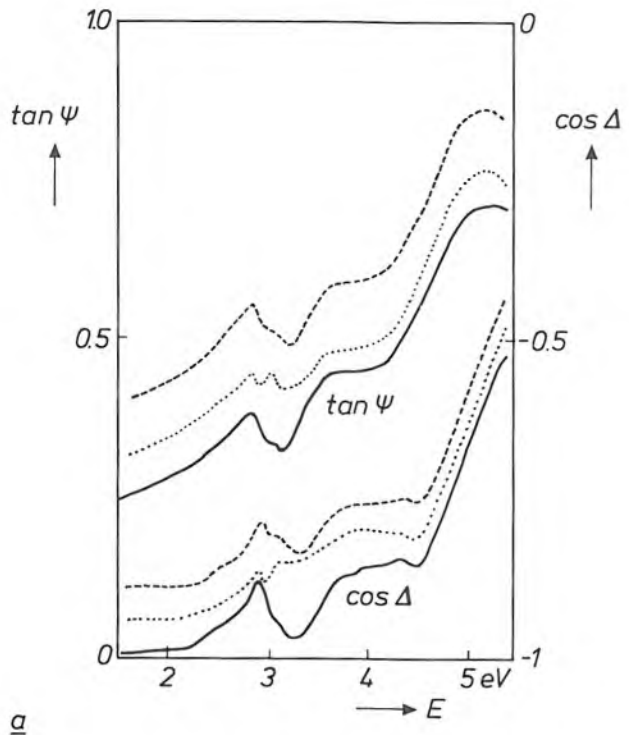

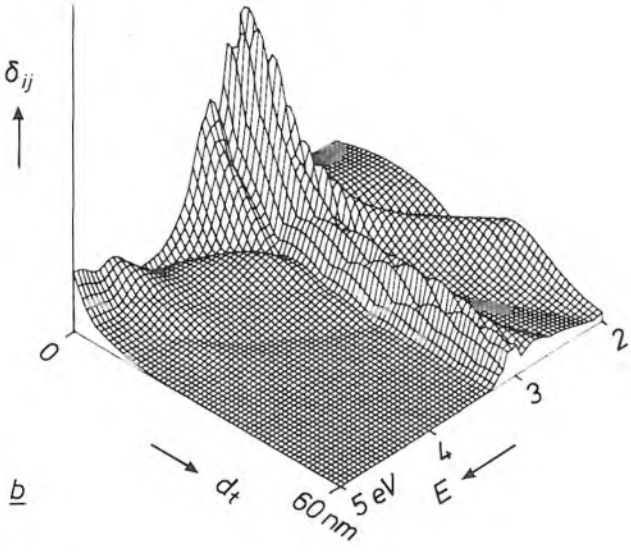

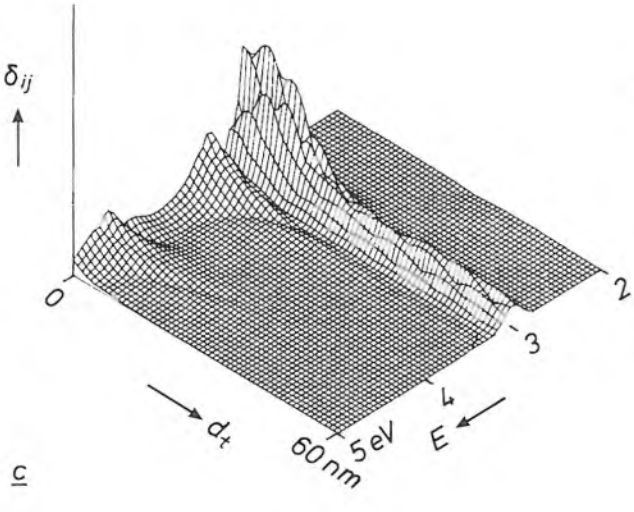

but rough on the atomic scale; this will be referred to as a 'physical' interface.

Investigations of different types of structures by spectroscopic ellipsometry have demonstrated the sensitivity of this method to the presence and nature of interface regions. As an example, *fig. 4a* gives the simulated curves of $\tan\psi$ and $\cos\Delta$ plotted against E for a structure with an ideal interface and for structures with chemical and physical interfaces. At the critical energy of about 3 eV (fig. 3) the curves for the ideal and physical interfaces are quite similar, while the curves for the chemical interface differ markedly. This is due to the presence of the intermediate composition at the chemical interface, giving rise to a shifted double-peak structure. This indicates that spectroscopic ellipsometry on $Al_xGa_{1-x}As$ structures will be especially sensitive to the presence of a chemical interface.

A more extensive comparison is obtained by considering the mean-square difference δ_{ij} between the cases i and j, given by

$$\delta_{ij} = (\tan\psi_i - \tan\psi_j)^2 + (\cos\Delta_i - \cos\Delta_j)^2. \quad (9)$$

In fig. 4*b* and 4*c* the calculated differences are given as a function of the incident light energy E and the total thickness d_t. Because of the optical absorption of the top layer, the interface region cannot be detected when $E \geqslant 3.5$ eV and $d_t \geqslant 15$ nm. The major contrast at about 3 eV between chemical and ideal is a factor of two greater than between physical and chemical. Even at this energy the contrast is strongly reduced when d_t becomes larger than 30 nm. This means that d_t should be of the order of 10 nm to achieve a satisfactory interface analysis. This limitation can be taken as an advantage when successive heterojunctions on the same substrate have to be investigated. An *in situ* analysis will be possible for each individual heterojunction, provided that sufficient material is deposited between two successive transitions.

The comparison between modelling and experiment will be illustrated by the results obtained

◁

Fig. 4. Theoretical comparison between the ellipsometry properties of three types of interface. *a*) Calculated curves of $\tan\psi$ and $\cos\Delta$ as a function of the energy E. The continuous curves refer to an ideal interface between GaAs and 10 nm $Al_{0.54}Ga_{0.46}As$, the dotted curves to a chemical interface region of 5 nm with the intermediate composition $Al_{0.27}Ga_{0.73}As$ and the dashed curve to a physical interface region that is a mixture of GaAs and $Al_{0.54}Ga_{0.46}As$. For clarity the curves have been shifted with respect to one another in the vertical direction. At about 3 eV, the deviation from the ideal interface is larger for the chemical interface than for the physical one. *b*) Mean-square difference δ_{ij}, given by eq. (9), between the chemical and ideal interfaces as a function of the total thickness d_t and the energy E. The greatest contrast is obtained at $d_t \approx 10$ nm and $E \approx 3$ eV. *c*) Mean-square difference δ_{ij} between the chemical and physical interfaces plotted against d_t and E. The maximum contrast is about half that in (*b*).

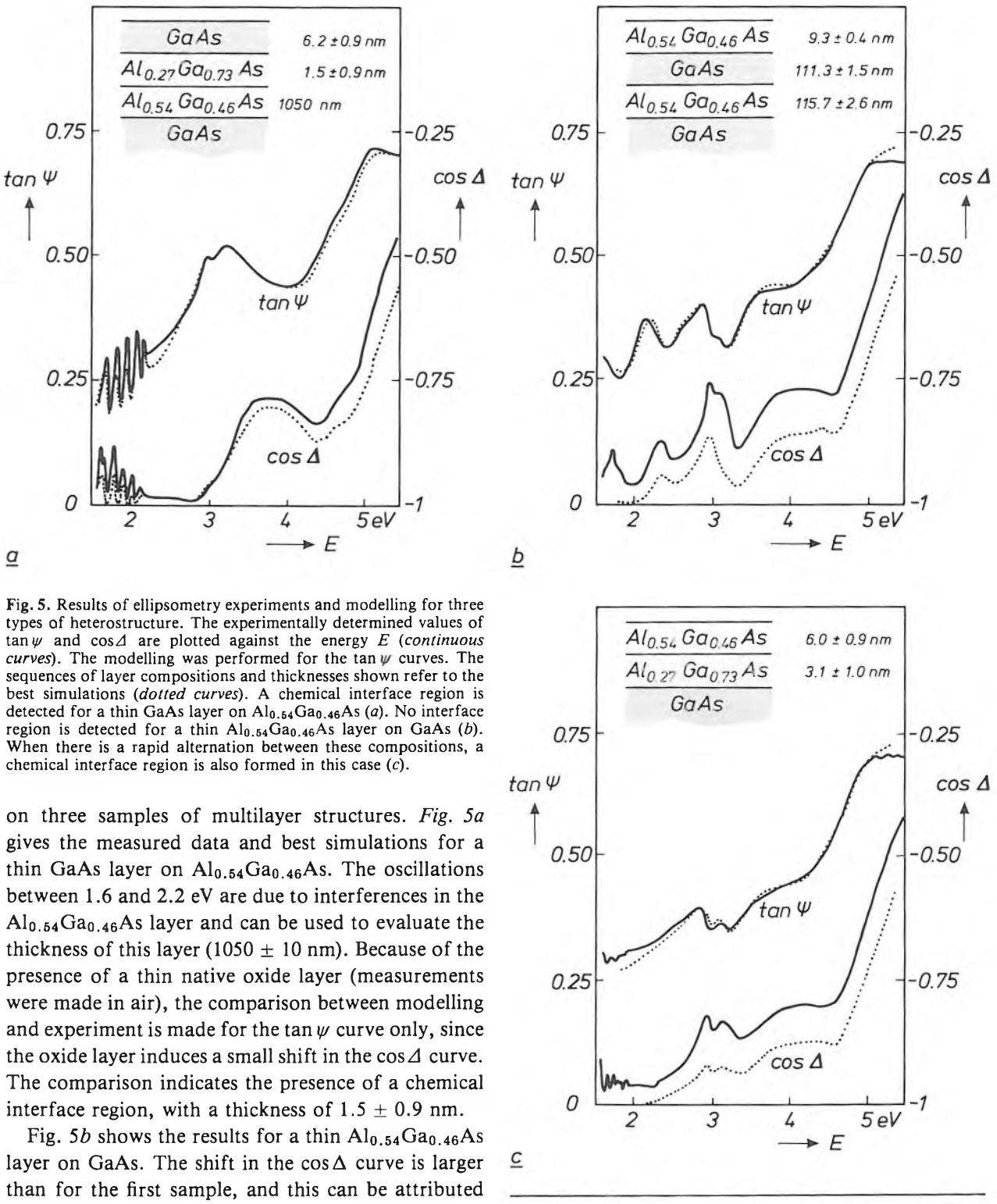

Fig. 5. Results of ellipsometry experiments and modelling for three types of heterostructure. The experimentally determined values of $\tan\psi$ and $\cos\Delta$ are plotted against the energy E (*continuous curves*). The modelling was performed for the $\tan\psi$ curves. The sequences of layer compositions and thicknesses shown refer to the best simulations (*dotted curves*). A chemical interface region is detected for a thin GaAs layer on $Al_{0.54}Ga_{0.46}As$ (*a*). No interface region is detected for a thin $Al_{0.54}Ga_{0.46}As$ layer on GaAs (*b*). When there is a rapid alternation between these compositions, a chemical interface region is also formed in this case (*c*).

on three samples of multilayer structures. *Fig. 5a* gives the measured data and best simulations for a thin GaAs layer on $Al_{0.54}Ga_{0.46}As$. The oscillations between 1.6 and 2.2 eV are due to interferences in the $Al_{0.54}Ga_{0.46}As$ layer and can be used to evaluate the thickness of this layer (1050 ± 10 nm). Because of the presence of a thin native oxide layer (measurements were made in air), the comparison between modelling and experiment is made for the $\tan\psi$ curve only, since the oxide layer induces a small shift in the $\cos\Delta$ curve. The comparison indicates the presence of a chemical interface region, with a thickness of 1.5 ± 0.9 nm.

Fig. 5*b* shows the results for a thin $Al_{0.54}Ga_{0.46}As$ layer on GaAs. The shift in the $\cos\Delta$ curve is larger than for the first sample, and this can be attributed to a thicker native oxide layer due to the presence of Al in the top layer. The best modelling is obtained by assuming no interface region (ideal interface). The conclusion can therefore be drawn that the $Al_xGa_{1-x}As/GaAs$ heterojunction (the 'normal' situation) is essentially abrupt and is better defined than the converse situation discussed earlier. A careful error analysis of the results shows that the maximum transition thickness is about 0.5 nm, compared with about 1.5 nm in the converse situation.

To test the ability of spectroscopic ellipsometry to detect an interface region we have also examined a structure in which a 3-nm interface region had been deliberately grown. This was done by rapid alternation of the gas flows corresponding to GaAs and $Al_{0.54}Ga_{0.46}As$ in such a way that the interface could be considered as a sequence of twenty layers of

alternating composition, with each individual layer about 0.15 nm thick. Since this thickness is below that of one monolayer a chemical mixture would be expected: the interface region should look like an $Al_{0.27}Ga_{0.73}As$ layer about 3 nm thick. This is confirmed experimentally; see fig. 5c. The modelling assuming a chemical interface gives the best fit with the experimental data, with fewer uncertainties in the layer thicknesses. The best simulation is obtained with an interface of 3.1 ± 1.0 nm.

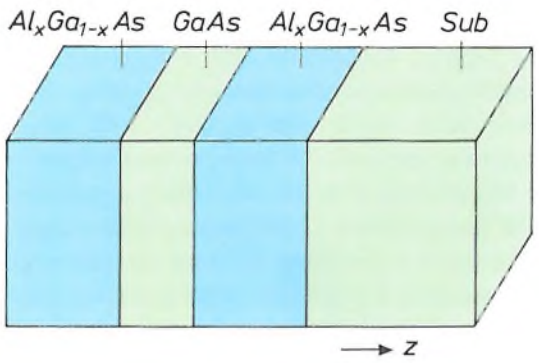

Quantum wells

When a GaAs layer is sandwiched between two $Al_xGa_{1-x}As$ layers that have a larger band gap, there are steps in the energy-level diagram at the interfaces [1]. The existence of energy bands is due to the periodicity of the crystals, but their configuration is essentially determined by interactions over a range of about one unit cell of the crystal. In fact, the magnitude of the band gap of each material appears to be maintained right up to the interface. The band-gap difference leads to discontinuities in the conduction and valence bands at the interfaces. The conduction-band discontinuity is related to the difference in electron affinity between the two materials and is now assumed to be about 60% of the band-gap difference [12].

An interesting quantization effect is observed when the GaAs layer becomes thinner than the mean free path of the electrons between two collisions with lattice vibrations (phonons), lattice imperfections such as point defects, or impurity atoms [13]. The electrons trapped in the GaAs layer can then be reflected many times between the two interfaces. If the half-wavelength of the electrons in the direction perpendicular to the interfaces does not fit into the quantum well an integer number of times, the state will only have a very short lifetime, because of extinction by interference. Only the particular states that do fit in this way can exist permanently. Thus for the movement perpendicular to the interfaces only discrete energy values are permissible.

In directions parallel to the interfaces the electrons can move freely, and to a first-order approximation this does not affect the wavelength of the perpendicular movement. This implies that the electrons may have some extra energy. Each permitted state in the perpendicular direction therefore gives rise to a discrete energy band, whose lower band edge, characterized by zero movement in the parallel directions, is determined by the energy necessary to give a wavelength of $2d/n$, where n is an integer and d is the well thickness plus an effective ('tunnelling') penetration

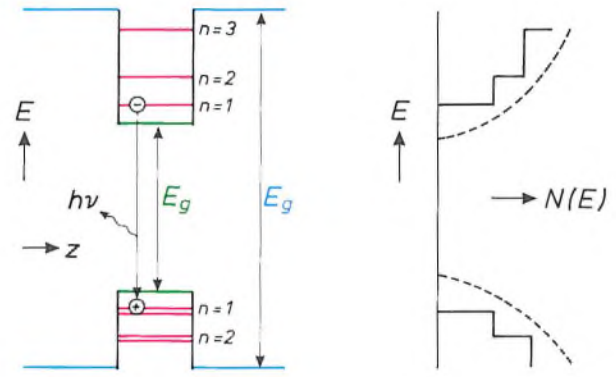

Fig. 6. Simplified energy-level diagram and density of states for a quantum well formed on a GaAs substrate *Sub* by a very thin GaAs layer between two $Al_xGa_{1-x}As$ layers with a larger band gap E_g. The confinement in the narrow potential well leads to discrete energy levels for electrons and holes that move perpendicular to the interfaces. These levels are characterized by the quantum number n. For each quantum state two valence levels exist, corresponding to 'heavy' holes and 'light' holes. The energy bands corresponding to movement parallel to the interfaces are not shown, their edges represent zero movement. The variations in the density of states $N(E)$ with E is not continuous as in the bulk material (*dashed curves*), but occurs in steps (*continuous curves*). This means that the luminescence resulting from the recombination of electrons and heavy holes with $n = 1$ can have a high efficiency. The energy difference between the states associated with the luminescence is larger than in the bulk material, so that the luminescence occurs at shorter wavelengths.

width of the wave into the barriers. The lowest-energy state will be the state with $n = 1$. There is an analogous effect for the holes, with the complication that two types of holes exist in GaAs, with light and heavy effective mass. The resulting energy-level diagram and density of states are shown in *fig. 6*.

Luminescence

If we create electron-hole pairs in a quantum well by shining light on it, the electrons and holes will lose energy through a number of rapid relaxation pro-

[12] R. C. Miller, D. A. Kleinman and A. C. Gossard, Energy-gap discontinuities and effective masses for GaAs-$Al_xGa_{1-x}As$ quantum wells, Phys. Rev. B 29, 7085-7087, 1984.

[13] The possible quantum states in heterostructures with ultra-thin semiconductor layers have been compiled by R. Dingle, Festkörperprobleme 15, 21-48, 1975.

cesses, and they will thermalize in the $n = 1$ states, with the particle distribution approaching a Fermi-Dirac distribution around a quasi-Fermi level. After this there is a much slower (e.g. 1000 times) recombination process. At each recombination, a photon will be emitted at the wavelength corresponding to the energy difference between an electron and a hole, both within a few times kT from the band edges of their respective $n = 1$ levels. With a thinner quantum well these band edges are more widely separated and the emitted photons will therefore have a shorter wavelength. A theoretical relation between the quantum-well thickness and the emission wavelength is given in *fig. 7*. This relation now permits us to assess the thickness of the GaAs quantum well directly by measuring the emission wavelength for small values of kT, e.g. at 4 K. A small correction is necessary because electrons and holes will first form excitons (mobile electron-hole 'pairs') before recombining completely. This effect reduces the photon energy by about 5-10 meV, depending on the thickness of the quantum well.

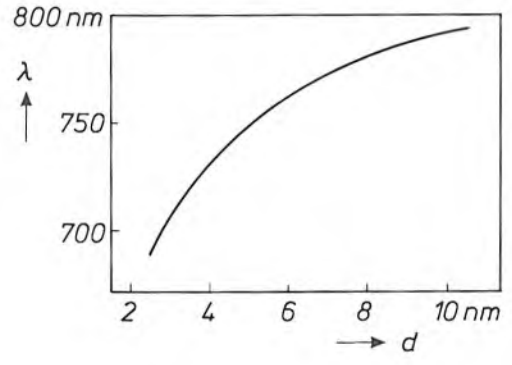

Fig. 7. Calculated relation between well thickness d and emission wavelength λ corresponding to the recombination of electrons and heavy holes in the $n = 1$ state, for a rectangular GaAs quantum well between $Al_{0.54}Ga_{0.46}As$ barriers. For a decrease in thickness from 12 to 2.5 nm the calculated reduction in wavelength is from 800 to 680 nm.

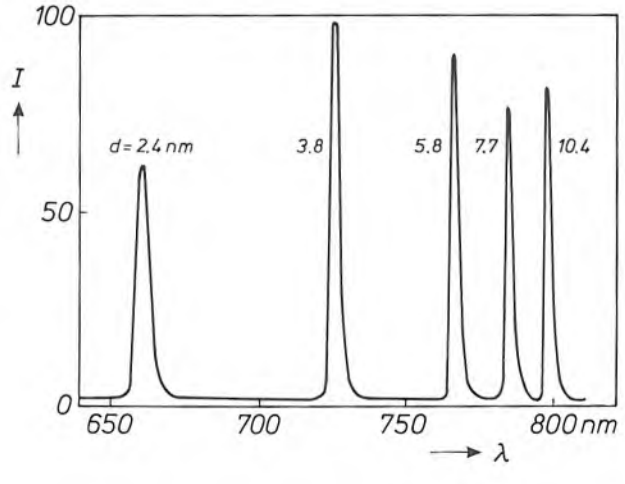

Fig. 8. Photoluminescence spectrum of a multiple-quantum-well sample on excitation at 4 K with radiation at 514.5 nm from an argon laser. The emission intensity I is plotted in arbitrary units as a function of the emission wavelength λ. The quantum wells have various thicknesses d and are separated by 50 nm of $Al_{0.6}Ga_{0.6}As$. The thinner wells were grown last, to prevent re-absorption of emitted radiation. Each well gives an emission peak due to the recombination of electrons and heavy holes with $n = 1$. The peak positions do not differ greatly from the theoretical values indicated in fig. 7. Broader peaks are observed with the thinner wells.

Fig. 8 shows the emitted spectrum of a sample containing five quantum wells of different sizes, which was excited by light from an argon laser at 514.5 nm. For each quantum well we only see the emission from the excitons associated with the $n = 1$ states. The polished surface of the substrates we used was at an angle of 6 degrees to the (001) plane of the crystal. The surface is 'step-like' during growth, with monolayer steps of 'height' 0.283 nm and about 2.8 nm apart. Addition of one GaAs molecule at each step site increases the mean grown thickness by 0.028 nm. In the plane of the quantum well, the excitons extend over about 30 nm, i.e. an order of magnitude larger than the distance between the steps, and the excitons will therefore not 'see' the steps but only the mean thickness of the GaAs layer, which varies in units of not more than 0.028 nm.

The width of the peaks is determined by the amount of (unintentionally incorporated) impurities in the epitaxial layer (5×10^{14} to 10^{15} cm^{-3}) and also by the amount by which the thickness of the quantum well varies over the light spot whose photoluminescence is measured. The tail of each peak on the low-energy side can be attributed to band-bending and to localized states due to impurities and thickness variations with a magnitude of a few tens of nm in the plane of the quantum well [14].

The width of the peaks is not related to the actual shape of the quantum wells, insofar as this is the same everywhere in the light spot, and does not therefore give information about the transition width of the composition profile at the interfaces. This transition will be fairly gradual because of the time necessary to change the gas composition over the wafer, and possibly because of adsorption or desorption at the walls of the reactor and tubing. Another possible source of gradual transition at the interface could be interdiffusion during growth, which may be enhanced when the interface is still close to the growing surface.

It has been shown [15] that the contribution of interdiffusion without surface-proximity enhancement is less than 0.1 nm for normal growth conditions. Since the time required for changing the gas concentration without adsorption or desorption is of the order of 0.1 s, its contribution will also be less than 0.1 nm. The two remaining mechanisms, adsorption/desorption and surface-proximity enhanced diffusion, are

most likely to provoke exponential tails at each compositional transition.

The effect of gradual compositional changes on the energy-level diagram is illustrated in *fig. 9*. Here the conduction-band edge in the well is lowered so little that the minimum is higher than the $n = 1$ electron level in pure GaAs. It is clear that the $n = 1$ electron level will shift to a higher energy and the $n = 1$ heavy-hole level to a lower energy. Thus the energy difference between the $n = 1$ states will be larger and the photoluminescence peak will be shifted to shorter wavelengths. For a given transition width, this shift is relatively larger for narrower quantum wells. This made it possible to assess the transition width by comparison of the relative positions of the photoluminescence peaks of a multiple quantum-well sample with the theoretical values for perfectly rectangular wells. The required exact knowledge of the ratios of the physical magnitude of the quantum wells was obtained by ensuring that the growth rate remained constant, and that there was no perturbation in the growth rate due to flow transients occurring when the gas flows are switched. The flow through the sources was stabilized by insertion of capillary tubes at the exit of the bubbling vessels.

The usefulness of these capillary tubes may be illustrated by the fact that, in our reactor, 50 cm^3 of saturated trimethyl-gallium vapour in the bubbler is sufficient to grow 500 nm of GaAs. An accuracy of 0.1 nm in the thickness of a quantum well means that we have to be able to displace a smallest unit of just 0.02% of this volume (0.01 cm^3) into the reactor chamber at the required instant. The result was checked by growing samples with superlattices consisting of alternating layers of GaAs and $Al_xGa_{1-x}As$. The ripple wavelengths in the depth profiles obtained by secondary-ion mass spectrometry (SIMS)[16] agree well with the periods in the superlattices.

From the observed relative shifts of the photoluminescence peaks in the spectra of multiple quantum wells that were subsequently grown, we concluded, assuming an exponential decay profile of the Al content at the interfaces, that the transition width is no larger than about 0.5 nm for all interfaces [17].

By forced depletion of the gas stream in the horizontal reactor chamber, a replica of a structure grown upstream can be grown downstream with layers less than a third of the thickness. In this way it was possible to show that even a 0.6-nm GaAs layer embedded in $Al_{0.35}Ga_{0.65}As$ acts as a quantum well and gives a well-defined photoluminescence peak [14], in the absence of significant interdiffusion of the layers during growth. The spectrum of a multilayer structure containing such a quantum well is shown in *fig. 10*. The emission wavelength of this well is very short, 620 nm.

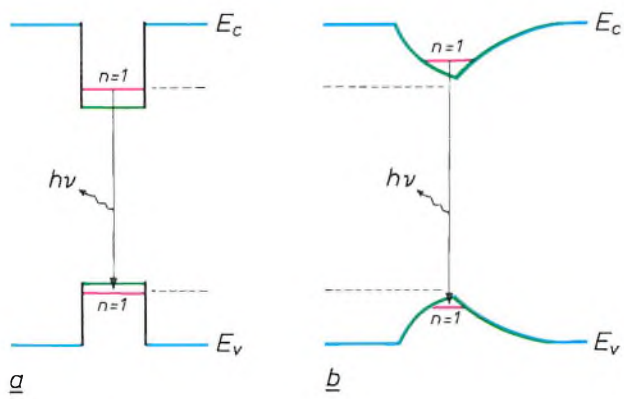

Fig. 9. The effect of gradual changes in composition on the energy-level diagram of a GaAs quantum well. With abrupt changes ideal interfaces are obtained, resulting in a rectangular well (*a*). If the composition changes slowly near the interfaces, the well becomes less deep (*b*). The edge of the conduction band E_c and the edge of the valence band E_v are modulated in such a way that the minimum of E_c becomes higher than the lowest conduction level of a rectangular well, whereas the maximum of E_v becomes lower than the highest valence level. The energy difference between the $n = 1$ states will therefore increase, so that the luminescence occurs at shorter wavelengths.

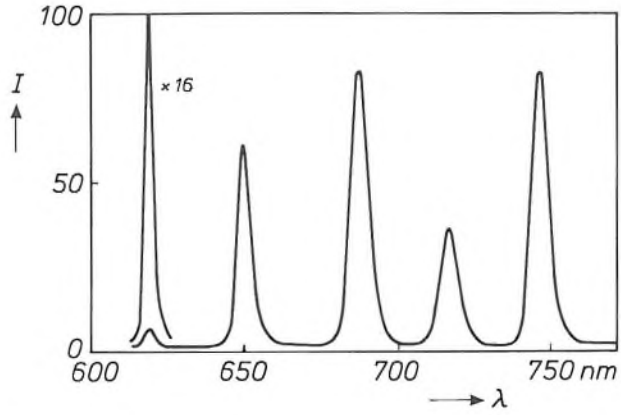

Fig. 10. Photoluminescence spectrum of a sample with five GaAs quantum wells, excited at 4 K with an argon laser emitting at 514.5 nm. The thinnest well, with an estimated thickness of only about 0.6 nm, has a weak emission peak at a very short wavelength (620 nm).

Application in lasers

The use of one or more quantum wells as the active layer permits the manufacture of separate confinement semiconductor lasers with shorter emission wavelengths, lower threshold currents, higher output power and a longer lifetime than conventional semi-

[14] P. M. Frijlink, J. P. André and J. L. Gentner, Very narrow interface multilayer III-V heterostructures by organometallic vapor phase epitaxy, J. Cryst. Growth 70, 435-443, 1984.

[15] R. M. Fleming, D. B. McWhan, A. C. Gossard, W. Wiegmann and R. A. Logan, X-ray diffraction study of interdiffusion and growth in $(GaAs)_n(AlAs)_m$ multilayers, J. Appl. Phys. 51, 357-363, 1980.

[16] See for example H. H. Brongersma, F. Meijer and H. W. Werner, Surface analysis, methods of studying the outer atomic layers of solids, Philips Tech. Rev. 34, 357-369, 1974.

[17] P. M. Frijlink and J. Maluenda, MOVPE growth of $Ga_{1-x}Al_xAs$-GaAs quantum well heterostructures, Jap. J. Appl. Phys. 21, L574-L576, 1982.

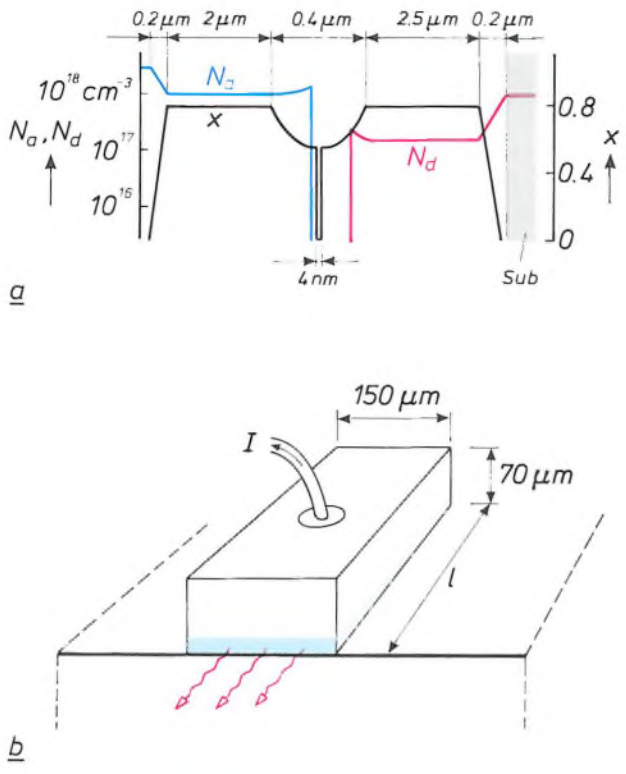

Fig. 11. *a*) Composition and doping profiles in a quantum-well laser manufactured at LEP. The quantum well consists of a 4-nm layer of pure undoped GaAs. Outside the well the Al content x increases gradually from 0.5 to 0.8. Near the substrate and the surface the Al content decreases again to zero. The barrier on one side of the quantum well is p-doped with acceptor concentration N_a (*blue*), the one on the other side is n-doped with donor concentration N_d(*red*). Both the substrate *Sub* and the surface layer are heavily doped (n^+ and p^+ respectively). *b*) Schematic structure of the laser. The laser chip has a height of 70 μm, a width of 150 μm and a length l. The chip is indium-soldered to a copper block with the epitaxial layers (*blue*) downwards. The other side is metallized with an AuGe-alloy. A current I above a threshold value generates laser emission (*red*) in the longitudinal direction.

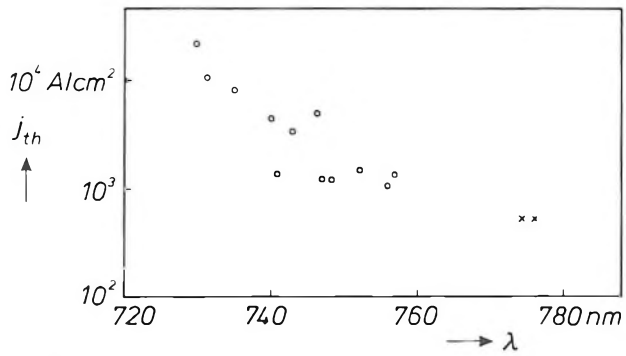

Fig. 12. Threshold current density j_{th} plotted against laser emission wavelength λ at room temperature for four-well lasers obtained from the same wafer (*circles*) and for two single-quantum-well lasers (*crosses*). The pulse duration was 2 μs with a repetition rate of 500 Hz. The shorter the emission wavelength, the higher the threshold for laser operation. No laser operation was detected below 730 nm.

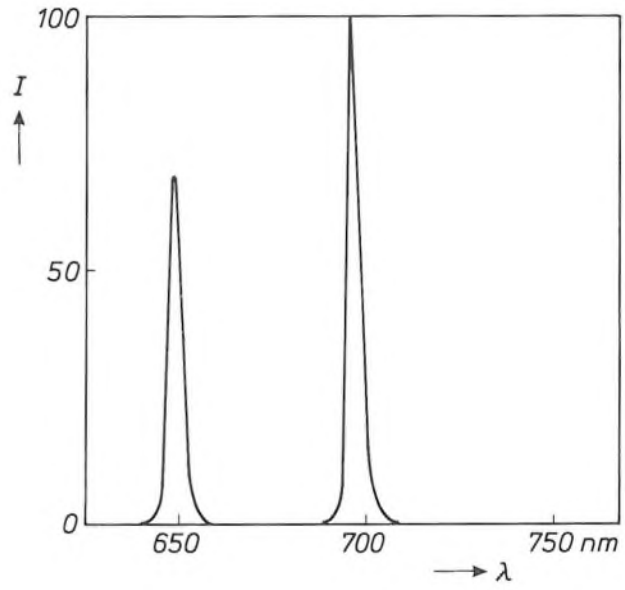

Fig. 13. Photoluminescence spectrum at 4 K on excitation with 514.5-nm argon-laser radiation of a sample containing two $Al_{0.2}Ga_{0.8}As$ quantum wells of thickness 3 and 8 nm and $Al_{0.5}Ga_{0.5}As$ barriers. The combination of a narrow well and Al incorporation gives a very short emission wavelength.

conductor lasers [18]. *Fig. 11a* shows the compositional and doping profiles of the epitaxial layers for such a laser, which consists of a single central GaAs quantum well that collects and confines electrons and holes coming from n- and p-$Al_xGa_{1-x}As$ respectively. The well is surrounded by an almost parabolic aluminium concentration profile (with x increasing from 0.5 to 0.8) of 0.2 μm on both sides, which confines the light by the gradient in the refractive index. Cladding layers of $Al_{0.8}Ga_{0.2}As$ with a low refractive index prevent coupling between the light in the central guide and the GaAs in the substrate and the top layer. To obtain good electrical contacts, a heavily n-doped GaAs substrate and a thin heavily p-doped GaAs top layer are used, and the transitions from $Al_{0.8}Ga_{0.2}As$ to GaAs at the extremities occur gradually within 0.2 μm.

After the deposition, the substrate is reduced in thickness by grinding and polishing the back, and both sides are metallized for electrical contacts. Cleaving and sawing provides individual laser chips, typically 500 by 150 μm, with the cleaved planes at the extremities acting as mirrors for obtaining optical resonance. The laser crystals are soldered, p-side down, to an indiated copper block (fig. 11*b*), which acts as a heat sink.

The threshold current for laser operation increases as the quantum well becomes thinner. In view of the thickness dependence of the emission wavelength (fig. 7) this implies that lasers with a shorter emission wavelength have a higher threshold current. *Fig. 12* shows the threshold current density as a function of the emission wavelength for quantum-well lasers with different well thicknesses [14]. No laser action was obtained for wavelengths shorter than 730 nm, prob-

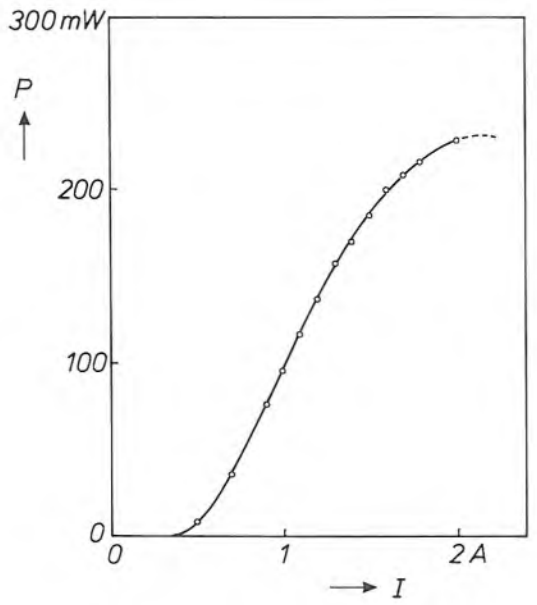

Fig. 14. Power P emitted per facet as a function of current I for a quantum-well laser of the type shown in fig. 11*b* with $l = 500$ μm, operating at room temperature and emitting at 775 nm. The threshold current is 0.50 A, corresponding to a current density of 660 A/cm^2. A maximum power of 230 mW is obtained.

ably because carrier capture becomes too inefficient for thinner wells.

The answer to this problem may be to use a large number of quantum wells, or $Al_xGa_{1-x}As$ instead of GaAs for the quantum well, which can then be thicker for the same emission wavelength. For a given thickness, the incorporation of Al in the active layer shortens the emission wavelength. *Fig. 13* shows the photoluminescence of 3-nm and 8-nm quantum wells with 20% of aluminium in the active layer. The emission wavelengths are considerably shorter than for pure GaAs wells of comparable thickness.

A laser structure that was more extensively studied, with a single quantum well and an emission at 775 nm, had a threshold current density of 530 A/cm^2 in the pulsed mode (2-μs pulses with a repetition rate of 500 Hz) and 660 A/cm^2 in CW operation. In *fig. 14* the CW light output at room temperature is plotted against the input current. The maximum available light output power per facet was about 230 mW. The cavity length was 500 μm. Still lower threshold current-density values, down to 300 A/cm^2 for a cavity length of 440 μm, were obtained using 15-nm quantum wells, emitting at 860 nm.

Modulation-doped heterostructures

Modulation-doped $Al_xGa_{1-x}As$/GaAs heterostructures have become a subject of intensive study in many laboratories. In these structures, GaAs is undoped whereas $Al_xGa_{1-x}As$ is n-doped with a typical donor concentration of between 10^{17} and 5×10^{18} cm^{-3}, except for a thin undoped layer next to the heterojunction, called a spacer layer. Owing to the difference in electron affinity and band gap between GaAs and $Al_xGa_{1-x}As$, there is a step in the conduction and valence bands at the heterojunction; see *fig. 15*. Induced electron transfer creates an electron-accumulation region on the GaAs side of the heterojunction and an electron-depletion region on the $Al_xGa_{1-x}As$ side. The potential well in the accumulation region gives quantization of the electron states in the direction perpendicular to the heterojunction. Since movement parallel to the interface remains free, a two-dimensional electron gas is formed.

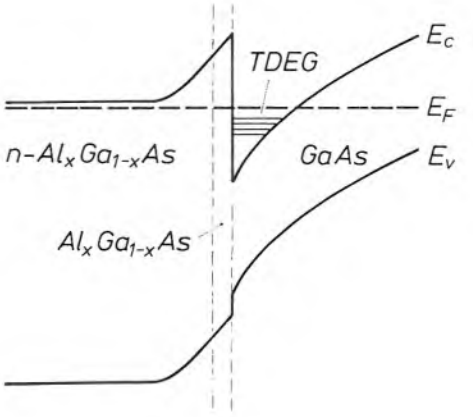

Fig. 15. Schematic energy-band structure of a modulation-doped heterostructure. E_v top of valence band; E_F Fermi level; E_c bottom of conduction band. The structure consists of an n-doped $Al_xGa_{1-x}As$ layer and an undoped GaAs layer, separated by a thin undoped $Al_xGa_{1-x}As$ layer or spacer. In the potential well on the GaAs side near the heterojunction, conduction electrons accumulate, forming a two-dimensional electron gas (*TDEG*). These electrons are spatially separated from the parent donor atoms in the n-doped layer.

The spatial separation between the accumulated electrons and the donor impurities greatly decreases the rate of impurity scattering. This results in a high electron mobility parallel to the heterojunction, which is increased at low temperatures as there is less optical phonon scattering. The combination of high electron density with high electron mobility in the accumulation region makes these structures very attractive for application in high-frequency devices.

An example of the modulation-doped heterostructures we have investigated [19] is shown in *fig. 16*.

[18] W. T. Tsang, Extremely low threshold (AlGa)As modified multiquantum well heterostructure lasers grown by molecular-beam epitaxy, Appl. Phys. Lett. **39**, 786-788, 1981;
D. R. Scifres, C. Lindström, R. D. Burnham, W. Streifer and T. L. Paoli, Phase-locked (GaAl)As laser diode emitting 2.6 W CW from a single mirror, Electron. Lett. **19**, 169-171, 1983.

[19] Investigations on modulation-doped heterostructures have also been described by J. Maluenda and P. M. Frijlink in Jap. J. Appl. Phys. **22**, L127-L129, 1983, and in J. Vac. Sci. & Technol. B **1**, 334-337, 1983.

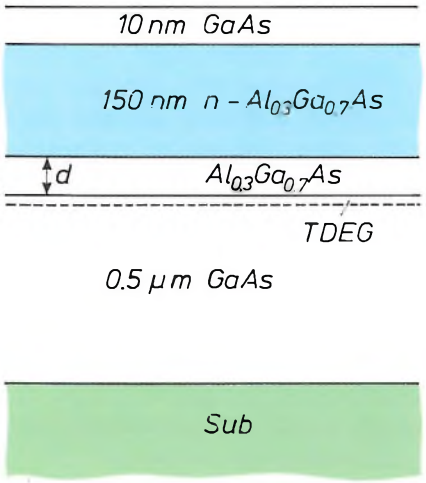

Fig. 16. Cross-section of a typical modulation-doped heterostructure on a Cr-doped semi-insulating GaAs substrate. Below the spacer of thickness d a two-dimensional electron gas (*TDEG*) is formed. The n-$Al_{0.3}Ga_{0.7}As$ layer contains 7.5×10^{17} cm^{-3} of Si atoms.

On a semi-insulating Cr-doped GaAs substrate there is a 0.5-μm non-doped GaAs layer and a 0.15-μm $Al_{0.3}Ga_{0.7}As$ layer doped with 7.5×10^{17} at. Si/cm^3, with a thin non-doped $Al_{0.3}Ga_{0.7}As$ spacer layer of variable thickness. A 10-nm cap layer of GaAs facilitates the formation of ohmic contacts. Hall measurements were made on these structures: orthogonal external electric and magnetic fields induce a voltage across the sample at right angles to both fields, and this voltage was determined. The reciprocal of this voltage is proportional to the free carrier concentration and the ratio of this to the electrical resistivity gives the electron mobility.

Results of the Hall measurements on these structures are shown in *fig. 17*. The sheet electron density and the electron mobility determined at 77 K are given as a function of the spacer thickness. The density decreases with larger spacer thickness, owing to a decreasing accumulation effect. The electron mobility has a maximum of 8×10^4 cm^{2}V^{-1}s^{-1} at a thickness of 12 nm, where the electron density is 8.3×10^{11} cm^{-2}.

The electron mobility in this structure at 77 K is determined by the scattering at residual impurities in the direct vicinity of the electrons and at intentionally incorporated donors with Coulomb fields extending into the accumulation region. A screening effect also has to be considered. Electrons tend to stay longer near positive scattering centres than elsewhere. These centres are therefore surrounded by a net negative charge, which partly screens their fields and therefore reduces the scattering. If the spacer is very thin, most of the scattering occurs at intentionally incorporated donors. With a larger thickness this scattering diminishes owing to the increasing separation between electrons and donors. This leads to a higher mobility, although the screening effect becomes weaker because of the lower electron density. With a thick spacer, scattering occurs mainly at residual impurities. The only result of an increase in thickness is then a lower electron density, so that there is less screening and hence a lower mobility.

The dependence of the electron mobility on the temperature is illustrated in *fig. 18* for one of our samples containing a 15-nm undoped spacer layer and a 45-nm n-doped layer of $Al_{0.35}Ga_{0.65}As$, with a 30-nm GaAs cap layer [14][20]. The sheet electron density was found to be 5×10^{11} cm^{-2}. At room temperature a mobility of 7.4×10^3 cm^{2}V^{-1}s^{-1} was measured. At lower temperatures, the decrease of optical

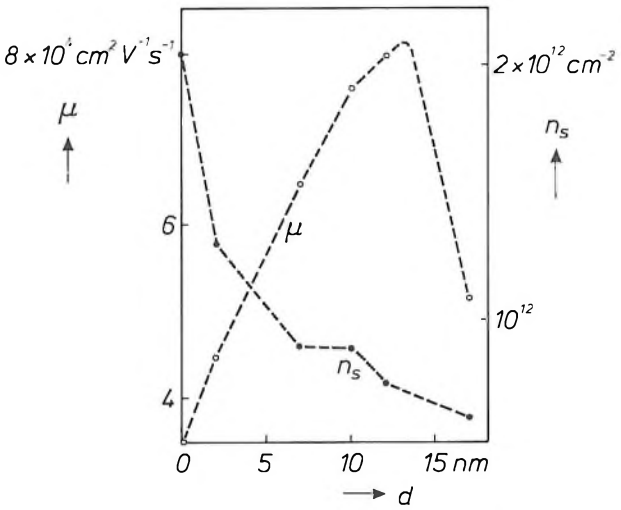

Fig. 17. Effect of spacer thickness d on the electron mobility μ at 77 K and the sheet electron density n_s, determined by Hall measurements on the modulation-doped heterostructures of fig. 16 [19]. With increasing spacer thickness the sheet electron density decreases monotonically, whereas there is a maximum in the electron mobility.

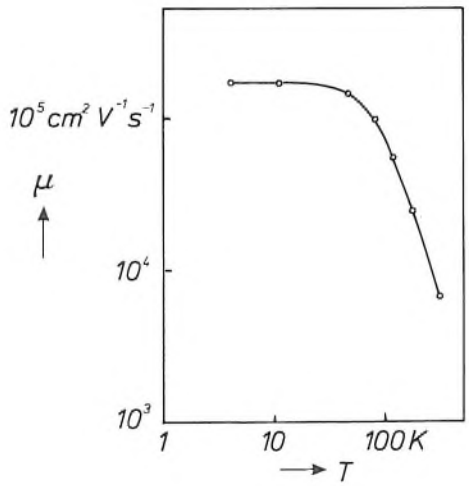

Fig. 18. Decrease in the electron mobility μ with temperature T for a modulation-doped heterostructure based on $Al_{0.35}Ga_{0.65}As$ and GaAs with a spacer thickness of 15 nm.

phonon scattering leads to markedly higher mobilities: 1.21×10^5 cm^{2}V^{-1}s^{-1} at 77 K and 1.73×10^5 cm^{2}V^{-1}s^{-1} at 4 K. The highest mobility obtained for one of our best samples was 2.7×10^5 cm^{2}V^{-1}s^{-1} at 4 K.

Application in transistors

The idea of a modulation-doped heterostructure has been used in the fabrication of a high-electron-mobility transistor (HEMT), a special type of field-effect transistor. Here the electrons are transferred between the source and drain electrodes via a very thin channel near the substrate surface. The current conductance between source and drain is modulated by the transverse electric field between the gate and the substrate. A characteristic feature of a HEMT device is that the conductance takes place in the undoped GaAs layer in the accumulation region near the heterojunction.

The technology used in the fabrication of HEMT devices is based on planar processes. Here again MO-VPE has been found to be an appropriate method for depositing the various layers. Device isolation is obtained by boron implantation. The ohmic drain and source contacts are formed by evaporated alloys of gold and germanium. Several device geometries have been considered, differing in the length and width of the gate and in the source-gate and drain-gate spacings.

The gain that can be obtained is proportional to the transconductance, i.e. the change in the drain-source current induced by a given change in the gate voltage. The transconductance can be derived experimentally by measuring the drain-source current as a function of drain-source voltage at different values of the gate voltage. In *fig. 19* the curves measured at 300 and 77 K are given for a non-optimized device in which the Al gate had a length of 100 μm and a width of 1000 μm and the source-gate and drain-gate spacings were 1 μm [19]. This particular device was in fact the first HEMT made with MO-VPE (instead of MBE), thus demonstrating the feasibility of this technique. The transconductance, determined by the distance between the curves for different gate voltages, increases markedly on going from 300 K to 77 K. This clearly demonstrates the higher electron mobility at lower temperatures.

The best values obtained so far for the transconductance are 250 S/m at 300 K and 450 S/m at 77 K. These values were measured for a HEMT device with a gate length of 1.1 μm, a gate width of 240 μm and a source-drain spacing of 4 μm. The test versions of the HEMT devices were found to have a good high-frequency performance, mainly because of the modulated doping and the small gate length. Microwave measurements indicate a noise figure of 2.1 dB with an associated gain of 5.1 dB at 12 GHz and a cut-off frequency of 30 GHz.

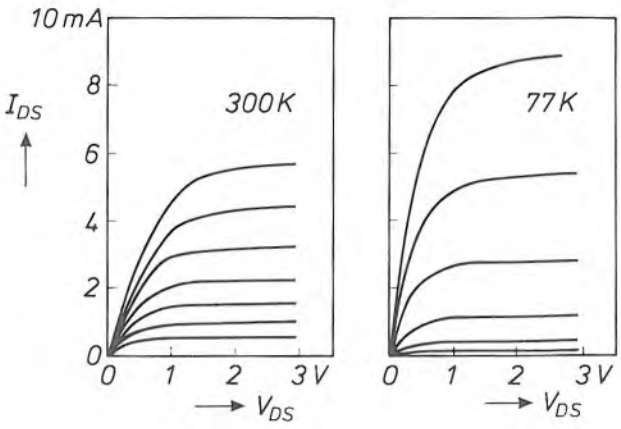

Fig. 19. Characteristic curves of drain-source current I_{DS} plotted against drain-source voltage V_{DS} for a HEMT device at 300 and 77 K, with the gate voltage varying in steps of 200 mV. The transconductance, derived from the spacings between the curves, increases threefold from 300 to 77 K.

Quantized Hall effect

An interesting effect associated with the presence of a two-dimensional electron gas in modulation-doped heterostructures is the 'quantized Hall effect'. This can be observed when the Hall voltage is measured at very low temperatures ($\lesssim$ 4 K) as a function of the

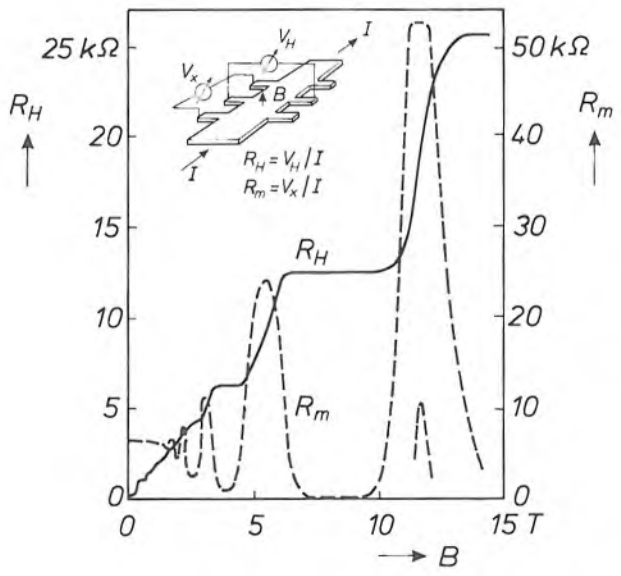

Fig. 20. Quantized Hall effect for a modulation-doped heterostructure based on $Al_{0.3}Ga_{0.7}As$ and GaAs, with a two-dimensional electron gas. The Hall resistance R_H (V_H/I) and magnetoresistance R_m (V_x/I), measured at 4 K, are given as a function of the magnetic flux density B (in the z-direction). At certain values of the flux density there is a plateau in the curve for R_H and there is a minimum for R_m.

[20] J. P. André, A. Brière, M. Rocchi and M. Riet, Growth of (Al,Ga)As/GaAs heterostructures for HEMT devices, J. Cryst. Growth 68, 445-449, 1984.

strong magnetic field. The Hall resistance R_H — the ratio between the measured Hall voltage and the electric current — does not increase linearly with the magnetic field but has a number of plateaus [21]. The resistance at these plateaus appears to be independent of the electron mobility, sample geometry and impurity concentration and is given to an accuracy of 1 in 10^8 by:

$$R_H = h/e^2 n, \qquad (10)$$

where h is Planck's constant, e the electronic charge and n an integer [22]. A plateau in the Hall resistance is associated with a minimum in the magnetoresistance.

The quantized Hall effect has been observed for several modulation-doped heterostructures grown in our Laboratories [23]. An example of the results is given in *fig. 20*, where the Hall resistance and magnetoresistance measured at 4 K are plotted against the magnetic field. The sample had a 7-nm spacer of undoped $Al_{0.3}Ga_{0.7}As$ between 500-nm undoped GaAs and 150-nm Si-doped $Al_{0.3}Ga_{0.7}As$. The value derived for the sheet carrier density in the accumulation region was 4×10^{11} cm^{-2} and the electron mobility measured at 77 K was 6×10^4 cm^{2}V^{-1}s^{-1}. The plateaus in the Hall resistance and the close correspondence with the variation in the magnetoresistance are clearly visible.

[21] The quantized Hall effect was first observed in silicon-MOS field-effect transistors, see K. von Klitzing, G. Dorda and M. Pepper, Phys. Rev. Lett. **45**, 494-497, 1980.
Shortly afterwards this effect was also observed in $Al_xGa_{1-x}As$/GaAs heterostructures, see D. C. Tsui and A. C. Gossard, Appl. Phys. Lett. **38**, 550-552, 1981.

[22] With strong pulsed magnetic fields plateaus also occur at fractions of n, see D. C. Tsui, H. L. Stormer and A. C. Gossard, Phys. Rev. lett. **48**, 1559-1562, 1982, and J. Wolter, this issue, pp. 111-117.

[23] The measurements of the quantized Hall effect were made by colleagues at Philips Research Laboratories, Eindhoven, and also at the Catholic University of Nijmegen. See for example R. E. Horstman, E. J. van den Broek, J. Wolter, R. W. van der Heijden, G. L. J. A. Rikken, H. Sigg, P. M. Frijlink, J. Maluenda and J. Hallais, Solid State Commun. **50**, 753-756, 1984;
R. Woltjer, J. Mooren, J. Wolter and J. P. André, Solid State Commun. **53**, 331-333, 1985.

Summary. Vapour-phase epitaxy with metal-organic reactants (MO-VPE) is a good method for growing multilayer structures of III-V semiconductor materials such as GaAs and $Al_xGa_{1-x}As$. Precise control of the growth parameters can give interfaces that are abrupt on an atomic scale. The quality of the interfaces and the depth profiling have been assessed by spectroscopic ellipsometry and confirmed by photoluminescence experiments on quantum wells consisting of a thin GaAs layer between two $Al_xGa_{1-x}As$ layers with a larger band gap. The emission wavelength of these wells can be varied in a controlled manner from 800 to 620 nm by decreasing the well width or incorporating aluminium in the well, or both. Laser operation has been obtained for quantum wells with emission wavelengths down to 730 nm. In modulation-doped heterostructures with GaAs and $Al_xGa_{1-x}As$ a two-dimensional electron gas is formed on the GaAs side near the heterojunction. The spatial separation of carriers and donor impurities gives high electron mobilities, particularly at low temperatures. This favours the application of such structures for obtaining transistors with a good high-frequency performance. At low temperatures the presence of a two-dimensional electron gas is responsible for the 'quantized Hall effect'.

Metal-organic vapour-phase epitaxy with a novel reactor and characterization of multilayer structures

M. R. Leys, M. P. A. Viegers and G. W. 't Hooft

Introduction

The previous article [1] explains how multilayer structures with $Al_xGa_{1-x}As$ can be grown on a GaAs substrate by metal-organic vapour-phase epitaxy (MO-VPE). The great importance of abrupt transitions in such structures prompted us to optimize the growth method to produce such transitions. A novel reactor was therefore developed that could be used to bring about very fast changes in the gas composition. Transmission-electron-microscope (TEM) investigations of the resulting structures have shown that the transition between layers of different composition can take place within approximately one monolayer. Investigations of the optical quality of the structures have shown that quantum wells consisting of a very thin GaAs layer between two $Al_xGa_{1-x}As$ layers can have a high luminescence efficiency. We have studied the temperature dependence of the radiative recombination coefficient for various quantum wells; this quantity is important for optoelectronic applications of quantum-well lasers. The measured temperature dependence and the variation with well thickness showed reasonably good agreement with calculations based on a simple model.

In this article we first describe the new reactor and the growth procedure. We then discuss the characterization by TEM, with special attention to the method of obtaining a good contrast between layers of different composition. TEM micrographs of structures that have been grown are then shown. Finally the temperature dependence of the radiative recombination coefficient in quantum wells is compared with the value in the bulk material and the consequences for laser applications are discussed.

Growth of multilayer structures with abrupt transitions

MO-VPE can be used to produce a multilayer structure on a substrate by appropriately changing the composition of the vapour phase above the substrate surface during epitaxial growth [1]. To obtain structures with abrupt transitions and very thin layers, good control of the gas composition is essential. This means that special precautions have to be taken with the design of the reactor and the processing conditions. A rapid change in the supply of the components does not necessarily produce the same rapid change near the

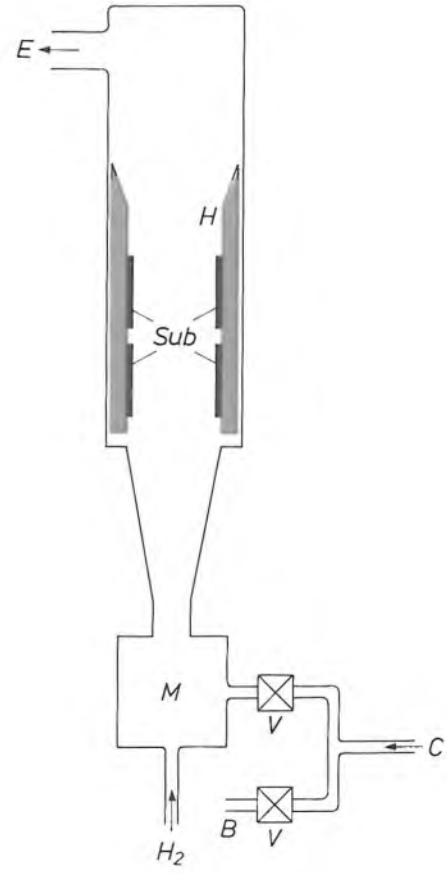

Fig. 1. Diagram of a novel reactor for MO-VPE of $Al_xGa_{1-x}As$ layers. The carrier gas (H_2) is supplied to the mixing chamber *M* at the bottom of the vertical reactor. A component *C* is admitted by a pneumatic valve *V* to the mixing chamber or switched by another valve to a bypass *B*. The substrates *Sub* are attached to the inner wall of a hollow susceptor *H*, which is heated by r.f. induction to a temperature of about 700 °C. Thin films are deposited on the substrates from the gas mixture (carrier gas plus components). *E* exhaust.

Drs M. R. Leys, formerly with Philips Research Laboratories, Eindhoven, is now with the University of Lund, Sweden; Dr M. P. A. Viegers and Dr G. W. 't Hooft are with Philips Research Laboratories, Eindhoven.

[1] P. M. Frijlink, J. P. André and M. Erman, Metal-organic vapour-phase epitaxy of multilayer structures with III-V semiconductors, this issue, pp. 118-132.

substrate surface. While the components are being transported through the reactor various recirculation effects can occur, with the result that the original fast change in the gas composition can be 'spread out' to give a gradual change in the composition in the actual structure. One important factor here is gas recirculation in the reactor; another is diffusion, especially from 'stagnant' volumes in the valves and in a boundary layer near the substrate surface. Our reactor has been designed to reduce this 'smoothing out' to a minimum [2].

The new reactor

Fig. 1 is a diagram of the new reactor used for producing multilayer structures with sharp transitions. *Fig. 2* shows part of the experimental arrangement used for producing the structures described in this article. The carrier gas (hydrogen) and the reactive components enter the vertical reactor from below after passing through a mixing chamber. The different components are supplied to the mixing chamber by separate lines (five in total). Each component enters the mixing chamber through a feed line or is switched to a bypass line. These lines have the same flow resistance, so that the transit times are the same and there are no pressure fluctuations when the valves are opened or closed. The inlet valves and the lines are purged constantly with hydrogen so that there are no stagnant volumes in the gas-feed system.

The geometry of the reactor is optimized for fast throughput of the gas mixture (carrier gas plus components). This means that the distances between inlet valves, mixing chamber and substrates are kept to a minimum. Recirculation of the gas mixture is largely eliminated by streamlining the input region, and by the vertical arrangement of the reactor. The gas mixture passes through a hollow susceptor with a rectangular internal cross-section; the substrates are attached to the inner wall of the susceptor. With this geometry the free convection — the tendency of hot (less dense) gases to rise, as in a chimney — helps rather than hinders the forced convection. This minimizes the effect of gas recirculation and reduces the thickness of the diffusion-boundary layer near the substrate surface.

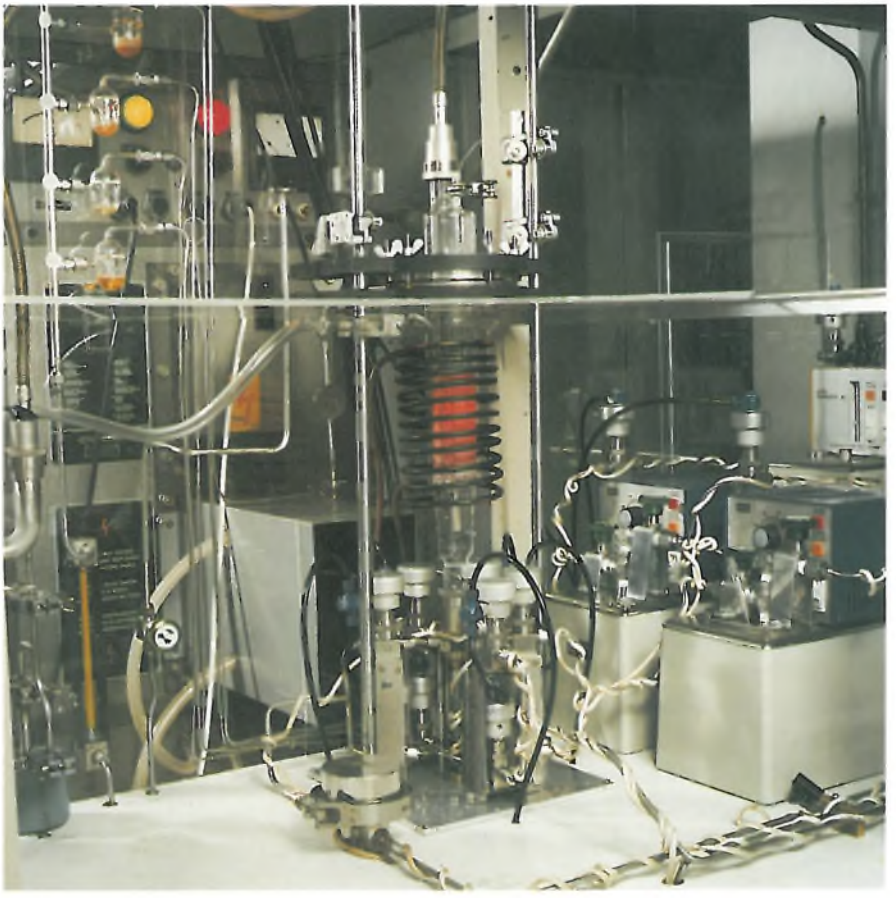

Fig. 2. Part of the experimental MO-VPE arrangement for growing layers of $Al_xGa_{1-x}As$. The reactor with gas inlet at the bottom is shown at the centre, and the valves for admitting the various components are arranged around it radially. The substrate is heated to the required temperature in the reactor by r.f. induction in the suspector. The thermostatic baths with bubbling vessels containing the metal-organic compounds are on the right.

The graphite susceptor contains two areas (each 35×70 mm^2) for positioning the substrates. It is heated by r.f. induction. The hydrogen acting as carrier gas is purified by a palladium diffusor. The system for the growth of $Al_xGa_{1-x}As$ also contains sources of the reactive components trimethyl aluminium ($Al_2(CH_3)_6$), trimethyl gallium ($Ga(CH_3)_3$) and arsine (AsH_3), as well as the reactive components for n-type or p-type doping. A microcomputer controls the supply of the various components during growth and keeps the susceptor at the correct temperature.

Growth procedure

The multilayer structures are grown on the (001) surface of a GaAs substrate. The susceptor is kept at 700 °C during the growth. The total gas flow through the reactor is 7.5 l/min and the total pressure in the reactor is 10^5 Pa (1 atm). The partial pressure of $Ga(CH_3)_3$ is 3 Pa, the partial pressure of AsH_3 is 75 Pa. Under these conditions the growth rate is 0.35 nm/s, corresponding to slightly more than one monolayer per second. The partial pressure of $Al_2(CH_3)_6$ can be varied from 0 to 12 Pa to grow $Al_xGa_{1-x}As$ layers with different compositions. The partial pressure of $Al_2(CH_3)_6$ for the growth of AlAs is 3.6 Pa.

To demonstrate how flexible the growth process is and how well the layer thickness can be controlled, we made a complicated test structure. The growth pattern of the structure is shown in *fig. 3*. At the start we grew alternate layers of GaAs and $Al_{0.55}Ga_{0.45}As$ by continuous introduction of $Ga(CH_3)_3$ and AsH_3 while alternately switching the flow of $Al_2(CH_3)_6$ from the mixing chamber to the bypass line. The first GaAs layer (called the buffer layer) and the first $Al_{0.55}Ga_{0.45}As$ layer are relatively thick; the others are extremely thin (down to about 0.7 nm grown in two seconds). Next some layers of $Al_xGa_{1-x}As$ with ascending x were grown. Before growing each layer the component supply was briefly interrupted (for about 5 s) until the partial $Al_2(CH_3)_6$ pressure had reached the appropriate value. In the final part of the growth $Ga(CH_3)_3$ and $Al_2(CH_3)_6$ were supplied alternately, to produce a quasi-superlattice, consisting of alternate 3.5-nm layers of GaAs and AlAs. Finally, a layer of AlAs and a top layer of $Al_{0.55}Ga_{0.45}As$ were grown.

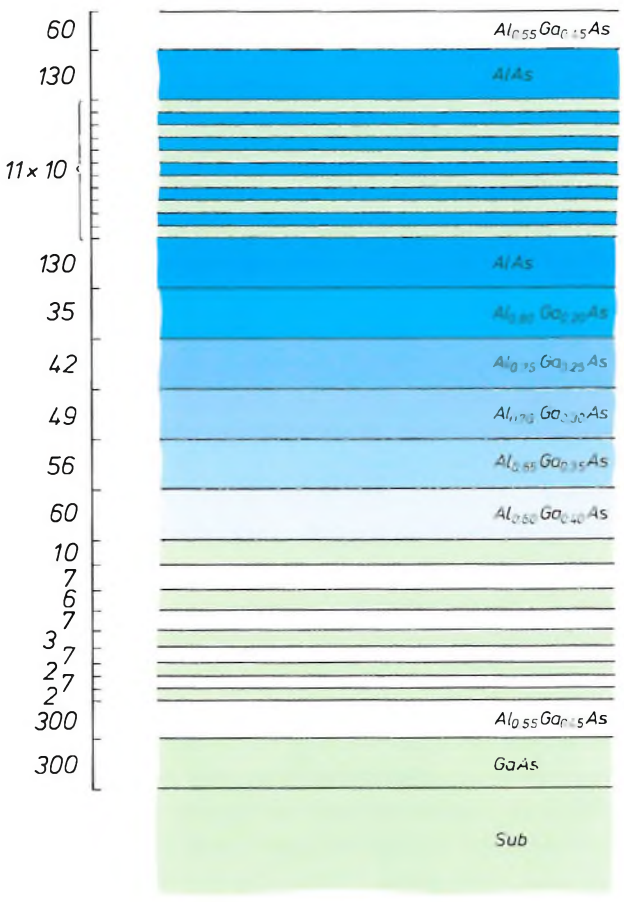

Fig. 3. Diagram of a test structure grown by MO-VPE, consisting of a large number of $Al_xGa_{1-x}As$ layers with different values of x. The growth time (in seconds) for each layer is plotted along the vertical axis. The layers and growth times are not shown to scale.

Characterization by transmission electron microscopy

It is difficult to obtain direct and unambiguous information about layer thickness and transition width in these multilayer structures. The previous article explains how luminescence spectra can be used for estimating the thicknesses of the layers and transition regions [1]. The model used, however, only applies for a direct-gap semiconductor ($Al_xGa_{1-x}As$ with $x \lesssim 0.35$) with a layer thickness between 2 and 20 nm. Analytical techniques such as Auger electron spectroscopy and secondary-ion mass spectroscopy [3] are limited by the fact that the depth resolution is no better than about 2 nm. Also, since these methods only give the composition as a function of depth, details at interfaces cannot be observed.

The method we used for characterization in our investigations was transmission electron microscopy (TEM). In principle a resolution of 0.2 nm can be obtained with TEM, so that structures can be studied on an atomic scale. The method can also reveal details with atomic dimensions at interfaces.

The basic requirement for TEM is a specimen thin enough to be transparent to electrons. This means that a multilayer structure has to be studied in cross-

[2] M. R. Leys, C. van Opdorp, M. P. A. Viegers and H. J. Talen-van der Mheen, Growth of multiple thin layer structures in the GaAs-AlAs system using a novel VPE reactor, J. Crystal Growth 68, 431-436, 1984.

[3] See H. H. Brongersma, F. Meijer and H. W. Werner, Surface analysis, methods of studying the outer atomic layers of solids, Philips Tech. Rev. 34, 357-369, 1974.

section, which requires a special technique for specimen preparation [4]. The TEM micrographs shown here were made with a Philips EM 420 ST microscope operated at 120 kV. It is possible to distinguish between layers of different composition in the structure because they diffract the electrons differently [5]. We shall now show how the composition of the layers affects the contrast in a TEM micrograph [6].

Contrast

In making a TEM micrograph of a single crystal a coherent electron beam is diffracted at the crystal planes in directions given by Bragg's law:

$$2d \sin \theta = \lambda, \tag{1}$$

where d is the distance between the planes, θ the angle between the incident beam and the planes (about 0.5°) and λ is the wavelength of the electrons. The diffracted beams are focused to form a diffraction pattern at the diaphragm in the back focal plane of the objective lens; see *fig. 4*. When the specimen is tilted so that only one set of planes exactly satisfies the Bragg relation, then apart from the transmitted beam only one other beam effectively reaches the back focal plane. An image can then be made through the aperture of a diaphragm at the back focal plane, either including the transmitted beam (bright field) or with the diffracted beam only (dark field).

Local deviations from the Bragg relation and local differences in the composition of the specimen produce a contrast (amplitude contrast) in the TEM micrograph. The multilayer structures considered here are always oriented in such a way that the Bragg condition is satisfied, so that the contrasts in the TEM photograph are a direct representation of the local differences of composition.

The amplitude of an electron beam that is diffracted from the (hkl) planes is determined by the structure factor F_{hkl}, defined as [6]:

$$F_{hkl} = \sum_{i}^{n} f_i \exp 2\pi \mathrm{j}(hx_i + ky_i + lz_i), \tag{2}$$

where n is the number of atoms in the unit cell of the crystal structure, j the imaginary unit ($\sqrt{-1}$), f_i the scattering factor of atom i, and x_i, y_i and z_i are the coordinates of this atom, expressed in fractions of the dimensions of the unit cell. For the Al and Ga atoms in $Al_xGa_{1-x}As$ the atomic scattering factors have to be weighted with the relative concentrations:

$$f_{Al/Ga} = xf_{Al} + (1 - x)f_{Ga}. \tag{3}$$

Since the scattering factor is proportional to the atomic number, f_{Al} is much smaller than f_{As} whereas f_{Ga} and f_{As} are not very different. The coordinates (x_i, y_i, z_i) of the atoms in the unit cell can be derived from the crystal structure of $Al_xGa_{1-x}As$. This corresponds to the zinc-blende structure of ZnS: the Al/Ga atoms form a cubic close-packed structure in which As atoms occupy half the number of tetrahedral interstices. *Fig. 5* shows the unit cell of $Al_xGa_{1-x}As$. The coordinates (x_i, y_i, z_i) of the atoms are:

$$\begin{aligned} &(0,0,0), (0,\tfrac{1}{2},\tfrac{1}{2}), (\tfrac{1}{2},0,\tfrac{1}{2}), (\tfrac{1}{2},\tfrac{1}{2},0) \quad \text{for Al/Ga} \\ &(\tfrac{1}{4},\tfrac{1}{4},\tfrac{1}{4}), (\tfrac{1}{4},\tfrac{3}{4},\tfrac{3}{4}), (\tfrac{3}{4},\tfrac{1}{4},\tfrac{3}{4}), (\tfrac{3}{4},\tfrac{3}{4},\tfrac{1}{4}) \quad \text{for As.} \end{aligned} \tag{4}$$

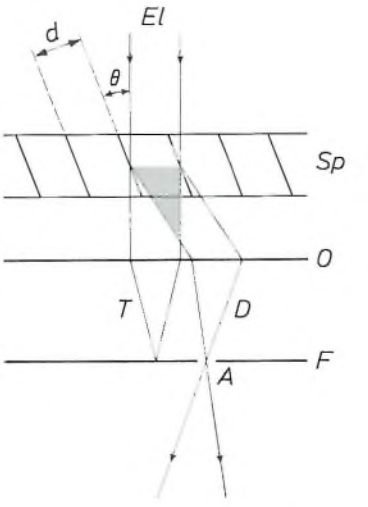

Fig. 4. Ray diagram for dark-field imaging with transmission electron microscopy (TEM). The single-crystal specimen *Sp* is oriented in such a way that the angle θ for the incident electron beam *El* only satisfies the Bragg relation given in eq. (1) for one set of planes (with spacing d). The diffracted beam *D* and the transmitted beam *T* are focused by an objective lens *O* on to the back focal plane *F*, where there is a diaphragm. The aperture *A* in the diaphragm only passes the diffracted beam. Contrasts in the micrograph are due to local deviations from the Bragg relation and local differences in composition.

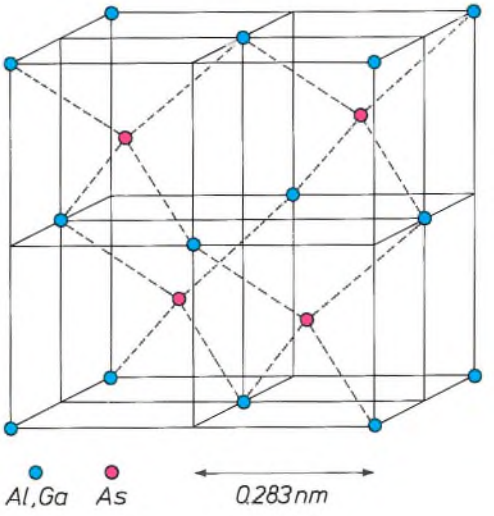

Fig. 5. Unit cell of $Al_xGa_{1-x}As$. The Al/Ga atoms form a face-centred cubic lattice: they are situated at the corners of the unit cell and at the centre-points of the six faces. The As atoms fill half the number of the available tetrahedral interstices. The coordinates of the atoms in the unit cell are given in equation (4). The lattice constant is 0.566 nm.

On substituting f_i and (x_i, y_i, z_i) in eq. (2) for different values of h, k and l it is found that the structure factor depends most strongly on x for diffraction from (002) planes [5]. In this case the structure factor is given by:

$$F_{002} = \sum_i^n f_i \exp(4\pi j z_i). \quad (5)$$

Substituting z_i from eq. (4), $f_{Al/Ga}$ from eq. (3) and f_{As}, we obtain:

$$F_{002} = 4x f_{Al} + 4(1 - x) f_{Ga} - 4 f_{As}. \quad (6)$$

With $f_{As} \approx f_{Ga}$ this becomes:

$$F_{002} \approx 4x(f_{Al} - f_{Ga}). \quad (7)$$

The composition dependence of the intensity I_{002} of the diffracted beam is then given approximately by:

$$I_{002} \propto F_{002}^2 \propto x^2. \quad (8)$$

This means that layers with a small x (for example GaAs, $x = 0$) will be dark compared with layers with a large x (for example AlAs, $x = 1$), if we make a dark-field image with I_{002} alone.

Another contribution to the contrast is connected with the number of electrons taking part in the imaging. In the presence of heavier atoms in the specimen, many electrons are scattered over such large angles that they fall outside the lens aperture. This effect is not so pronounced in specimens consisting of lighter atoms (they have less scattering power). Although this effect does not greatly enhance the contrast, it operates in the same sense as the amplitude contrast: areas with GaAs appear darker and those with AlAs appear brighter.

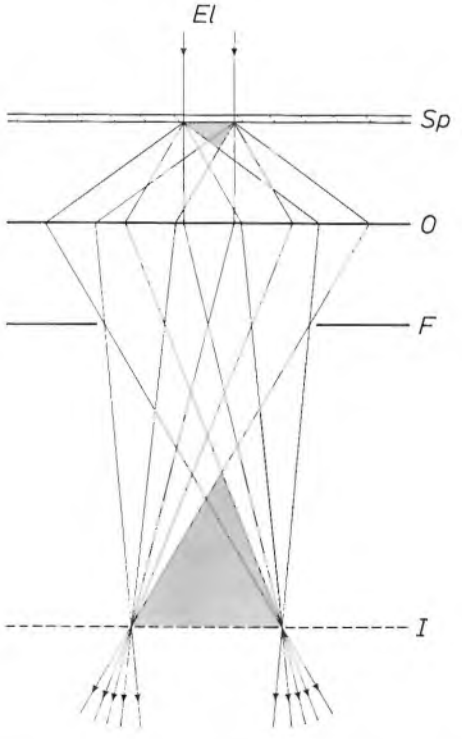

Fig. 6. Ray diagram for a high-resolution TEM micrograph. The electron beam *El* is incident on the specimen *Sp* in the direction of (say) the [110] axis. The beams produced by diffraction from the crystal planes are focused by an objective lens *O* on to the back focal plane *F*. The diffraction pattern formed by the combination of a large number of diffracted beams results in an image of the crystal lattice at the image plane *I*.

The resolution of the dark-field image is determined by the diameter of the aperture of the diaphragm in the back focal plane of the objective lens. This aperture cannot be made arbitrarily large: the maximum diameter is equal to the distance between the transmitted and the diffracted beams. This means that the resolution cannot be better than the spacing of the (002) planes; in GaAs this is 0.283 nm. In practice it is about 0.5 nm.

A higher resolution can be obtained by quite a different method, in which the electron beam is incident parallel to one of the crystal axes with a low index, e.g. the [110] axis. In this case the beam is diffracted from many crystal planes, all nearly parallel to the incident beam. An image of the crystal lattice is formed by combination of a large number of these diffracted beams, as shown in *fig. 6*. Calculation of the contrast is very complicated in this case because there are so many beams. Nevertheless, because of the difference in scattering between Al and Ga, the GaAs regions appear darker than the AlAs regions.

Results

Several TEM micrographs were made of the structure that was grown in the pattern shown in fig. 3. *Fig. 7* shows a dark-field image made with I_{002}. The different layers are easily distinguished from each other. At the top of relatively thick AlAs layers a wavy interface can be seen; the 'waves' have an amplitude of about 2 nm and a wavelength of about 100 nm. This effect has not yet been completely understood. It is probable that the interface structure is due to surface instability during growth, caused by adsorption of impurity atoms, notably oxygen and carbon. These may accumulate at 'steps' already present on the growing crystal surface. Such impurities slow down

[4] M.P.A. Viegers, A.F. de Jong and M.R. Leys, Characterization of structural features in thin layers of GaAs,Al(x)Ga($1-x$)As and AlAs by means of structure factor imaging and high resolution electron microscopy, Spectrochim. Acta **40B**, 835-845, 1985.

[5] P. M. Petroff, Transmission electron microscopy of interfaces in III-V compound semiconductors, J. Vac. Sci. & Technol. **14**, 973-978, 1977.

[6] Good books on diffraction theory for TEM include:
P. B. Hirsch, A. Howie, R. B. Nicholson, D. W. Pashley and M. J. Whelan, Electron microscopy of thin crystals, Butterworth, London 1965;
G. Thomas and M. J. Goringe, Transmission electron microscopy of materials, Wiley, New York 1979.

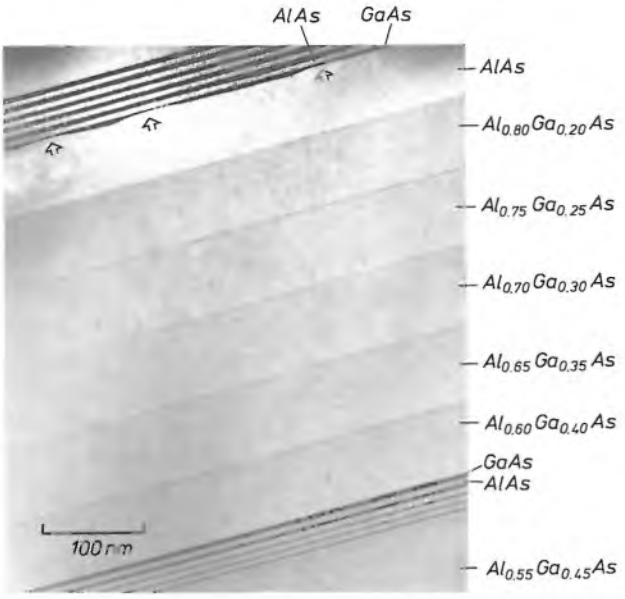

Fig. 7. TEM dark-field image, with (002) diffraction, of a multilayer structure of $Al_xGa_{1-x}As$ grown as in the diagram of fig. 3. Layers with low x (Al-poor) appear dark compared with layers with high x (Al-rich), as indicated by eq. (8). The arrows indicate undulations at the AlAs surface.

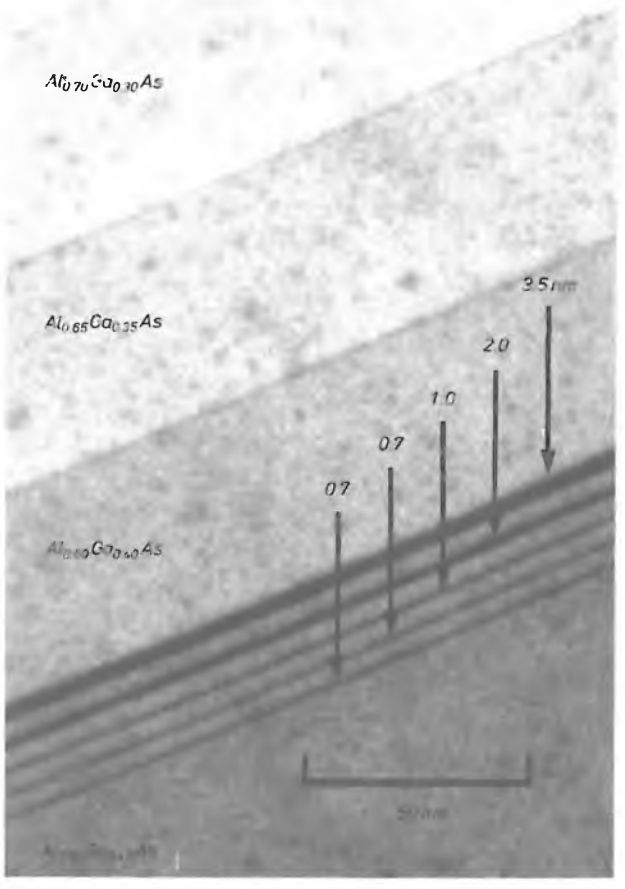

Fig. 8. TEM dark-field image, with I_{002}, of the bottom part of the multilayer structure of fig. 3. The GaAs layers (dark) have a thickness ranging from 0.7 to 3.5 nm. The $Al_xGa_{1-x}As$ layers become brighter as x increases; an increase of 0.05 is clearly visible.

the advance of a step over the surface. During the growth of 'thick' layers (> 60 nm), with prolonged adsorption of impurities, this may have the effect of disturbing the two-dimensional growth required for a planar surface. Pure GaAs is much less sensitive to oxygen and carbon than AlAs, and will therefore maintain a planar interface much more easily. It is remarkable that the growth of a thin layer of 3.5 nm of GaAs is nevertheless sufficient to produce a smooth interface on a surface with undulations 2 nm high. It appears that the flatness of a surface is largely kinetically determined, e.g. by the surface mobility and the adsorption of impurities. The flatness is therefore not determined by the abruptness of the changes in composition, which depends on the technology of the MO-VPE reactor.

The lower part of the structure is shown in more detail in *fig. 8*. The stepwise changes of 5% in the aluminium content are clearly visible in the TEM micrograph as differences in grey tone. It can also be seen that the changes in composition take place within 0.5 nm, which is approximately equal to the attainable resolution and corresponds to a transition region of one or two monolayers. In considering the minimum thickness of the GaAs layers, we have to remember that only an integral number of monolayers can be deposited. This means that the thickness of the GaAs layers must always be a multiple of half the lattice constant (0.283 nm). The thinnest layer, grown in 2 s at an average rate of 0.35 nm/s will therefore have a thickness varying in steps between 0.57 and 0.85 nm.

By combining several beams (fig. 6) a more detailed image of the structure is obtained. *Fig. 9* shows a TEM micrograph made with the electron beam incident along a [110] direction for an image of the quasi-superlattice of GaAs and AlAs (fig. 3). The structure in the micrograph bears a direct relation to the atomic order in the GaAs and AlAs layers. Each round 'spot' visible in the micrograph corresponds to a combination of a Ga (or Al) atom and an As atom; see *fig. 10*. The growth steps at the interfaces are clearly visible, especially at the transition from AlAs to GaAs. It is clear that the transition from GaAs to AlAs, and vice versa, takes place within approximately one monolayer (0.283 nm). The growth steps observed at the in-

[7] W. K. Burton, N. Cabrera and F. C. Frank, The growth of crystals and the equilibrium structure of their surfaces, Phil. Trans. R. Soc. London A 243, 299-358, 1950/51.

[8] J. H. Neave, B. A. Joyce, P. J. Dobson and N. Norton, Dynamics of film growth of GaAs by MBE from RHEED observation, Appl. Phys. A 31, 1-8, 1983.
See also the article by B. A. Joyce and C. T. Foxon, Molecular beam epitaxy of multilayer structures with GaAs and $Al_xGa_{1-x}As$, this issue, pp. 143-153.

[9] G. W. 't Hooft, M. R. Leys and H. J. Talen-van der Mheen, Temperature dependence of the radiative recombination coefficient in GaAs-(Al,Ga)As quantum wells, Superlattices & Microstructures 1, 307-310, 1985.

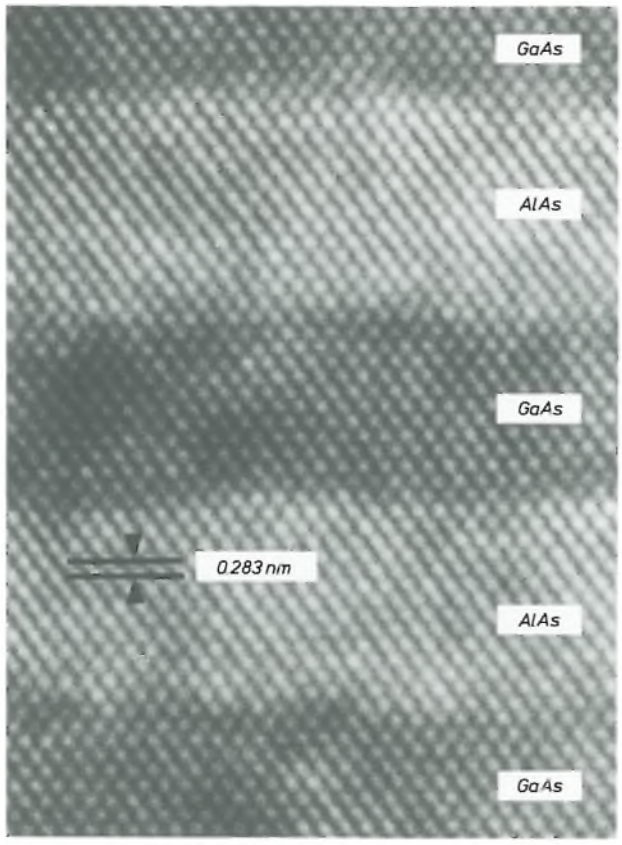

Fig. 9. TEM high-resolution micrograph, with the electron beam in a [110] direction, of part of the quasi-superlattice of GaAs and AlAs, grown as shown in fig. 3. The transition from GaAs to AlAs (and vice versa) takes place within about one monolayer. Growth steps are visible at the interfaces.

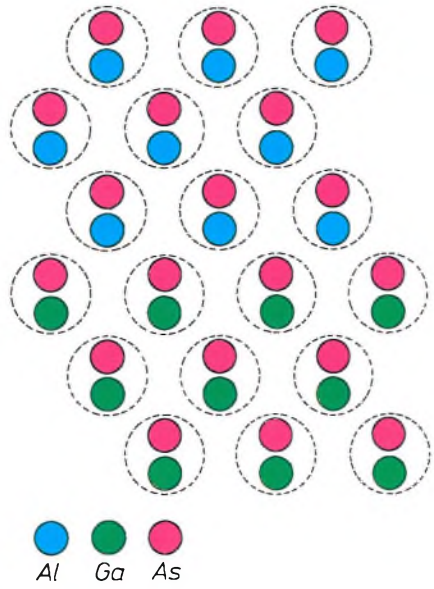

Fig. 10. Projection in the (110) plane of a structure with a GaAs layer and an AlAs layer. Dashed circles are drawn around the Ga (or Al) and As atoms that lie close together in this projection. These correspond to the round spots visible in the TEM image in fig. 9.

terfaces are due to the presence of surface islands during the (two-dimensional) growth. The occurrence of surface islands during epitaxial growth is known from crystal-growth theory [7] and has also been demonstrated in the growth of GaAs with MBE [8].

Temperature dependence of the radiative recombination coefficient in quantum wells

The reactor described in this article can be used for the fabrication of quantum-well lasers of the type described in the previous article [1]. Under optimum growth conditions it is possible to obtain quantum wells that have a high value of the luminescence efficiency, defined as the number of emitted photons divided by the number of injected charge carriers. A high efficiency means that the probability of a spontaneous radiative electron-hole recombination, given by the coefficient B, is large compared with the probability of non-radiative transitions. The dependence of these probabilities on temperature is of practical importance for optoelectronic devices. In general, the coefficient B decreases with increasing temperature whereas the probability of non-radiative transitions increases. This leads to a fall in the luminescence efficiency and increases the threshold current for laser operation at higher temperatures.

Theoretically, B is less strongly dependent on the temperature in a quantum well than in the bulk material; this has an advantageous effect on the luminescence efficiency and on the threshold current for laser operation when quantum wells are incorporated as the active layer. We have studied the temperature dependence of B experimentally by measuring the luminescence decay times at different temperatures [9]. The measurements were performed on bulk GaAs and on quantum wells, which have such a high efficiency at these temperatures that, as a first approximation, the effect of non-radiative transitions can be neglected. Before looking at the results, we shall first show, in simple theoretical terms, how the temperature dependence of B in a quantum well differs from that in the bulk material [9].

Theory

The radiative recombination coefficient B is defined as:

$$B = L/np, \tag{9}$$

where L is the photon generation rate (number of photons per unit time and per unit volume) and n and p are the concentrations of electrons and holes in the conduction and valence bands, respectively. To establish the temperature dependence we assume that holes

of only one type are present in the valence band. The values of n, p and L are determined by the densities of states ϱ_e and ϱ_h and by their occupation probabilities f_e and f_h in the conduction and valence bands [10]:

$$n = \int_{E_c}^{\infty} \varrho_e f_e \, dE_e, \tag{10}$$

$$p = \int_{-\infty}^{E_v} \varrho_h (1 - f_h) \, dE_h, \tag{11}$$

$$L \propto \int_{E_g}^{\infty} \varrho_{red} f_e (1 - f_h) \, d(E_e - E_h), \tag{12}$$

where E_e is the energy of an electron in the conduction band with minimum energy E_c and E_h is the energy of a hole in the valence band with maximum energy E_v; see *fig. 11*. In eq. (12) E_g is the band gap $(E_c - E_v)$ and ϱ_{red} is the reduced density of states for electron-hole pairs:

$$\varrho_{red} = \tfrac{1}{2}(\varrho_e^{-1} + \varrho_h^{-1})^{-1}. \tag{13}$$

The occupation probabilities f_e and f_h depend on temperature in accordance with Fermi-Dirac statistics. At low concentrations of conduction electrons and holes, approximate values of f_e and f_h are given by Boltzmann's formula:

$$f_e = \exp\{(E_{F,e} - E_e)/kT\}, \tag{14}$$

$$f_h = 1 - \exp\{(E_h - E_{F,h})/kT\}, \tag{15}$$

where $E_{F,e}$ and $E_{F,h}$ are the 'quasi-Fermi energies' for electrons and holes.

The difference in the temperature dependence of the radiative recombination coefficient B for a quantum well and for bulk material can be traced back to the differences in ϱ_e and ϱ_h. In bulk GaAs the conduction and valence bands are a parabolic function of the wave number k (fig. 11). For a conduction electron this means that the energy E_e is given by:

$$E_e = E_c + \frac{h^2 k^2}{8\pi^2 m_e}, \tag{16}$$

where h is Planck's constant and m_e is the effective electron mass. The number of energy levels at E_e in an interval dE_e is equal to the number of k-states in the corresponding interval dk. This number is proportional to the contents of a spherical shell in the k-space (hence proportional to $k^2 dk$), so that:

$$\varrho_e \propto k^2 dk/dE_e. \tag{17}$$

Since it follows from eq. (16) that k is proportional to $(E_e - E_c)^{\frac{1}{2}}$ it is clear that:

$$\varrho_e \propto (E_e - E_c)^{\frac{1}{2}}. \tag{18}$$

In the same way we find:

$$\varrho_h \propto (E_v - E_h)^{\frac{1}{2}}, \tag{19}$$

and taking account of the k-selection rule (conservation of momentum) in the recombination:

$$\varrho_{red} \propto (E_e - E_h - E_g)^{\frac{1}{2}}. \tag{20}$$

Substituting eqs (14) and (18) in eq. (10) gives:

$$n \propto \int_{E_c}^{\infty} (E_e - E_c)^{\frac{1}{2}} \{\exp(E_{F,e} - E_e)/kT\} \, dE_e. \tag{21}$$

If we put $\varepsilon = (E_e - E_c)/kT$, we obtain:

$$n \propto (kT)^{\frac{3}{2}} \exp\{(E_{F,e} - E_c)/kT\} \int_0^{\infty} \varepsilon^{\frac{1}{2}} \exp(-\varepsilon) \, d\varepsilon. \tag{22}$$

The integral here is independent of temperature, so that the temperature dependence of n is given by:

$$n \propto T^{\frac{3}{2}} \exp\{(E_{F,e} - E_c)/kT\}. \tag{23}$$

In the same way we find:

$$p \propto T^{\frac{3}{2}} \exp\{(E_v - E_{F,h})/kT\}, \tag{24}$$

$$L \propto T^{\frac{3}{2}} \exp\{(E_v - E_c + E_{F,e} - E_{F,h})/kT\}. \tag{25}$$

When eqs (23), (24) and (25) are substituted in eq. (9)

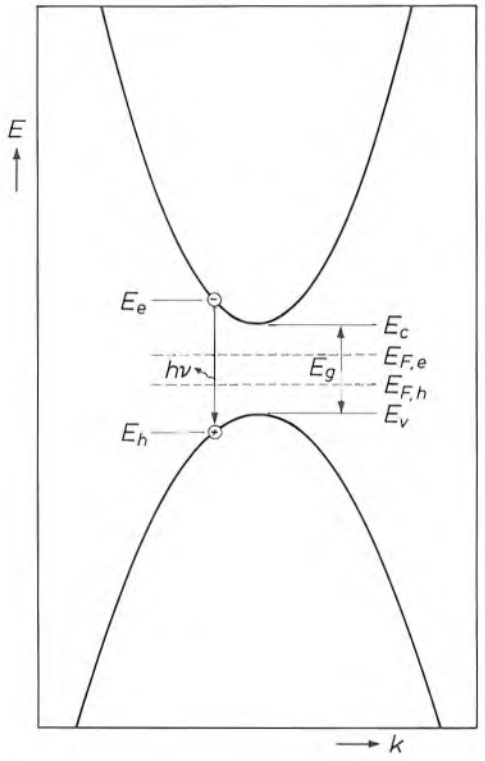

Fig. 11. Parabolic variation (schematic) of the energy E of the electrons in GaAs, as a function of the wave number k (momentum). GaAs is a direct-gap semiconductor: the minimum E_c of the conduction band and the maximum E_v of the valence band lie at about the same value of k. The difference between E_c and E_v is the band gap E_g. $E_{F,e}$ and $E_{F,h}$ are the quasi-Fermi energies for electrons and holes, respectively. A photon is generated when an electron (with energy E_e) in the conduction band recombines with a hole (energy E_h) in the valence band. This recombination must comply with the selection rule that the electron and the hole should have the same value of k (conservation of momentum).

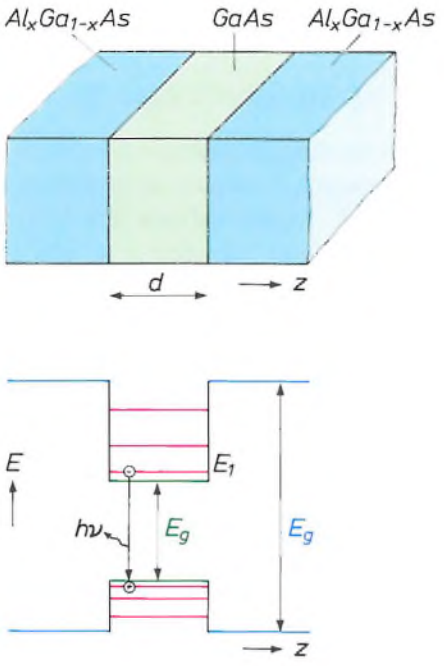

Fig. 12. Diagram of a quantum well consisting of a GaAs layer (thickness d) between two $Al_xGa_{1-x}As$ layers with a larger band gap E_g. The layers are grown in the z-direction on a GaAs substrate. In a very thin GaAs layer the movements of electrons and holes in the z-direction correspond to discrete levels with energy differences that are much greater than the thermal energy kT. The electrons and holes produce photons on recombination. Almost all the electrons have the energy of the lowest conduction level (E_1) and almost all the holes have the energy of the highest valence level, in addition to the thermal energy for free movement parallel to the interfaces.

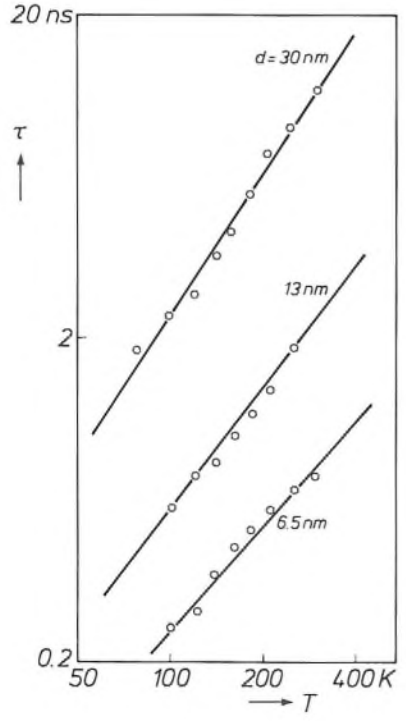

Fig. 13. Log-log plots of the luminescence decay time τ against the absolute temperature T, for three quantum wells of GaAs (thickness d) between two layers of $Al_{0.33}Ga_{0.67}As$. The exponent of the temperature dependence can be derived from the slopes of the lines.

the exponential factors cancel, so that the temperature dependence of the radiative recombination coefficient B_b in bulk GaAs is given by:

$$B_b \propto T^{-\frac{3}{2}}. \tag{26}$$

In a quantum well, consisting of a thin layer of GaAs between two layers of $Al_xGa_{1-x}As$, with a larger band gap, discrete energy levels exist for the electron movements perpendicular to the interfaces [1]; see *fig. 12*. At these levels the increase in the density of states ϱ_e with energy then takes place in steps. For a very thin well the energy difference between these levels is much greater than kT, so that almost all the electrons occupy the lowest level at energy E_1. The density of states may then be assumed to be constant over the energy range where the occupancy f_e has a reasonable value, so that eq. (10) becomes:

$$n \propto \int_{E_1}^{\infty} \exp\{(E_{F,e} - E_e)/kT\}\, dE_e. \tag{27}$$

After substituting $\varepsilon = (E_e - E_1)/kT$, we then find for the temperature dependence:

$$n \propto T \exp\{(E_{F,e} - E_1)/kT\}. \tag{28}$$

The pre-exponential factor here is now T^1 instead of $T^{\frac{3}{2}}$, as in eq. (23). The same applies for p and L with respect to equations (24) and (25). Since the exponential factors are eliminated again on substituting in eq. (9), it follows that the temperature dependence of the radiative recombination coefficient B_q in a quantum well is given by:

$$B_q \propto T^{-1}. \tag{29}$$

As the well thickness increases the energy levels come closer together, so that the densities of states may no longer be assumed to be constant and the temperature dependence of B_q will change from T^{-1} to $T^{-\frac{3}{2}}$.

Experimental results

The temperature dependence of B can be determined experimentally by measuring the decay time τ of the luminescence. This is given by:

$$\tau^{-1} = Bn_0 + \tau_{nr}^{-1}, \tag{30}$$

where n_0 is the concentration of the majority carriers and τ_{nr}^{-1} is the probability of non-radiative transitions. If the luminescence efficiency is high, the second term can be neglected, so that τ^{-1} at constant n_0 has the same temperature dependence as B.

The measurements of τ were made for quantum wells of GaAs between $Al_{0.33}Ga_{0.67}As$, grown by MO-VPE with the reactor described here, producing

[10] See for example C. Kittel, Introduction to solid state physics, 4th edition, Wiley, New York 1971.

transition regions of one or two monolayers. *Fig. 13* shows a log-log plot of the measured values of τ against temperature for three wells of different thicknesses. In all three cases a reasonably straight line is found, so that $\tau \propto T^a$. The value of a corresponding to the slope is 1.07 for a thickness d of 6.5 nm, 1.22 for $d = 13$ nm and 1.41 for $d = 30$ nm. There is therefore good qualitative agreement with the predicted temperature dependence as a function of the layer thickness. A quantitative interpretation of the results is difficult because the variation of the energy levels with layer thickness is not accurately known.

Because of the smaller temperature dependence of τ in a quantum well the threshold current I_{th} for laser operation is also less dependent on temperature. In the ideal case ($\tau_{nr}^{-1} = 0$, no non-radiative processes) the value of I_{th} is determined solely by τ, so that the temperature dependence is given by:

$$I_{th} \propto T^a. \tag{31}$$

Usually an empirical relation is used to represent the temperature dependence of the threshold current:

$$I_{th} \propto \exp(T/T_0), \tag{32}$$

where the value of T_0 characterizes the temperature behaviour. From equations (31) and (32) it can be shown that:

$$I_{th}\,(\mathrm{d}I_{th}/\mathrm{d}T)^{-1} = T/a = T_0. \tag{33}$$

For a conventional semiconductor laser at room temperature a is about 1.5, so that the maximum value of T_0 is about 200 K. In an ideal quantum well with high luminescence efficiency the value of a may approach 1, so that T_0 is about 300 K. The smaller increase in threshold current with temperature will lengthen the life of quantum-well lasers.

In the work described here Ing. H. J. Talen-van der Mheen took part in the growth experiments and C. W. T. Bulle-Lieuwma and Drs A. F. de Jong contributed to the TEM investigations.

Summary. A novel type of reactor has been developed for making MO-VPE multilayer structures, in which very sharp transitions can be obtained between layers of different composition. The perfection of the structures produced is very well demonstrated by means of transmission electron microscopy. It is demonstrated for instance that the transition regions are no thicker than approximately one monolayer. The optical quality of the quantum wells is determined by measuring the decay time of the luminescence. It appears that the decay time in quantum wells is less dependent on temperature than in bulk material, so that the threshold current for laser operation is also less temperature-dependent.

Molecular beam epitaxy of multilayer structures with GaAs and $Al_xGa_{1-x}As$

B. A. Joyce and C. T. Foxon

Introduction

As indicated in the opening article of this issue [1], thin epitaxial films of some III-V semiconductors have properties which are important in high-frequency and optoelectronic applications. Such films can be prepared by conventional growth techniques such as liquid-phase epitaxy (LPE) or vapour-phase epitaxy (VPE). For particular applications it may be advantageous to use metal-organic vapour-phase epitaxy (MO-VPE), discussed in the previous articles [2][3], or molecular beam epitaxy (MBE) [4].

MBE is a refined form of ultra-high vacuum evaporation. In this technique thermally generated collision-free molecular (or atomic) beams of the constituent elements, formed in Knudsen sources, are deposited on a heated substrate where they react to form an epitaxially related crystalline film. Growth temperatures are usually somewhat lower than those used in the more conventional growth techniques, while growth rates are in the range 0.01 to 1 nm/s. Because the molecular beam fluxes can be started or stopped rapidly using a simple mechanical shutter, atomically abrupt interfaces can be obtained. Using *in situ* analysis it is possible to measure directly the intensity of the various molecular beams and as a result films of high crystalline quality with precise control of the thickness, composition and doping level can be obtained. Changes in composition and doping level on an atomic scale facilitate the formation of well-defined multilayer structures with special properties [5].

The growth of III-V semiconductor films by MBE has been studied extensively at Philips Research Laboratories in Redhill, England. This study included the preparation of various types of III-V compounds and layered structures, investigation of the mechanisms controlling the growth and dopant incorporation, characterization of surfaces and interfaces, measurements of film or layered-structure properties and the improvement of the MBE equipment. The film properties have been studied *in situ* using non-destructive surface analysis. The III-V semiconductors grown by MBE have included mainly the binary compound GaAs and the related ternary alloy $Al_xGa_{1-x}As$ but some work has also been carried out both on the fundamental properties controlling growth and on measurements of film properties for other alloys such as InGaAs, InGaP, GaAsP, InAsP and InGaAsP. In all cases single-crystal films were grown epitaxially on GaAs or for InGaAs on InP.

The progress of MBE technology has led to films and multilayer structures having adequate quality for device applications. Background donor and acceptor levels can be as low as 2×10^{14} cm^{-3}. In a hetero-structure of GaAs and $Al_xGa_{1-x}As$ a two-dimensional electron gas is formed in the GaAs material near the interface, showing extremely high electron mobilities at low temperatures: $> 3 \times 10^6$ cm^{2}V^{-1}s^{-1} at 4 K. With structures of GaAs between $Al_xGa_{1-x}As$ barriers multiple quantum-well lasers have been grown in which the GaAs wells are as thin as 1.3 nm, corresponding to about five monolayers of material. At

Dr B. A. Joyce and Dr C. T. Foxon are with Philips Research Laboratories, Redhill, Surrey, England.

[1] J. Wolter, Research on layered semiconductor structures, this issue, pp. 111-117.
[2] P. M. Frijlink, J. P. André and M. Erman, Metal-organic vapour phase epitaxy of multilayer structures with III-V semiconductors, this issue, pp. 118-132.
[3] M. R. Leys, M. P. A. Viegers and G. W. 't Hooft, Metal-organic vapour phase epitaxy with a novel reactor and characterization of multilayer structures, this issue, pp. 133-142.
[4] See for example: L. L. Chang, L. Esaki, W. E. Howard, R. Ludeke and G. Schul, Structures grown by molecular beam epitaxy, J. Vac. Sci. & Technol. **10**, 655-662, 1973;
A. Y. Cho and J. R. Arthur, Molecular beam epitaxy, Progr. Solid State Chem. **10**, 157-191, 1975.
[5] A. C. Gossard, P. M. Petroff, W. Wiegmann, R. Dingle and A. Savage, Epitaxial structures with alternate-atomic-layer composition modulation, Appl. Phys. Lett. **29**, 323-325, 1976.
See also: G. H. Döhler, Solid-State superlattices, Sci. Am. **249** (No. 5), 118-126, 1983;
D. W. Shaw, Advanced multilayer epitaxial structures, J. Cryst. Growth **65**, 444-453, 1983.

this well width a visible laser emission is obtained at 704 nm [6]. To our knowledge this is the shortest wavelength reported for a room-temperature injection laser with only GaAs in the wells.

In this article the discussion on MBE will be restricted to certain aspects of the growth of GaAs and $Al_xGa_{1-x}As$. Among the III-V compounds and alloys these materials are the most widely investigated and the most promising for practical devices. Before dealing with some results of our investigations a general description of the MBE process will be given. The results to be discussed concern the surface chemistry of growth, the control of the $Al_xGa_{1-x}As$ composition and the growth dynamics. Special attention will be given to the interface between GaAs and $Al_xGa_{1-x}As$ films. Finally some properties and possible applications will be discussed.

The MBE process

It will be useful to define at the outset the important features of the MBE process in terms of the apparatus used, process parameters and source materials [7].

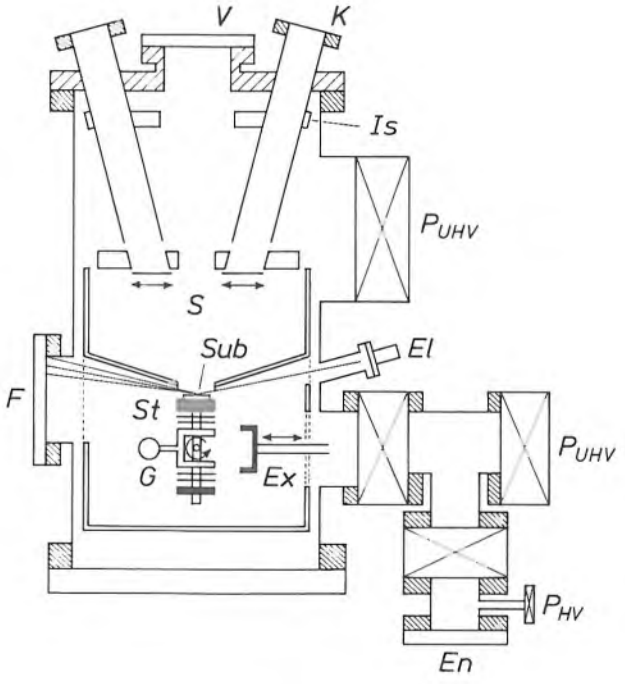

Fig. 1. Schematic diagram of an MBE system showing the essential features required for the growth of III-V compound semiconductor films. Atomic or molecular beams of the film constituents are produced in the heated Knudsen effusion cells *K*. By opening the shutters *S* the beams are directed to the heated substrate *Sub* on the stage *St*, which can be rotated. The beam fluxes are monitored by the ion gauge *G*. Substrates are introduced via a sample entry lock *En* and a sample exchange mechanism *Ex*. A RHEED system consisting of an electron gun *El* and a fluorescent screen *F* is used to study the substrate surface before growth and the film surface during growth. Other facilities for *in situ* analysis such as a quadrupole mass spectrometer and an Auger electron spectrometer are not shown. *Is* water-cooled thermal isolator. P_{HV} pump for obtaining intermediate vacuum. P_{UHV} pump for obtaining ultra-high vacuum. *V* view port.

Although MBE is simply a refined form of vacuum evaporation in which directed neutral thermal atomic and molecular beams impinge on a heated substrate under ultra-high vacuum conditions, the apparatus required to achieve this with the necessary degree of control has become rather complex. The essential elements of a system suitable for growth of III-V compound films are illustrated schematically in *fig. 1*. It is based on a two- or three-chamber stainless-steel ultra-high-vacuum system ($< 10^{-9}$ Pa), usually ion-pumped or cryopumped, and incorporates large areas of liquid-nitrogen-cooled panels. The provision of a vacuum interlock, to enable the substrate to be introduced into the growth chamber without breaking the vacuum, is essential if films having high-quality electrical and optical properties are to be prepared.

The atomic or molecular beams are formed in heated Knudsen effusion cells. An example of such a cell is shown in *fig. 2*. The material to be evaporated is contained in a crucible, which is heated by radiation from a separate winding. In the cell we attempt to ensure that the liquid or solid phase and the vapour are in equilibrium (Knudsen evaporation). The mean free path of the vapour (atoms or molecules) is much

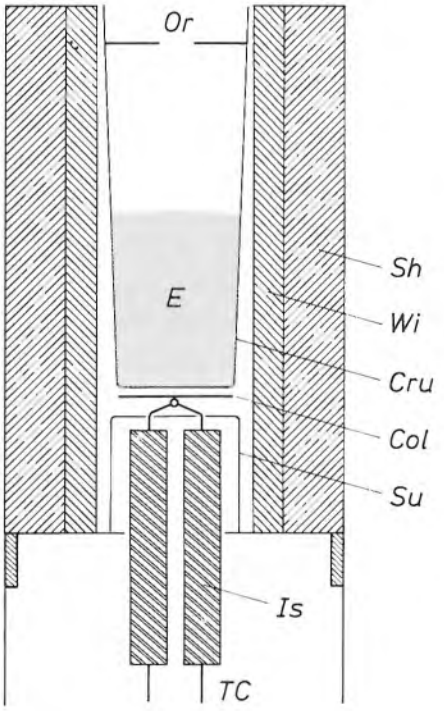

Fig. 2. Schematic diagram of a typical Knudsen effusion cell, acting as source of the Group III element (Ga or Al) for the MBE growth of III-V-films. The evaporation source *E* is contained in a crucible *Cru* of boron nitride. The heater winding *Wi* is surrounded by heat-shields *Sh* of tantalum. The beam of evaporated particles leaves the cell through the orifice *Or*. The temperature is read by a thermocouple *TC* passing through the insulators *Is* and connected to a radiation collector *Col* of tantalum. *Su* thermocouple support of boron nitride.

larger than the cell orifice, ensuring molecular flow. The inner crucible is made either of reactor-grade graphite or, preferably, pyrolytic boron nitride, so that the possible contamination of the molecular beams is minimized. Beam intensities are controlled by the cell temperatures and for molecular flow are given by [7]:

$$J_i = \frac{a p_i \cos\theta}{\pi d^2 (2\pi m_i kT)^{\frac{1}{2}}},$$

where J_i is the flux per unit area at a distance d from the source, which has an orifice of area a and contains atoms (molecules) of mass m_i having an equilibrium vapour pressure p_i at temperature T (in K). θ is the angle between the beam and the substrate surface normal. Individual cells are thermally isolated by a succession of heat shields and the flux is regulated by a shutter operating in front of each aperture. A single microcomputer can be used to control all of the cell temperatures (within $\pm$ 0.25 K) and all of the shutters to achieve any growth sequence.

Fluxes are usually monitored by an ion gauge which can be rotated in and out of the beams. Other analytical facilities may include a quadrupole mass spectrometer for residual gas analysis and leak-checking [8], and a reflection high-energy electron diffraction (RHEED) arrangement for assessment of surface structure [9]. Additionally there may be an Auger electron spectrometer to determine surface composition and purity [10]. Some or all of these facilities may be housed in a separate analysis/preparation chamber mounted between the sample-insertion interlock and the growth chamber. A general view of the equipment used for our MBE experiments is shown in *fig. 3*.

A RHEED arrangement consists simply of a 5-20 keV electron gun and a fluorescent screen. The electron beam is incident at a very shallow angle (1° – 3°) to

Fig. 3. General view of the MBE equipment (Varian GEN II) at the Philips Research Laboratories in Redhill. The growth occurs in the vacuum chamber on the left by effusing molecular beams from the tubular Knudsen cells. The growth rates for GaAs and $Al_xGa_{1-x}As$ can be deduced from RHEED intensity variations measured in the growth chamber. The vacuum system on the right is used for the introduction and preparation of substrates.

[6] K. Woodbridge, P. Blood, E. D. Fletcher and P. J. Hulyer, Short wavelength (visible) GaAs quantum well lasers grown by molecular beam epitaxy, Appl. Phys. Lett. **45**, 16-18, 1984.

[7] Various MBE aspects have been extensively reviewed by K. Ploog, Molecular beam epitaxy of III-V compounds, in: H. C. Freyhardt (ed.), Crystals — growth, properties and applications, Vol. 3, Springer, Berlin 1980, pp. 73-162. A review more directly related to the work described in this article has been given by C. T. Foxon, Molecular beam epitaxy, Acta Electron. **21**, 139-150, 1978.

[8] In a quadrupole mass spectrometer the ions formed in the ionizer are mass-separated using r.f. and d.c. fields generated by four electrodes.

[9] The importance of *in situ* RHEED studies in the MBE development has been demonstrated by (for example):
A. Y. Cho, J. Appl. Phys. **41**, 2780-2786, 1970, and **42**, 2074-2081, 1971, and by J. H. Neave and B. A. Joyce, J. Cryst. Growth **44**, 387-397, 1978.

[10] A survey of various surface-analysis methods, including electron diffraction and Auger electron spectroscopy has been given by H. H. Brongersma, F. Meijer and H. W. Werner, Surface analysis, methods of studying the outer atomic layers of solids, Philips Tech. Rev. **34**, 357-369, 1974.

the substrate surface. The diffracted electron beams form a characteristic pattern on the fluorescent screen, which provides information on the morphology and the symmetry of the surface. Because of the small incidence angle the information obtained in RHEED is derived from the first few atomic layers. Temporal variation in the intensity of diffraction features during MBE growth can be related to growth dynamics.

Since the atomic or molecular beams are neutral and collimated they are necessarily divergent, and usually non-axial with respect to the substrate. To obtain uniform growth rate or composition (in the case of alloy films) over a large substrate (diameter 5 to 8 cm), the substrate stage is rotated at speeds between 0.03 and 2.0 Hz. It was shown that with this technique a growth-rate variation of $< 1\%$ could be obtained across a 5-cm substrate, with comparable control of alloy composition [11]. For alloy growth, however, the time taken for a complete revolution must be shorter than the time to grow a monolayer, to avoid a periodic modulation of alloy composition in the direction of growth.

To provide the basis of high-quality films, a substrate surface free of crystallographic and other defects and clean on an atomic scale ($\lesssim$0.01 monolayer of impurities) must be prepared. This usually involves free etching by an oxidative process which removes any carbon and leaves the surface covered with a protective volatile oxide, which is subsequently removed in the vacuum system by heating in a beam of arsenic. The final quality of the substrate surface can be checked by RHEED and Auger spectrometry, for example.

Growth is initiated by bringing the substrate to the appropriate temperature (typically in the range 500-700 °C) in a beam of arsenic and then opening the shutter of the Group III element source. Growth rates are in the range 0.03-3 nm/s (0.1-10.0 μm/h), corresponding to beam fluxes from 5×10^{13} to 5×10^{15} at. $cm^{-2}s^{-1}$. The arsenic flux is typically 3-5 times greater than that of the Group III element, but it is the latter which determines the growth rate.

Source materials are usually elemental, and all of the Group III elements produce monoatomic beams. The arsenic source is rather more complex, however, both in terms of the species produced and the methods used to produce them. When evaporation takes place directly from the element, the flux consists entirely of tetratomic molecules (As_4), but if GaAs is used as the source, the arsenic flux is dimeric [12]. Alternatively, dimers can be produced from the element by using a two-zone Knudsen cell in which a tetramer flux is formed conventionally and passed through an optically baffled high temperature stage, which can be designed to produce a complete conversion to a dimeric flux [13].

Dopant beams are also produced from Knudsen effusion cells. The elements used for doping in MBE are principally Be for the preparation of p-type films and Si or Sn for the preparation of n-type films. All these elements evaporate as monomers. Free-carrier concentrations can be controlled over the range between 10^{14} and 10^{19} carriers per cm^3. The upper limit is set by the limited solid solubility in the lattice, the lower by the presence of background impurities.

Surface chemistry of growth

Surface kinetic data on growth and doping can be obtained by using modulated molecular beam techniques [12][14]. The flux of an incident species can be modulated by opening and closing the shutter of the Knudsen cell periodically or by placing a beam chopper inside the vacuum system. The perturbation of the incident flux gives rise to a time-varying concentration of chemisorbed atoms and molecules on the substrate surface. This leads to a time-dependent desorption rate, which can be measured mass-spectrometrically. Alternatively, by modulating the desorption flux with a beam chopper, atomic and molecular species which are leaving the surface directly can be identified and distinguished from background vapour species.

The kinetic parameters to be extracted from modulated molecular-beam experiments include the surface residence time, desorption energy, sticking coefficient and order of reaction in which the adsorbed and desorbed species are involved. From these data detailed interaction mechanisms have been deduced, especially for the reaction of gallium and arsenic on (100)

[11] A. Y. Cho and K. Y. Cheng, Growth of extremely uniform layers by rotating substrate holder with molecular beam epitaxy for applications to electro-optic and microwave devices, Appl. Phys. Lett. **38**, 360-362, 1981;
K. Y. Cheng, A. Y. Cho and W. R. Wagner, Molecular-beam epitaxial growth of uniform $Ga_{0.47}In_{0.53}As$ with a rotating sample holder, Appl. Phys. Lett. **39**, 607-609, 1981.

[12] C. T. Foxon, J. A. Harvey and B. A. Joyce. The evaporation of GaAs under equilibrium and non-equilibrium conditions using a modulated beam technique, J. Phys. & Chem. Solids **34**, 1693-1701, 1973.

[13] J. H. Neave, P. Blood and B. A. Joyce, A correlation between electron traps and growth processes in *n*-GaAs prepared by molecular beam epitaxy, Appl. Phys. Lett. **36**, 311-312, 1980.

[14] C. T. Foxon, M. R. Boudry and B. A. Joyce, Evaluation of surface kinetic data by the transform analysis of modulated molecular beam measurements, Surf. Sci. **44**, 69-92, 1974.

[16] C. T. Foxon and B. A. Joyce, Interaction kinetics of As_2 and Ga on |100| GaAs surfaces, Surf. Sci. **64**, 293-304, 1977.

[16] C. T. Foxon and B. A. Joyce, Interaction kinetics of As_4 and Ga on |100| GaAs surfaces using a modulated molecular beam technique, Surf. Sci. **50**, 434-450, 1975.

[17] C. T. Foxon and B. A. Joyce, Surface processes controlling the growth of $Ga_xIn_{1-x}As$ and $Ga_xIn_{1-x}P$ alloy films by MBE, J. Cryst. Growth **44**, 75-83, 1978.

substrates of GaAs. It has been demonstrated that the use of an As_4 flux (from an elemental arsenic source) and that of an As_2 flux (from a GaAs source) lead to substantially different surface reactions [15] [16].

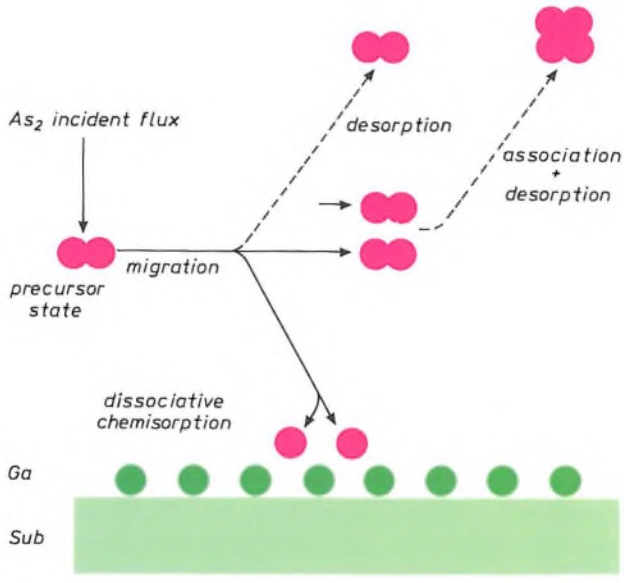

Fig. 4. Model of the chemistry of growth of a GaAs film from molecular beams of Ga and As_2. The As sticking coefficient approaches unity when the substrate is already covered with a monolayer of Ga atoms. An As_2 molecule is first adsorbed into a weakly bound precursor state, in which it can migrate on the surface. Dissociative chemisorption can occur on Ga adatoms with a sticking coefficient $\lesssim 1$. Excess As_2 molecules can either desorb from the precursor state or associate at low temperatures, leading to desorption of an As_4 molecule.

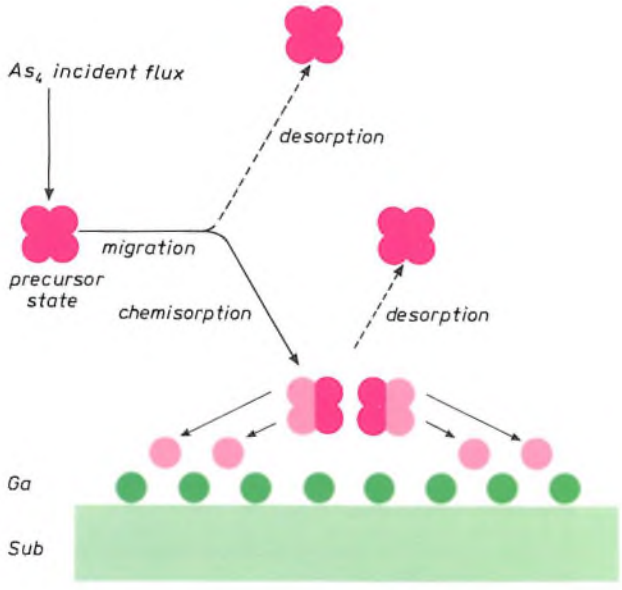

Fig. 5. Model of the chemistry of growth of a GaAs film from molecular beams of Ga and As_4. Here an As_4 molecule, adsorbed into a weakly bound precursor state, migrates on the substrate. The molecules can desorb or be chemisorbed on adjacent Ga adatoms. Pairwise interaction of two chemisorbed As_4 molecules on adjacent Ga atoms leads to the incorporation of four As atoms in the lattice and to desorption of another four As atoms as an As_4 molecule. As a result the sticking coefficient of As_4 is $\lesssim 0.5$.

The interactions of the As_2 flux and gallium on a GaAs substrate are summarized in the growth model shown in *fig. 4* [16]. According to this model the As_2 molecules are first adsorbed into a mobile, weakly bound precursor state. The surface residence time of molecules in this state is less than 10^{-5} s. The basic process for As incorporation during thin-film growth is a simple first-order dissociative chemisorption on surface Ga atoms. When the Ga flux is lower than half the As_2 flux, one As atom sticks for each Ga atom supplied. The maximum value of the As_2 sticking coefficient is unity, which is obtained when the surface is covered with a complete monolayer of Ga atoms (as in fig. 4). At relatively low substrate temperatures (< 600 K) there is an additional association reaction to form As_4 molecules. These desorb very slowly by a first-order reaction. At substrate temperatures above 600 K some dissociation of GaAs may occur.

By contrast, the reaction mechanism with an incident As_4 flux is significantly more complex [16]. The model for this is shown in *fig. 5*. Here the As_4 molecules are first adsorbed into a mobile precursor state. The migration of the adsorbed As_4 molecules has an activation energy of about 0.25 eV. The surface residence time is temperature dependent, from which a desorption energy of about 0.4 eV may be determined. A crucial finding is that the sticking coefficient of arsenic never exceeds 0.5, even when the Ga flux is much higher than the As_4 flux or when the surface is completely covered with a monolayer of Ga atoms (as in fig. 5). This is explained by assuming a pairwise dissociation of As_4 molecules chemisorbed on adjacent Ga atoms. This second-order reaction is the key feature of the thin-film growth of GaAs with an As_4 flux. From any two As_4 molecules four As atoms are incorporated in the GaAs lattice, while the other four desorb as an As_4 molecule.

Composition control for $Al_xGa_{1-x}As$ films

For the MBE growth of the ternary III-III-V alloy $Al_xGa_{1-x}As$, beams of Al, Ga and excess As_2 or As_4 are directed simultaneously at the substrate surface. In this way films of good crystallographic perfection can be obtained. A critical factor, however, in alloy-film growth by MBE is the production of films having a homogeneous composition.

Growth reactions for III-III-V alloys, in so far as the Group V element is concerned, are similar to those observed in the growth of binary compounds. The only problem is to establish those kinetic factors which can influence the ratio of the Group III elements [17]. An important point to note, however, is that the thermal stability is determined by the less stable of the two

binary compounds of which the alloy may be considered to be composed. In the case of $Al_xGa_{1-x}As$ films AlAs is more thermally stable than GaAs. Thus by using growth parameters comparable to those for GaAs, films of good compositional uniformity and control can be prepared.

At comparatively low substrate temperatures (<575 °C) the sticking coefficients of Al and Ga are both unity, so the alloy composition is determined simply by the ratio of the two atomic fluxes. However, to obtain adequate electrical and/or optical properties it is frequently necessary to use significantly higher substrate temperatures. In that case preferential desorption of the more volatile Ga occurs, which means that the sticking coefficient of Ga is less than unity. The value for Al, on the other hand, does not change significantly over the entire temperature range used (≈ 650-750 °C). The effective loss of Ga can be readily calculated from its known vapour pressure over GaAs.

Growth dynamics

It is possible to explore some features of the growth dynamics of MBE by monitoring temporal variations in the intensity of various features in the RHEED pattern. It has been found that damped oscillations in the intensity of both the specular and diffracted beam occur immediately after initiation of growth [18]. A typical example for the specular beam is shown in *fig. 6*. The period of oscillation corresponds exactly to the growth of a single monolayer, i.e. a complete layer of Ga and As atoms, which in the [001] direction is equal to the thickness of half the lattice constant. The period is independent of the azimuth of the incident beam and of the particular diffraction feature being measured [19]. The amplitude, however, is strongly dependent on both of these parameters. For evaluation of growth dynamics most of the information is contained in the specular beam, so we shall limit the discussion to this feature.

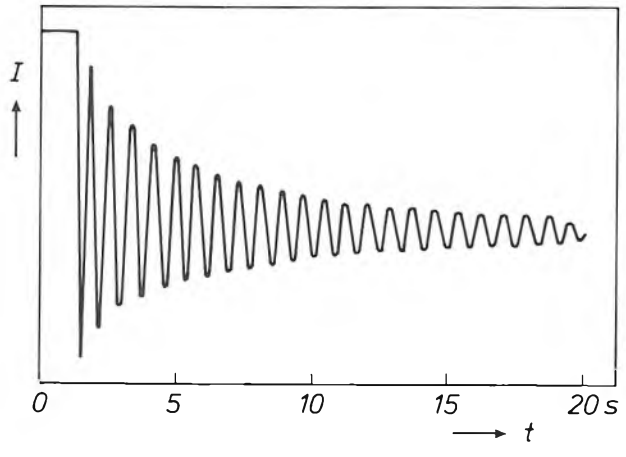

Fig. 6. Oscillations of the intensity of the specular beam in the RHEED pattern from a (2×4) reconstructed surface in the [110] azimuth, during the growth of a thin GaAs film on a (001) substrate of GaAs[17]. The notation (2×4) indicates an enlargement of the surface unit cell by a factor of two and four in the [$\bar{1}$10] and [110] directions respectively. The growth is initiated by an incident flux of Ga atoms at the heated substrate which is maintained in a flux of either As_2 or As_4. The intensity I is given in arbitrary units as a function of the growing time t. The oscillation period corresponds to the growth of a monolayer of GaAs.

Similar oscillatory effects have been observed during epitaxial growth of thin metal or silicon films, when studied *in situ*, for example by Auger spectroscopy or low-energy electron diffraction (LEED) [20]. The observation of these effects is usually associated with a layer-by-layer growth process (i.e. two-dimensional nucleation). Detailed analysis of the oscillations provides important information on growth dynamics.

If we equate changes in intensity of the specular beam in the RHEED pattern with changes in surface roughness, a smooth equilibrium surface corresponds to high reflectivity. On commencement of growth, clusters are formed at random positions on the crystal surface, leading to a decrease in the reflectivity. This decrease can be predicted for purely optical reasons, since the de Broglie wavelength of the electrons is about 0.012 nm while the bi-layer step height is about 0.28 nm; i.e. the wavelength is at least an order of magnitude less than the size of the scatterer, so diffuse scattering will result. Nucleation is not restricted to a single layer, but can reoccur before the preceding monolayer is complete. In the early stages, however, one monolayer is likely to be almost complete before the next monolayer starts, so the reflectivity will increase as the surface again becomes smooth on the atomic scale, but with subsequent roughening as the next monolayer develops. This repetitive process will cause the oscillations in reflectivity to be gradually damped as the surface becomes statistically distributed over several incomplete monolayers.

In *fig. 7* we show a real-space representation of the formation of two monolayers which illustrates how the oscillations in the intensity of the specular beam

[18] J. H. Neave, B. A. Joyce, P. J. Dobson and N. Norton, Dynamics of film growth of GaAs by MBE from RHEED observations, Appl. Phys. A **31**, 1-8, 1983.

[19] J. J. Harris, B. A. Joyce and P. J. Dobson, Oscillations in the surface structure of Sn-doped GaAs during growth by MBE, Surf. Sci. **103**, L90-L96, 1981.

[20] V. Bostanov, R. Roussinova and E. Budevski, Multinuclear growth of dislocation-free planes in electrocrystallization, J. Electrochem. Soc. **119**, 1346-1347, 1972;
Y. Namba, R. W. Vook and S. S. Chao, Thickness periodicity in the Auger line shape from epitaxial (111) Cu films, Surf. Sci. **109**, 320-330, 1981;
K. D. Gronwald and M. Henzler, Epitaxy of Si(111) as studied with a new resolving LEED system, Surf. Sci. **117**, 180-187, 1982.

occur. There is a maximum in reflectivity for the initial and final smooth surfaces and a minimum (or maximum in diffuse scattering) for the intermediate stage when the growing monolayer is approximately half complete. We have, however, also established that the amplitude of the intensity oscillations is dependent on the direction of the primary electron beam, being greater for the beam incident along [110] than for the beam incident along [$\bar{1}$10]. This would suggest, if we take our optical model one stage further, that most of the steps which develop on the surface are along the [$\bar{1}$10] direction, as shown in fig. 7, i.e. they cause maximum diffuse scattering when their longer edges are normal to the incident beam.

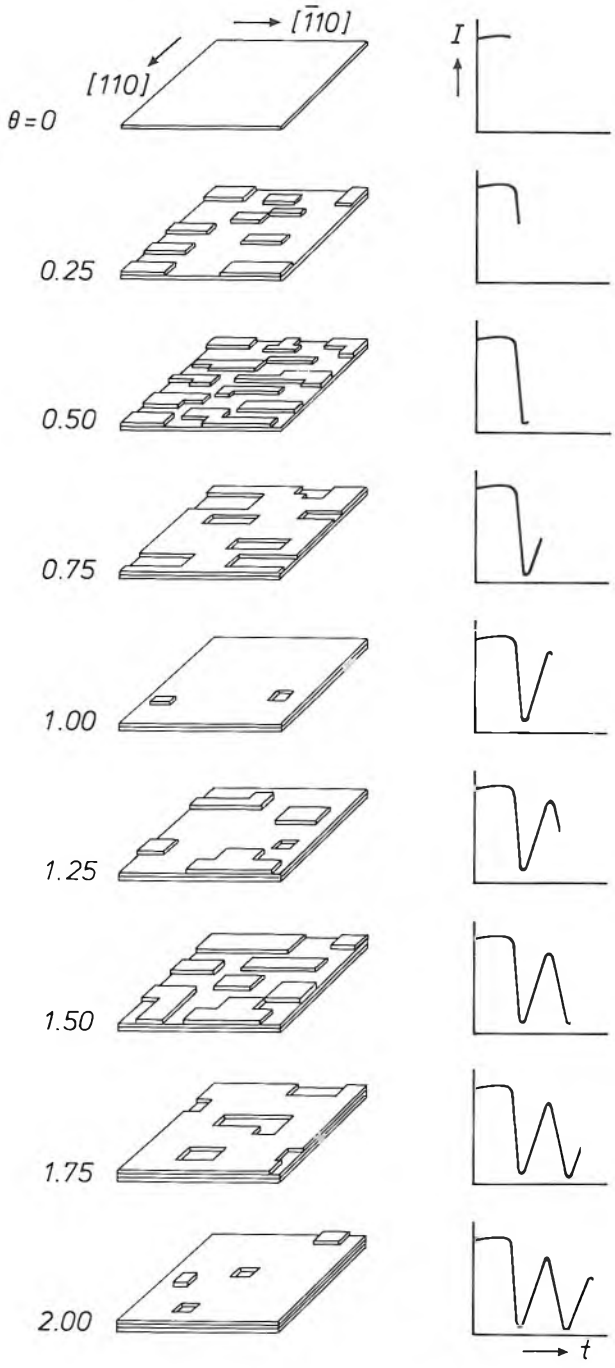

Fig. 7. Real-space representation of the formation of the first two monolayers of GaAs (*left*) with the corresponding RHEED oscillations (*right*). The intensity I is given as a function of time t for various numbers θ of monolayers deposited. When a smooth substrate is progressively covered with less than half a monolayer, the reduction in smoothness leads to a continuous decrease of reflectivity and hence of intensity. At higher coverages, up to one monolayer, the surface again becomes smoother. The intensity maximum at $\theta = 1$ is however lower than that at $\theta = 0$ because the growth of a monolayer is not perfectly two-dimensional. Similar intensity variations occur between $\theta = 1$ and $\theta = 2$. The increasing influence of the deviation from two-dimensional growth leads to a progressive damping of the amplitude of the oscillation, as shown in fig. 6.

From the results obtained we may conclude that growth occurs principally by a two-dimensional monolayer-by-monolayer process, but new monolayers are able to start before preceding ones have been completed. The oscillation period provides a continuous and absolute growth rate monitor with atomic-layer precision.

GaAs-$Al_xGa_{1-x}As$ interfaces

The MBE method described here has been used to prepare various multilayer structures based on GaAs and $Al_xGa_{1-x}As$. These include: single-heterojunction twodimensional electron-gas structures and multiple-quantumwell (MQW) structures formed from thin semiconductor films (usually GaAs) confined by layers of higher band-gap material (usually AlGaAs); when the structure is periodic and the confining barriers are thin enough for the wells to be electronically coupled the structure is known as a superlattice. For the properties of such structures the quality of the interfaces is very important, as has been indicated in the previous articles of this issue.

It is clear from the RHEED study of growth dynamics [18] that films of GaAs and $Al_xGa_{1-x}As$ grow predominantly by a process of two-dimensional nucleation of new monolayers. The damped intensity oscillations are however indicative of some non-ideality, i.e. growth is not perfectly two-dimensional. It is not yet possible to extract quantitative information on the structure and composition of GaAs-$Al_xGa_{1-x}As$ interfaces from the RHEED observations, but several other techniques have been utilized. It is important to emphasize, however, that experimentally realizable interface perfection is so high that conventional methods of profiling do not have the required resolution to test it. These methods involve ion sputtering to section the material followed by some means of composition determination, such as Auger electron spectrometry and secondary-ion mass spectrometry (SIMS) [10].

The best claimed (and probably optimistic) resolution limit of 1 nm was based on a 90%-10% peak-height range of the Auger signal of Al, from which an

interfacial width of 1.3 nm was deduced for a GaAs-$Al_{0.6}Ga_{0.6}As$ interface [21]. Even when a superlattice of GaAs and $Al_{0.3}Ga_{0.7}As$ was 'expanded' by a factor of 2400 using a very shallow angle bevelling technique, the minimum well width of GaAs in which the Auger signal of Al went to zero (< 1% Al) was 5 nm, probably due to ion beam mixing and other sputtering effects [22].

To put these results in context, it has been demonstrated by other characterization techniques that superlattices of alternate monolayers of GaAs and AlAs can be grown successfully with MBE [5] [7]. The available methods of obtaining structural and compositional information with the necessary level of spatial resolution are limited to transmission electron microscopy (TEM) of cross-sections, and to optical techniques using photoluminescence and excitation spectroscopy.

Characterization with TEM

In TEM cross-sections, when the superlattice period is greater than a few atomic layers it becomes very difficult to form a dark-field image from the superlattice spots since they are then too close to the main lattice reflections. However, because Ga and Al have significantly different scattering factors, the superlattice can still be imaged [3], as shown in *fig. 8a*. Here the dark bands correspond to GaAs and the light bands to $Al_xGa_{1-x}As$, but it is clear that the resolution is not adequate to define the interface on an atomic scale.

It is also possible to produce lattice-plane images of superlattices at extremely high resolution, but it is only possible to obtain a reasonable contrast distinction between the two materials for GaAs-AlAs structures. For GaAs-$Al_xGa_{1-x}As$ structures the interfaces are not clearly defined, but it is nevertheless evident that there is lattice-point alignment with no crystallographic disorder across the interface. An example of this is shown in fig. 8*b*, a cross-section image of a quantum well consisting of GaAs between two $Al_xGa_{1-x}As$ layers. The compositional variation cannot be precisely determined, however.

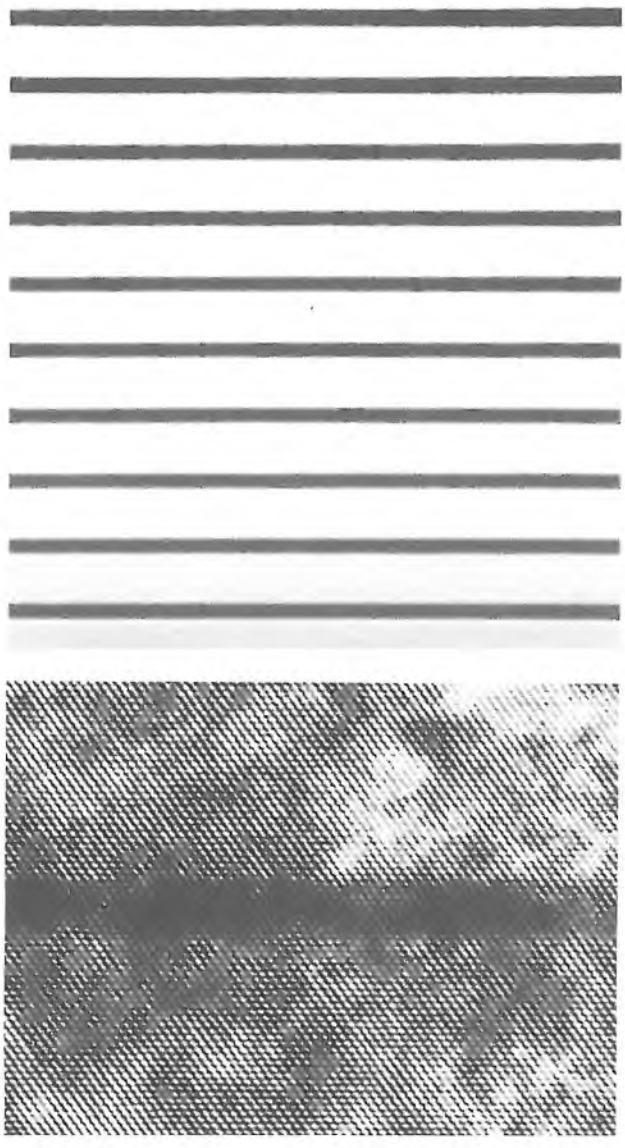

Fig. 8. *Above:* (110) cross-sectional TEM micrograph of a multiple quantum-well structure. The GaAs wells (dark) are 5.5 nm thick, the $Al_xGa_{1-x}As$ barriers (light) 17.5 nm. The micrograph was taken under dark-field conditions using the (002) diffraction. *Below*: high resolution (110) cross-sectional TEM micrograph (dark-field image) of a 2.7-nm quantum well of GaAs (dark) between two $Al_xGa_{1-x}As$ barriers (light). The samples were grown by K. Woodbridge and the micrographs were taken by J. P. Gowers and D. J. Smith (University of Cambridge).

Luminescence investigations

Probably the best available method for investigating interface disorder effects in superlattices or multiple quantum-well structures relies on their optical characterization [23]. The measurements are of photoluminescence and excitation spectra, typically at about 4 K, and the features observed are due to free or bound excitons, i.e. weakly bound mobile electron-hole pairs. Typical photoluminescence and excitation spectra for a sample which was grown in our Varian GEN II system at 650 °C are shown in *fig. 9*. The sample consists of five GaAs quantum wells 5.5 nm thick between barriers of $Al_xGa_{1-x}As$.

Exciton linewidths become broader as the well width decreases, but this could result from two possible effects. The first is a layer-to-layer thickness variation, leading to different energy levels for the conduction electrons in the different layers. The confinement of the conduction electrons in GaAs wells between the potential barriers of $Al_xGa_{1-x}As$ gives rise to the occurrence of discrete levels, as in the theoretical example of a particle confined in a box. The approximate value of the confinement energy E_n, as-

suming infinitely deep wells, is given by:

$$E_n = \frac{n^2 h^2}{8 m_e d^2},$$

where n is an integer, m_e is the effective mass of conduction electrons, h is Planck's constant and d the well thickness. For a thickness variation Δd which is independent of d, the variation of the confinement energy (ΔE_n) is given by:

$$\Delta E_n = c\, d^{-3},$$

where c is a constant.

The second alternative is for a thickness variation within each layer, but with a constant average layer thickness. This is the case corresponding to a growth process which is not perfectly two-dimensional. It will lead to a modification of the exciton energy provided the lateral scale of the interface roughness is greater than the exciton diameter, which is about 30 nm in bulk GaAs. When the lateral scale of the interface roughness becomes smaller than the diameter it will 'feel' an average potential, so that the energy levels will be sharp and narrow luminescence peaks will be observed. A study of the linewidths alone can therefore give information only if the lateral scale of the roughness is greater than the exciton diameter.

It is not possible to distinguish between these alternatives in transmission and luminescence measurements, since all the layers are then probed simultaneously, but a distinction can be made by excitation spectroscopy. In this technique the luminescence intensity at a fixed wavelength is measured as the exciting wavelength is varied. If there is a layer-to-layer thickness variation, luminescence peaks will be observed at energies corresponding to each thickness, since recombination at a given energy can only originate from wells of a specific thickness. If there is no average thickness variation, however, identical peaks will be observed in the excitation spectra for the different luminescence energies at which the spectra are obtained. Apparently this is the case in the sample of fig. 9. From the peak width of 3.5 meV a thickness variation of less than one monolayer can be deduced.

Excellent agreement between theory and experiment was obtained for well widths between 8 nm and 15 nm for the model in which there was no average thickness variation, but with an interfacial roughening on the scale of one (0.28 nm thick) monolayer [23]. In the experiment the wells of GaAs and the barriers of $Al_{0.24}Ga_{0.76}As$ were deposited at a substrate temperature of 690 °C. For very similar structures of GaAs and $Al_{0.21}Ga_{0.79}As$ barriers, deposited at 670 °C, the halfwidths of free exciton luminescence were studied as a function of well thickness [24]. It was deduced

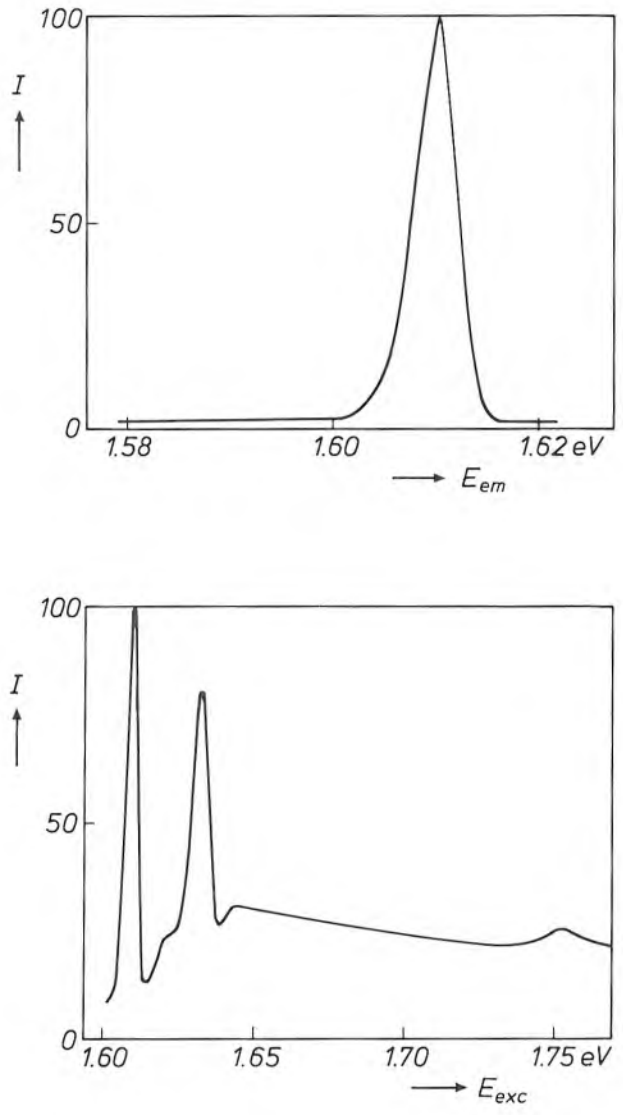

Fig. 9. *a*) Low temperature photoluminescence spectrum (relative intensity I as a function of the emission energy E_{em}) from a five-period quantum-well structure with 5.5-nm GaAs wells and 17.5-nm $Al_xGa_{1-x}As$ barriers. *b*) Corresponding excitation spectrum, obtained by measuring the relative photoluminescence intensity I as a function of the excitation energy E_{exc} at a fixed emission energy of 1.601 eV. The well-resolved peaks correspond to the formation of conduction electrons in the quantum state $n = 1$ and heavy and light holes in the $n = 1$ state. Note that the emission peak and the first excitation peak occur at the same energy. The peak width of 3.5 meV corresponds to a thickness variation which is less than one monolayer. The spectra were measured by P. J. Dobson and K. J. Moore.

[21] C. M. Garner, C. Y. Su, Y. D. Shen, C. S. Lee, G. L. Pearson, W. E. Spicer, D. D. Edwall, D. Miller and J. S. Harris, Jr., Interface studies of $Al_xGa_{1-x}As$-GaAs heterojunctions, J. Appl. Phys. 50, 3383-3389, 1979.

[22] L. P. Erickson and B. F. Phillips, Examination of MBE GaAs/$Al_{0.3}Ga_{0.7}As$ superlattices by Auger electron spectroscopy, J. Vac. Sci. & Technol. B 1, 158-161, 1983.

[23] C. Weisbuch, R. Dingle, A. C. Gossard and W. Wiegmann, Optical characterization of interface disorder in GaAs-$Ga_{1-x}Al_xAs$ multi-quantum well structures, Solid State Commun. 38, 709-712, 1981.

[24] H. Jung, A. Fischer and K. Ploog, Photoluminescence of $Al_xGa_{1-x}As$/GaAs quantum well heterostructures grown by molecular beam epitaxy; II. Intrinsic free-exciton nature of quantum well luminescence, Appl. Phys. A 33, 97-105, 1984.

that more than 65% of the interface within the photo-excited area (100 μm diameter) was atomically sharp, and any roughness in the remaining area only extended over one monolayer.

In conclusion, the analytical methods with sufficient resolution have undoubtedly demonstrated the high structural and compositional perfection of the interfaces between some MBE-grown layers. For GaAs-$Al_xGa_{1-x}As$ heterojunctions we can be confident that it is possible to prepare interfaces by MBE so that compositional changes occur over no more than one monolayer. They are free of extended defects.

Some properties and possible applications

Important properties of MBE-grown layers are the donor and acceptor concentrations and the free carrier concentration and mobility. These properties can be obtained by electrical characterization methods such as measurements of the Hall coefficient [25] and the electrical resistivity. The donor and acceptor concentrations can be derived by careful analysis of the temperature dependence of the free carrier concentration and mobility [26].

GaAs layers grown in our laboratory by MBE in a Varian GEN II equipment were found to have a low background acceptor level. This was determined by studying the electron mobility in 10-12 μm thick films lightly n-doped with silicon. The mobilities measured are typically 7.8×10^3 $cm^2V^{-1}s^{-1}$ at 300 K and 1×10^5 $cm^2V^{-1}s^{-1}$ at 77 K. The free electron concentrations allowing for depletion are 3×10^{14} cm^{-3} and the sum of the donor and acceptor concentrations can be estimated to be about 7×10^{14} cm^{-3} [26]. Hence a value of 2×10^{14} cm^{-3} is derived for the background acceptor concentration. Unintentionally doped films of similar thickness are fully depleted and this implies that the background donor concentration is also about 2×10^{14} cm^{-3}. Two-dimensional electron-gas structures prepared in the same MBE equipment were found to have mobilities as high as 3×10^6 $cm^2V^{-1}s^{-1}$ at 4 K, which also indicates how pure such samples are.

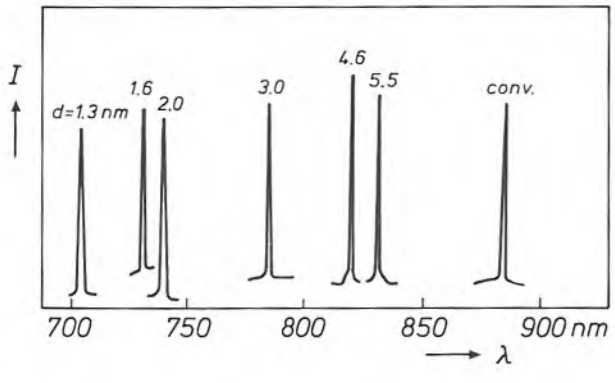

Fig. 10. Laser emission (relative intensity I plotted against emission wavelength λ) for a series of multiple quantum-well structures of GaAs wells and $Al_xGa_{1-x}As$ barriers and for a conventional semiconductor laser. The structures show emission at progressively shorter wavelengths as the well thickness d is reduced. The structure with the thinnest well (1.3 nm) operates in the visible part of the spectrum, the emitting wavelength being 704 nm. The multiple quantum well lasers were made by P. Blood, E. D. Fletcher and P. J. Hulyer from layers grown by K. Woodbridge.

Multiple-quantum-well GaAs-AlGaAs injection lasers have been grown by MBE in our laboratory-constructed equipment. The GaAs well width was varied from 5.5 to 1.3 nm to study its effect on the wavelength of the laser emission [6]. The smallest well width (1.3 nm) corresponds to only about five monolayers of GaAs. The wells are separated by 8 nm wide $Al_xGa_{1-x}As$ barriers.

In *fig. 10* the laser emission spectrum is given for quantum-well structures with various well widths and for a conventional laser with GaAs in the active region, which emits at about 880 nm. A decrease of the well width from 5.5 to 1.3 nm results in a progressive reduction in operating wavelength from 837 to 704 nm [6]. The emission at 704 nm is in the visible part of the spectrum. To our knowledge it is the shortest emission wavelength achieved with a room-temperature injection laser with only GaAs (and no Al) in the wells. Quantum-well lasers with such a short-wavelength emission are of interest in view of their possible use in optical information read-out systems.

The reduction of well width, particularly below about 3 nm, leads however to a strong increase of the threshold current for laser emission. This forms the only limitation for the realization of practical short-wavelength quantum-well lasers: as demonstrated, extremely thin wells with sufficiently abrupt interfaces can readily be obtained by MBE. Recently the influence of the number of wells on the threshold current was investigated, using a structure with a fixed waveguide [27]. It was shown that a small number of wells (preferably a single well) is favourable for obtaining lower threshold currents. For broad-area devices with a well of only 2.5 nm in a wide optical waveguide a threshold current density of about 1 kA/cm^2 was measured. This implies that it should

[25] The Hall coefficient represents the voltage induced by external electric and magnetic fields orthogonal to each other, which appears across a sample in a direction at right angles to both fields. The reciprocal of this coefficient is proportional to the free carrier concentration, and the ratio of the Hall coefficient to the electrical resistivity gives the free carrier mobility.

[26] G. E. Stillman and C. M. Wolfe, Electrical characterization of epitaxial layers, Thin Solid Films **31**, 69-88, 1976.

[27] P. Blood, E. D. Fletcher, K. Woodbridge and P. J. Hulyer, Short wavelength (visible) quantum well lasers grown by molecular beam epitaxy, Physica **129B**, 465-468, 1985.

be possible to obtain narrow stripes (5 μm wide) of production-type lasers with threshold currents below 50 mA.

In our MBE research and development at PRL invaluable assistance was given by Mr J. H. Neave. Many other members of the MBE group at PRL also contributed to the work described in this article, and there were many other contributions from members of other groups and other Philips colleagues.

Summary. The growth of thin films of GaAs and $Al_xGa_{1-x}As$ on GaAs substrates by molecular beam epitaxy (MBE) has been investigated extensively within the Philips Research Laboratories at Redhill. High-quality films and multilayer structures with controlled thickness and composition have been deposited. Detailed information has been obtained on the surface chemistry and the dynamics of growth. It is possible to produce abrupt interfaces between GaAs and $Al_xGa_{1-x}As$ layers, where the compositional changes occur over no more than one monolayer. GaAs layers have been grown with low background impurity concentrations (2×10^{14} cm^{-3}) and this has enabled us to achieve high electron mobilities at low temperatures (3×10^6 cm^{2}V^{-1}s^{-1} at 4 K) in two-dimensional electron-gas structures. Multiple quantum-well structures prepared by growing very thin GaAs wells between $Al_xGa_{1-x}As$ barriers showed laser emission at wavelengths down to 704 nm.

Philips Tech. Rev. 43, No. 5/6, 154-165, May 1987

Silicon molecular beam epitaxy on GaP and GaAs

P. C. Zalm, C. W. T. Bulle-Lieuwma and P. M. J. Marée

Introduction

Most products emerging from today's semiconductor industry are manufactured from silicon. Only for applications such as light-emitting diodes, microwave devices [1] and lasers for optical communication [2], Compact Disc players [3] and digital optical recording [4] are III-V semiconductors employed. New and technologically interesting possibilities can be envisaged if single-crystal wafers containing both types of semiconductor can be prepared. Such monolithic wafers can be used for the fabrication of devices combining the high-frequency and optoelectronic features of III-V compounds with modern silicon VLSI technology. It might even be possible to integrate a laser diode, a detector (for the reflected laser light) and the circuits for drive and signal processing all on a single chip. But there are many difficulties to be mastered in achieving this goal.

Because of the similarity in crystal structure, silicon can be deposited epitaxially on a substrate such as the well-known III-V semiconductor GaAs. A problem is the difference in interatomic distances: the lattice constant of Si is about 4% smaller than that of GaAs. Such a mismatch may lead to incorporation of crystal defects in the layer or film, and these can adversely affect the electrical properties. Deposition of III-V material on Si poses an additional problem, connected with the presence of atomic steps and 'kinks' in the surface and with the different bonding of the two components to Si; see *fig. 1*. A slight bonding preference for one component (e.g. As) may induce 'anti-phase boundaries', dependent on the growth mechanism. This may also affect the electrical properties. It was therefore decided to investigate the growth of Si on III-V substrates. The intention was to obtain a better understanding of the effect of the lattice mismatch on the crystal quality and to assess the potential and limitations of these systems.

A large number of experiments were performed with GaP as the substrate material. This only has a slight lattice mismatch (0.36%) with Si. We expected that a study of the combination of Si and GaP would shed some light on the onset of crystal defects due to lattice mismatch. Substrates that give a much larger mismatch are also of interest. A good representative of this category, which includes all the III-V materials of technological significance, is GaAs. The growth of silicon on GaAs was therefore extensively investigated as well.

A suitable growth technique is molecular beam epitaxy (MBE), essentially a controlled deposition by evaporation in ultra-high vacuum [5]. It has been shown that MBE of Si films on an Si substrate below 800 °C gives material of excellent quality for device manufacture [6]. Low deposition temperatures reduce diffusion across the interface, so that very abrupt changes in composition can be obtained. In addition, the decomposition of III-V compounds at higher temperatures limits the temperature range for epitaxial growth.

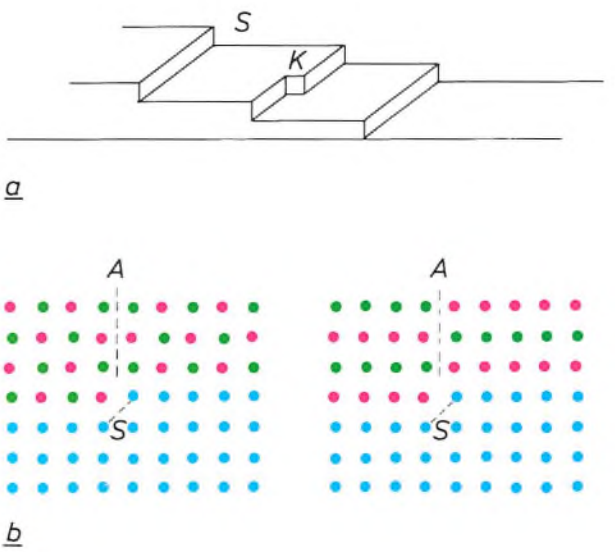

Fig. 1. *a*) Schematic representation of a surface of a single-crystal substrate showing steps *S* and a kink *K*. *b*) Two examples of atomic arrangements for a binary compound (e.g. GaAs) grown epitaxially on a substrate containing only one type of atom (e.g. Si). The difference in bonding leads to anti-phase boundaries *A* at steps *S* in the substrate surface.

Dr P. C. Zalm and C. W. T. Bulle-Lieuwma are with Philips Research Laboratories, Eindhoven; Drs P. M. J. Marée is with the FOM Institute for Atomic and Molecular Physics, Amsterdam.

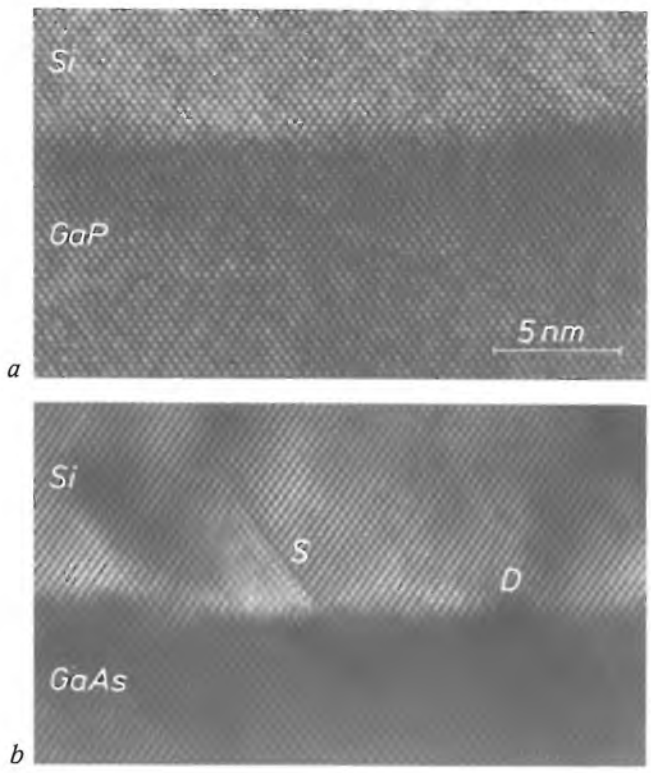

Fig. 2. High-resolution lattice images, made along the [110] direction by transmission electron microscopy (TEM), of MBE-grown Si on (001) GaP (*a*) and (001) GaAs (*b*). The interface region on GaP does not have any crystal imperfections. The interface region on GaAs has 60° dislocations *D* close to the interface and stacking faults *S* on (111) planes. The gradual interface transitions of about five monolayers can be attributed to an intermixing of elements or to the roughness of the substrates after the cleaning procedure.

The growth experiments described in this article were performed at the FOM Institute for Atomic and Molecular Physics (AMOLF) in Amsterdam, where a silicon MBE facility with associated analysis equipment is available for research purposes. Supplementary information on the properties of the films was obtained with various surface-analysis techniques at Philips Research Laboratories in Eindhoven.

Our studies showed that Si could be deposited epitaxially on (001) GaP, with no lattice defects for film thicknesses up to 75 nm. A cross-sectional lattice image made with a high-resolution transmission electron microscope is shown in *fig. 2a*. In films thicker than 75 nm misfit dislocations are introduced. The critical thickness for the onset of dislocation formation is much larger than predicted by current theory. In Si films deposited on (001) GaAs many crystal defects such as misfit dislocations and stacking faults are observed; see fig. 2*b*. The way in which the lattice mismatch induces the observed crystal imperfections is now fairly well understood. This may be important for the fabrication of thick perfectly epitaxial heterostructures. Before discussing the results in more detail, we shall first give a description of the MBE equipment and the procedure.

Experimental arrangement and procedure

Because of the fairly high temperature (> 1400 °C) required for significant evaporation, and the high reactivity of molten Si, effusion cells of the Knudsen type [5] cannot be used as a source. A good alternative is the electron-beam evaporator depicted in *fig. 3*. Here a high-power beam of electrons, with an energy of about 10 keV and a current of about 0.1 A, is focused by a magnetic field on to a Si 'slug', resulting in localized heating, melting and evaporation. The beam is scanned over an area of about 0.5 cm^2.

A problem with such a source is the limited evaporation rate. Above a certain power input 'sputtering' occurs: droplets or clusters containing many Si atoms are ejected and deposited on to the substrate. Whereas atoms that arrive individually can diffuse over the surface until they arrive at a suitable lattice position, these droplets form immobile amorphous islands, because they do not disintegrate sufficiently well on impact.

To prevent this effect the deposition rate must be limited to less than about 2 nm/s, corresponding to a silicon flux of less than 10^{16} at.$cm^{-2}s^{-1}$. This in turn necessitates growth in ultra-high vacuum to prevent

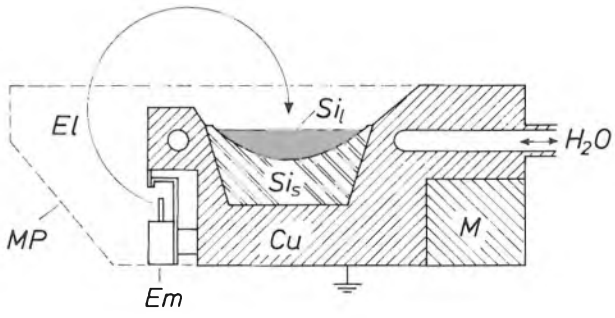

Fig. 3. Schematic representation of the electron-beam evaporator used as source for silicon MBE. Evaporation is produced by heating with an electron beam *El* emitted by the emitter assembly *Em* and deflected by a magnetic field on to a silicon slug. Si_s solid silicon, Si_l molten silicon, *M* magnet, *MP* magnet pole pieces. A deflection of 270° is used to avoid tungsten contamination from the filament. The copper holder *Cu* for the silicon slug is water-cooled to prevent melting and outgassing.

[1] P. Baudet, M. Binet and D. Boccon-Gibod, Low-noise microwave GaAs field-effect transistor, Philips Tech. Rev. **39**, 269-276, 1980.
[2] G. A. Acket, J. J. Daniele, W. Nijman, R. P. Tijburg and P. J. de Waard, Semiconductor lasers for optical communication, Philips Tech. Rev. **36**, 190-200, 1976.
[3] Special issue 'Compact Disc Digital Audio', Philips Tech. Rev. **40**, 149-180, 1982.
[4] K. Bulthuis, M. G. Carasso, J. P. J. Heemskerk, P. J. Kivits, W. J. Kleuters and P. Zalm, Ten billion bits on a disk, IEEE Spectrum **16**, No. 8 (August), 26-33, 1979.
[6] Details of the MBE growth of III-V compounds have been given in the previous article in this issue by B. A. Joyce and C. T. Foxon.
[6] Various aspects of silicon molecular beam epitaxy have been described in an extensive review article by Y. Ota, Thin Solid Films **106**, 3-136, 1983.

excessive contamination. Even at 10^{-8} Pa the rate of incidence of molecules from the residual gas is about 3×10^{10} $cm^{-2}s^{-1}$. If all these molecules were to 'stick' and remain on the surface the relative contamination level would be 3×10^{-6}, corresponding to an undesired doping level of 1.5×10^{17} cm^{-3}. This would not only be disastrous for the electrical properties, but would also prevent perfect crystal growth. Although the sticking probability is generally much less than unity (typically 10^{-3}), great care has to be taken with the design and operation of an MBE system, so that these problems can be avoided.

For our experiments we used an earlier version of the present silicon-MBE system at the FOM institute AMOLF, designed by T. de Jong *et al.* [7] and shown schematically in *fig. 4*. It has the basic features found in many research-oriented systems, and consists of three linked vacuum chambers. Substrates mounted on holders are introduced twelve at a time into the load-lock annexe to the storage chamber; the twelve holders are placed on a carrousel. After loading, the storage chamber is sealed, pumped down and baked for about ten hours at 150 °C. The final pressure is a few times 10^{-7} Pa. Then the valve to the main chamber is opened and a holder with substrate is picked up and transferred with the aid of a magnetically coupled transfer rod. During the transfer the main chamber remains at low pressure (10^{-8} Pa). The desired substrate temperature is obtained by direct-current heating and checked with an infrared pyrometer to an accuracy of ± 25 °C.

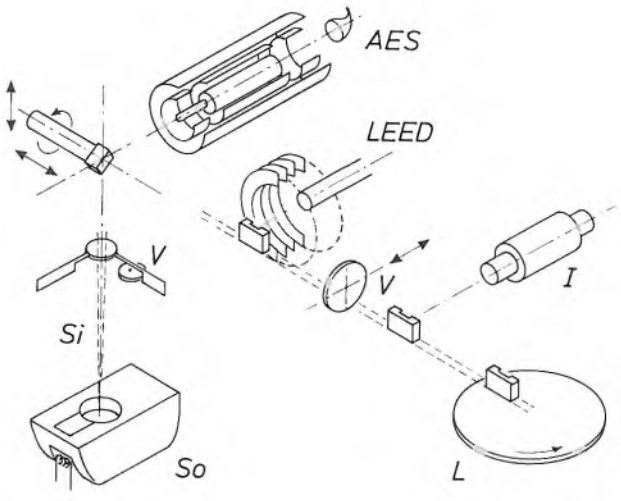

Fig. 4. Schematic diagram of an earlier version of the silicon MBE system at AMOLF. The system contains three vacuum chambers which can be connected by the gate valves *V*. A holder with a substrate is supplied via a load lock *L*. An ion gun *I* is used for cleaning the substrate surface. In the main vacuum chamber the surface is investigated by low-energy electron diffraction (LEED) and Auger electron spectroscopy (AES). The growth is started by introducing silicon vapour from the chamber with the Si source *So*. The diagram does not show the equipment for substrate heating and temperature measurement, the microbalance for growth-rate monitoring, or the quadrupole mass spectrometer for residual-gas analysis.

The source chamber is mounted below the main chamber. When the evaporator is turned on, residual gas adsorbed on the slug surface and the filament is released. This is pumped away and the valve to the main chamber is only opened when the source is stabilized at the desired evaporation or deposition rate, measured by a quartz-crystal oscillator microbalance. The pressure in the main chamber rises by less than an order of magnitude during the growth; the additional gas is mainly relatively harmless H_2 from the bulk of the Si slug.

Substrate preparation and analysis

Successful MBE growth of Si on GaP and GaAs requires careful attention to the preparation and cleaning of the substrate and the analysis of its surface. It is known that epitaxial Si films can be deposited on (001) Si from 200 °C, whereas the deposition on (111) Si requires much higher temperatures (> 600 °C) [6]. It was therefore decided to use (001) substrates only. These are cut from liquid-encapsulated Czochralski-grown crystals, polished and degreased. The GaP substrates of thickness 1 mm are too small to be mounted directly on the holder, and are therefore attached by small amounts of indium to a 7 mm $\times$ 25 mm silicon carrier. The indium provides a uniform thermal and electrical contact for the substrate heating, and does not affect the purity of the films. The GaAs substrates are 0.4 mm thick and can be cut immediately to the dimensions required for direct mounting in the holder.

Although the substrates are treated with the utmost care, their surface will always be covered by a thin film of oxide. Nor can slight contamination by carbon, from CO_2 in the atmosphere or from organic cleaning fluids, be avoided in practice. These contaminants are removed by sputter-etching with an Ar^+ beam at an energy of 600 to 800 eV and a total dose of about 10^{16} cm^{-2}. As ion bombardment makes the substrate surface amorphous, post-annealing is necessary to restore the crystallinity by solid-phase epitaxial regrowth [8]. This is done at 550 °C for 30 min (GaP) and at 600 °C for 90 min (GaAs).

A problem with this cleaning procedure is that the two components may be sputtered at different rates. In addition, at the temperatures necessary for reasonable regrowth rates (> 1 nm/min) there will be some evaporation. Since the two components evaporate at different rates, there will be a depletion of one of the components (usually the group V element) at the surface. Consequently the surface, although crystalline, will have a non-stoichiometric composition after cleaning. In principle this deficiency can be corrected by supplying the 'missing' component through adsorption from the gas phase, or by first growing a

stoichiometric crystalline film of the III-V material on the substrate, as described in the previous article [6].

The effectiveness of the cleaning procedure was checked by Auger Electron Spectroscopy (AES) [9]: an energetic (a few keV) electron beam removes a strongly bound electron from a target atom, and the 'hole' created is 'filled' by a more weakly bound electron. The energy gained is used to eject another weakly bound (Auger) electron with an element-specific energy between 10 and 2000 eV. Determining the number of Auger electrons therefore provides information about the composition of the surface. This technique is surface-sensitive since the escape depth (without energy loss) of the Auger electrons is less than about 2 nm. Residual impurities with a surface concentration greater than 1 % can be detected. Our AES measurements revealed that the cleaned surfaces of GaP and GaAs contain less than 0.01 of a monolayer of carbon, nitrogen or oxygen.

Another surface-sensitive technique, low-energy electron diffraction (LEED) [9], was used to check the recrystallization of the surface. In LEED, a low-energy (< 200 eV) electron beam is reflected by the sample. Diffraction occurs, and if the surface is crystalline there will be constructive interference of the reflected beams in certain directions only. A phosphor screen placed in the path of the reflected and subsequently post-accelerated electrons will then emit light locally. Spot patterns thus obtained are characteristic of the ordering of the surface atoms. The distance between the various spots is inversely proportional to the interatomic distances on the surface in a specific direction.

Methods of investigating the films.

Once the substrates had been cleaned sufficiently, Si films were deposited with thicknesses ranging from a few tenths of a nanometer to a few hundred nanometres. The films were investigated by *in situ* analysis with the integrated AES and LEED equipment (fig. 4) and further characterization was performed outside the MBE system [10] [11].

The structural quality of the layers was investigated by transmission electron microscopy (TEM). The observed defects were correlated to the strain induced by the lattice mismatch with the substrate. The occurrence of strain and defects was studied further by measuring the back-scattering of light ions in various directions, which is sensitive to the exact positions of the atoms in the lattice. Additional information was obtained by Raman scattering, where the frequency shift of the scattered light is a measure of the stress caused by atomic displacements from bulk lattice sites. The variation of composition with depth was studied in some samples by secondary-ion mass spectroscopy (SIMS). In this technique the ions that are successively sputtered from the surface by an ion bombardment are analysed [9].

Not all of the Si films were grown on GaP and GaAs. Some were grown 'homo-epitaxially', i.e. on an Si substrate. Investigations by TEM revealed that these films were completely free of defects, thus verifying the quality of the MBE system and the procedure.

Results of *in situ* analysis

Figs 5 and *6* show LEED patterns from cleaned GaP and GaAs surfaces and from Si films deposited

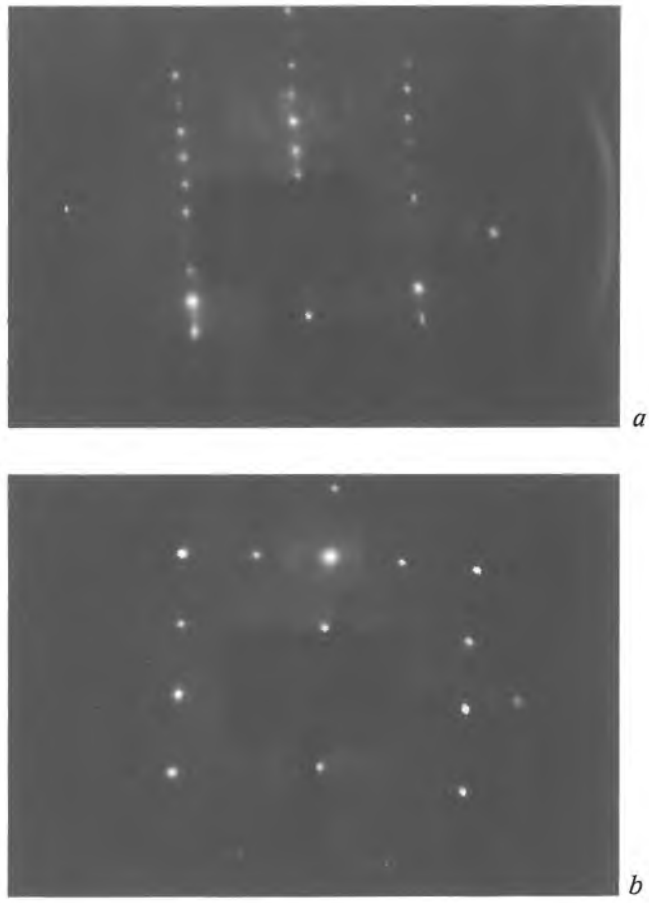

Fig. 5. LEED patterns from a (001) GaP substrate (*a*) and a silicon film (*b*). The patterns indicate that when silicon is deposited the surface reconstruction changes from (4×2) to (2×1).

[7] A description of this MBE system has been given by T. de Jong, W. A. S. Douma, L. Smit, V. V. Korablev and F. W. Saris, J. Vac. Sci. & Technol. B **1**, 888-898, 1983.

[8] T. de Jong, F. W. Saris, Y. Tamminga and J. Haisma, Solid phase epitaxy of silicon on gallium phosphide, Appl. Phys. Lett. **44**, 445-446, 1984.

[9] See for example H. H. Brongersma, F. Meijer and H. W. Werner, Surface analysis, methods of studying the outer atomic layers of solids, Philips Tech. Rev. **34**, 357-369, 1974.

[10] Si MBE on GaP has been reported previously by T. de Jong, W. A. S. Douma, J. F. van der Veen, F. W. Saris and J. Haisma, Appl. Phys. Lett. **42**, 1037-1039, 1983.

[11] Some of the investigations on Si MBE on GaAs have been reported by P. C. Zalm, P. M. J. Marée and R. I. J. Olthof, Appl. Phys. Lett. **46**, 597-599, 1985.

on them. For (001) GaP the surface reconstruction is characterized as (4×2), indicating that the periodicities along the [110] and [1$\bar{1}$0] directions are four times as large and twice as large as in the bulk material. The LEED pattern from (001) GaAs gives a $c(8 \times 2)$ reconstruction indicating an eight times two enlarged unit cell as compared with the bulk material, with a centre of symmetry. These results are typical of crystalline GaP and GaAs surfaces after ion bombardment and annealing.

Only a few Si monolayers have to be deposited on GaP or GaAs for the LEED patterns to indicate a (2×1) reconstruction, which is typical of (001) Si surfaces. The distance between corresponding diffraction spots, however, remains unchanged. It appears that the interatomic spacing in the Si film is the same as in GaP or GaAs, i.e. the growth is coherent or pseudomorphic on the substrate. This can only be established reliably for Si on GaAs, of course; the lattices of Si and GaP are too similar (a difference of only 0.36%) for any change in LEED spacings to be noticed. For thicker films on GaAs the diffraction spots broaden and become more diffuse. This is a strong indication of increasing crystal imperfection. Moreover, the distance between the spots increases by 4%, corresponding to a decrease in interatomic spacing to the value for bulk Si. Finally, for very thick films the LEED spots (not shown here) become somewhat sharper again, suggesting an improvement in the crystal quality.

To determine the surface composition, Auger spectra were recorded for various Si coverages, see *fig. 7*. The Auger signals from the substrate atoms decay exponentially with thickness up to 1 nm, suggesting layer-by-layer growth rather than a formation of islands. At a greater thickness ($\gtrsim$ 10 nm), however, the Auger spectra still indicate the presence of Ga and P (or As) with a total surface concentration of 5×10^{14} cm^{-2}, indicating some segregation.

Normal bulk diffusion of substrate atoms through the Si film is negligible at the temperatures used here, but there are other possible causes for the segregation observed. Detailed inspection of AES spectra and LEED patterns of various films have revealed two competing mechanisms. First there is surface diffusion of Ga and P or As from the sides and base of the substrate, an 'infinite' supply. This can be eliminated by reducing the growth temperature. Secondly, there is a position-exchange reaction with the incident Si atoms at the surface. The orientation [12] and shape of the LEED pattern for a silicon monolayer on GaAs can only be explained if the Si atoms are assumed to expel Ga atoms from their lattice positions, so that

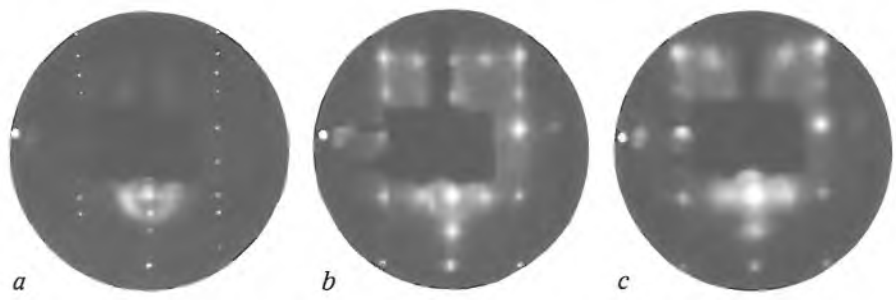

Fig. 6. LEED patterns from a (001) GaAs substrate (*a*) and Si films of thickness 1.4 nm (*b*) and 14 nm (*c*). On deposition, the surface reconstruction changes from $c(8 \times 2)$ to (2×1); the diffraction spots become more diffuse, indicating more crystal defects. The distance between the spots indicates that the 1.4-nm film has almost the same lattice constant as GaAs, whereas the lattice constant of the 14-nm film is 4% less and has the same value as for bulk Si.

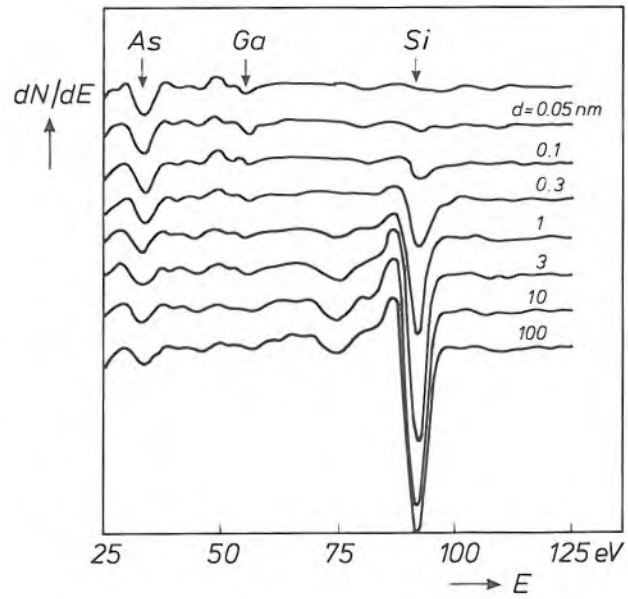

Fig. 7. Auger spectra of a cleaned (001) GaAs substrate and of Si films of thickness d deposited at 600 °C. The derivative dN/dE is shown in arbitrary units as a function of the electron energy E, where N is the number of Auger electrons detected. The arrows denote the peak positions corresponding to the characteristic Auger transitions of As (31 eV), Ga (55 eV) and Si (92 eV). For $0 < d < 1$ nm, the Ga and As peaks decrease exponentially with film thickness and the Si peak increases exponentially. When the thickness exceeds 10 nm the Ga and As peaks do not vanish.

they can bond directly with As atoms. This is rather surprising, since there are unoccupied As sites above the Ga atoms that form the upper layer of the Ga-enriched (001) surface. The exchange between Si and Ga atoms is corroborated by the Auger spectra of a monolayer, which showed that there was some Ga on top of the Si layer. A similar bonding preference has been reported for the deposition of germanium on GaAs [13].

Characterization by transmission electron microscopy

A technique such as LEED can give useful information about crystalline properties but is not very suitable for characterization of the crystal perfection because of its low sensitivity to defects. Transmission electron microscopy (TEM), however, can give more detailed structural information [14] [15]. Two examples have already been given in fig. 2, showing cross-sectional images of Si on GaP and GaAs obtained by high-resolution electron microscopy. Useful information can also be derived by making TEM 'plane-view' images at a much lower magnification. Before discussing some of the results, we shall first give a short description of the procedure for our TEM investigations.

Procedure

The samples are first made transparent to electrons. The preparation techniques required for the two kinds of imaging are very different.

For the preparation of samples for plane viewing, 3-mm discs are drilled from the wafer ultrasonically. The discs are reduced in thickness from the rear by jet-etching with a chlorinated-methanol etchant until the substrate has been completely removed from a small central area of diameter say 0.5 mm. The Si film can be examined here without interference from the substrate. At the edges the interface region can be studied.

For cross-sectional imaging, samples of {110} orientation are prepared [16]. Two strips less than 3 mm wide are cut from the wafer along one of the {110} planes, bonded together with the epitaxial films facing each other and then embedded in resin; see *fig. 8*. Thin slices are cut, mechanically polished and reduced in thickness by Ar-ion milling on a rotating sample holder at grazing incidence (about 10° to the surface) and a low voltage (≈ 4 kV) to make the surface smooth and minimize the formation of an amorphous top layer.

Images were obtained with a Philips EM 420 ST microscope operating at 120 kV. The contrast observable in TEM images has been described in an earlier article in this issue [17]. An area of GaP or GaAs appears dark compared with a silicon area because of the difference in atomic scattering. The plane-view images are made in 'bright field' (with the transmitted beam) or in 'dark field' (with one diffracted beam) under dynamic diffraction conditions. Defects can then be observed because of local variations in the diffraction conditions (amplitude contrast). The cross-sectional images are made with the electron beam along the [110] direction, so that there is strong simultaneous excitation of many diffracted beams. Recombination of the transmitted beam and several of the diffracted beams results in a high-resolution image (phase contrast).

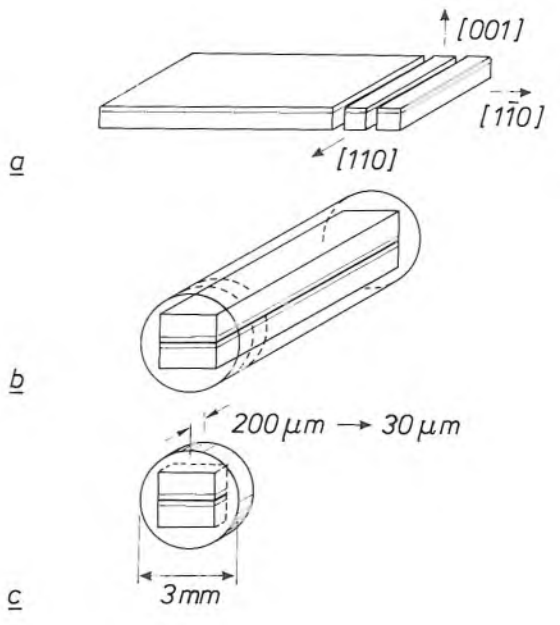

Fig. 8. Schematic illustration of the preparation of (110) samples for cross-sectional TEM imaging. Two bars are cut along one of the {110} planes (*a*). The bars are bonded together with the epitaxial films facing each other and are embedded in resin (*b*). They are then sawn into thin slices (*c*). The slices are further reduced in thickness by Ar ion milling on a rotating sample stage.

[12] A. J. van Bommel and J. E. Crombeen, Experimental determination of the correlation between the LEED pattern and the Ga-As bond vectors in the surface of GaAs (001), Surf. Sci. **57**, 437-440, 1976.

[13] B. J. Mrstik, LEED and AES studies of the initial growth of Ge epilayers on GaAs (100), Surf. Sci. **124**, 253-266, 1983.

[14] M. P. A. Viegers, C. W. T. Bulle-Lieuwma, P. C. Zalm and P. M. J. Marée, Misfit dislocations in epitaxial layers of Si on GaP (001) substrates, Mater. Res. Soc. Symp. Proc. **37**, 331-336, 1985.

[15] C. W. T. Bulle-Lieuwma, P. C. Zalm and M. P. A. Viegers, Characterization of MBE grown Si on (001) GaAs by transmission electron microscopy, Proc. Microscopy of Semiconductor Materials Conf., Oxford 1985 (Inst. Phys. Conf. Ser. **76**, section 4), pp. 123-128.

[16] C. W. T. Bulle-Lieuwma and P. C. Zalm, Suppressing of surface topography development in ion-milling of semiconductors, to be published in Surface and Interface Analysis, Vol. **10**, 1987.

[17] M. R. Leys, M. P. A. Viegers and G. W. 't Hooft, this issue, pp. 133-142.

Si on GaP

Plane viewing of Si on GaP gives almost featureless images for thicknesses up to 75 nm, indicating film growth with no misfit dislocations. It appears that the Si lattice is strained to match GaP, giving a coherent interface. At thicknesses above 75 nm, misfit dislocations are introduced. This is energetically more favourable when the strain energy becomes too high. An example of a TEM image with dislocations is given in *fig. 9*. This shows a rectangular network of misfit dislocations near the interface, and stacking faults intersecting the Si film and also forming a rectangular pattern.

The critical thickness observed (75 nm) for dislocation formation is considerably larger than the value of 14 nm derived from J. H. van de Merwe's theory assuming a thermodynamic equilibrium between an array of misfit dislocations along the interface and the strained layer [18]. A barrier to dislocation formation appears to exist. An understanding of its origin may be important for the production of perfect thick epitaxial heterostructures. We therefore studied the lattice defects of films thicker than 75 nm in more detail.

A complete characterization reveals that the dislocations are of the 60° type: 'Burgers vectors', describing the direction and magnitude of the atomic displacements, are at an angle of 60° to the dislocation lines in [110] and [1$\bar{1}$0] directions in the (001) interface; see *fig. 10a*. This is a common configuration for dislocations nucleating at the surface of a strained layer and gliding towards the interface along {111} slip planes [19]. These intersect the interface along the [110] and [1$\bar{1}$0] directions of the dislocation lines.

The presence of stacking faults (fig. 9) can be explained by considering the atomic arrangement in the slip planes. This is shown in fig. 10*b* for a face-centred cubic (fcc) lattice with a biaxial strain field in the (001) plane. The resolved shear stress $\vec{t}$ on a (111) plane is in the [11$\bar{2}$] direction. The unit displacement described by the Burgers vector $\vec{b}$ is achieved by two movements $\vec{b}_1$ and $\vec{b}_2$, producing 90° and 30° Shockley partial dislocations [20]. The force on the 90° dislocation ($\propto \vec{b}_1 \cdot \vec{t}$) is twice that on the 30° dislocation ($\propto \vec{b}_2 \cdot \vec{t}$). The principle just outlined is the same for all four {111} planes and is applicable to Si [21]. The special geometry in Si on (001) GaP therefore ensures that the 90° dislocation, which experiences the larger force, nucleates first. It moves to the interface and produces a stacking fault there. The defect structure thus initially consists of stacking faults bounded by 90° dislocations at the interface. As the film grows, the 30° dislocations also nucleate because of the stacking-fault energy. This means that the stacking faults disappear, giving perfect 60° dislocations. In fig. 9 these form a rectangular network, while the stacking faults can be associated with the situation where the 30° dislocations have not yet nucleated.

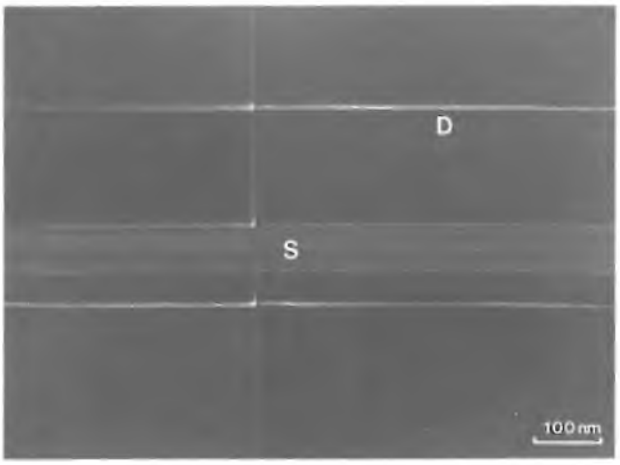

Fig. 9. Transmission electron micrograph of a planar section of an MBE-grown Si film 100 nm thick on (001) GaP, showing dislocations *D* along the interface and stacking faults *S* intersecting the Si film.

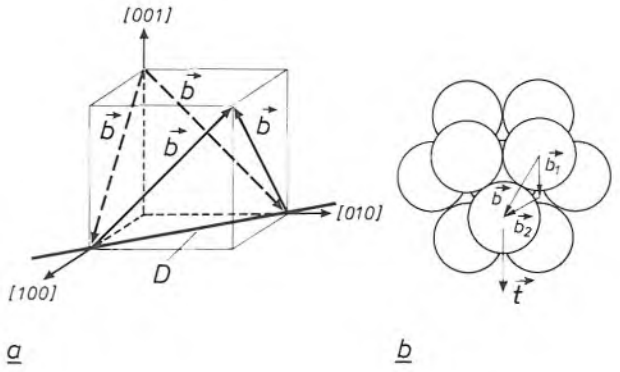

Fig. 10. *a*) Schematic illustration of the four possible Burgers vectors $\vec{b}$ of a 60° dislocation *D*, along one of the two ⟨110⟩ directions on the (001) interface. The vectors, which describe the magnitude and direction of the atomic displacement, are at an angle of 60° to the dislocation line. *b*) Schematic illustration of the atomic arrangement in one of the {111} planes of a face-centred cubic lattice, for a (001) film with a biaxial strain field. The resolved shear stress $\vec{t}$ on a (111) plane is in the [112] direction. The unit displacement $\vec{b}$, which results in a 60° dislocation, is produced by $\vec{b}_1$ and $\vec{b}_2$, giving 90° and 30° Shockley partial dislocations. The vectors are given by: $\vec{b}_1 = \frac{1}{6}a[112]$, $\vec{b}_2 = \frac{1}{6}a[2\bar{1}\bar{1}]$ and $\vec{b} = \frac{1}{2}a[10\bar{1}]$, where a is the lattice constant.

An example of incompletely formed (dissociated) 60° dislocations is shown in the high-resolution image

[18] J. H. van der Merwe and C. A. B. Ball in: J. W. Matthews (ed.), Epitaxial growth, part B, Academic Press, New York 1975.
[19] J. W. Matthews in: J. W. Matthews (ed.), Epitaxial growth, part B, Academic Press, New York 1975.
[20] A. H. Cottrell, Dislocations and plastic flow in crystals, Oxford Univ. Press, London 1953.
[21] J. Hornstra, Dislocations in the diamond lattice, J. Phys. & Chem. Solids **5**, 129-141, 1958.
[22] A. Gomez, D. J. H. Cockayne, P. B. Hirsch and V. Vitek, Dissociation of near-screw dislocations in germanium and silicon, Phil. Mag. **31**, 105-113, 1975.

of *fig. 11*. Close to the interface, the dislocations are found to have an average separation of about 10 nm. This is substantially larger than the equilibrium distance at 880 °C [22]. This may indicate that the local strains in the interface region differ considerably from the mean strain in the bulk of the film.

Finally, we note that the above geometrical effects depend strongly on the crystallographic orientation of the strained film and on the sign of the stress field. For example, in a compressive field it is not the 90° dislocations but the 30° dislocations that will have to nucleate first because of the different atomic arrangement. Since the 30° dislocations are subject to a smaller force from the shear stress, there may be a greater barrier to their nucleation than with a tensile force. Thus, films free from epitaxial defects may be thicker for compressed GaP on (001) Si than for strained Si on (001) GaP. We can assume that the nucleation of the 90° dislocations will immediately follow the nucleation of the 30° dislocations, because they are subject to a larger force from the shear stress. This means that the defect structure would consist only of perfect 60° dislocations.

Si on GaAs

Plane-view images of Si on (001) GaAs reveal Moiré fringes; see *fig. 12*. This indicates a small difference in atomic spacing between film and substrate, with no rotational misorientation on average. The periodicity corresponds to the 4% lattice mismatch between Si and GaAs. The fringes are bent locally and sometimes interrupted. Most of these distortions can be attributed to the presence of dislocations. In regions where the substrate has been removed completely, a high density of dislocations is observed. Stereomicroscopy reveals that they extend from the surface to the interface and back, with only short segments along the interface. The dislocations in the Moiré fringes of fig. 12 are more pronounced for diffraction at (220) planes than for diffraction at (400) planes. This means that they are preferably located in (110) planes. When gliding on (111) planes, they have to move along ⟨112⟩ directions. As shown in *fig. 13*, these dislocations can be clearly seen in cross-sectional images. As expected, their directions are very close to the ⟨112⟩ directions.

Investigations of the interface region (fig. 2) indicate that thin Si films grow coherently on GaAs in spite of the 4% lattice mismatch. The defect structure observed consists of dislocations close to the interface and stacking faults in (111) planes with the density increasing towards the interface. Because LEED indicated non-pseudomorphic growth above 1.4 nm, we attribute this defect structure to the relaxation of the misfit stress. Below 1.4 nm there is a planar tensile stress in the Si film, leading to a strain equal to the lattice mismatch. This stress can initially cause a homogeneous tetragonal distortion, giving rise to pseudomorphic growth. Above 1.4 nm relaxation occurs by the formation of 60° dislocations in the same way as for considerably thicker Si films on GaP. The larger lattice mismatch

Fig. 11. High-resolution electron microscopy (HREM) cross-sectional image along the [110] direction of MBE-grown Si on (001) GaP, showing dissociated 60° dislocations close to the interface.

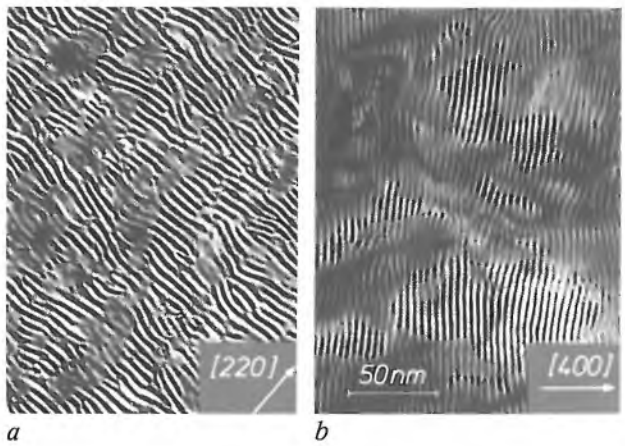

Fig. 12. Bright-field TEM images of a planar section of an Si film 200 nm thick on (001) GaAs for diffraction at (220) planes (*a*) and (400) planes (*b*). Both images show Moiré fringes, approximately perpendicular to the diffraction vector in the [220] and [400] directions. The periodicity corresponds to the 4% lattice mismatch. The distortions of the fringes are due to the presence of dislocations, which are more pronounced in (*a*) than in (*b*).

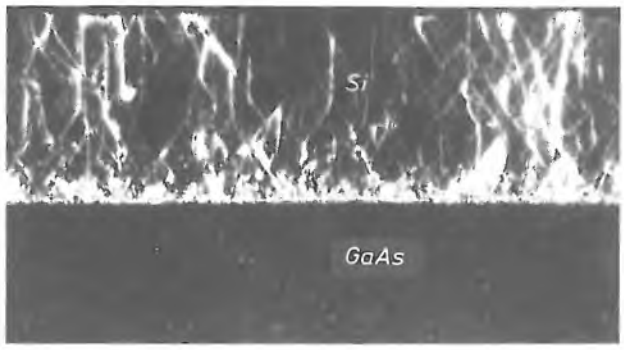

Fig. 13. Dark-field cross-sectional TEM image along the [110] direction of 200-nm MBE-grown Si on (001) GaAs. The Si film has a high density of dislocations, whereas no defects are observed in the GaAs substrate. Many dislocations run in ⟨112⟩ directions.

gives a stronger strain field, however, and hence a higher dislocation density. In plane-view images we only see short segments in the interfacial plane, indicating that the glide process has been disturbed by interactions between the dislocations.

Films of thickness 200 nm grown at 600 °C and films of thickness 25 nm grown at 500, 550 and 600 °C are found to have about the same lateral defect density. This indicates that there is no thermodynamic equilibrium between strain and dislocations. It points either to a complete relaxation of misfit strain below 25 nm or to the existence of a barrier to dislocation formation. In the latter case extended defects can be avoided, e.g. by preventing the occurrence of nucleation sites or by reducing the growth temperature, which reduces the mobility of the dislocations.

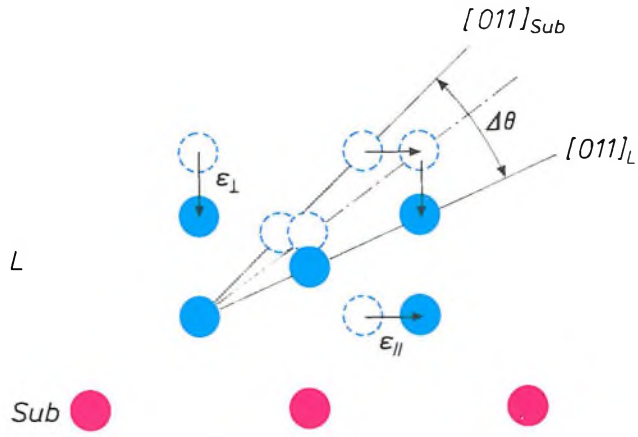

Fig. 14. Schematic illustration of the tetragonal lattice distortion in a film L with a smaller lattice constant than the substrate *Sub*. The parallel elongation by the coherency strain $\varepsilon_{\parallel}$ induces a perpendicular stress $\varepsilon_{\perp}$ leading to a contraction (Poisson effect). The resulting tetragonal distortion corresponds to a tilt $\Delta\theta$ in the [011] direction with respect to the substrate.

Further characterization

For perfect epitaxial growth on GaP, the Si atoms will be displaced laterally with respect to their natural lattice positions by 0.36% at room temperature and 0.46% at the actual growth temperature of 570 °C. This parallel elongation leads to a contraction perpendicular to the interface — the Poisson effect; see *fig. 14*. A direct consequence of the resulting tetragonal deformation is a tilt $\Delta\theta$ in the non-normal crystallographic axes, e.g. the [011] axis. Measurements of $\Delta\theta$ (by ion back-scattering) or the perpendicular lattice spacing (by X-ray diffraction) give valuable information about the strain [23].

Unfortunately, X-ray diffraction can only be used with films thicker than 0.5 μm. Measurements of $\Delta\theta$ are possible, however, if ion back-scattering is used in conjunction with ion blocking. *Fig. 15* shows the principles of this technique for measuring $\Delta\theta$ for the [011] axis, for which the largest shift was expected. Light positive ions (H^+ or He^+) with an energy of 100-200 keV are incident on the surface. Upon penetration, an ion only changes direction when it passes so closely (10^{-5} nm) to an atomic nucleus that scattering occurs. The ion loses energy because of the scattering process and the interaction with electrons as it travels through the film. The spectrum of a large number of back-scattered ions therefore gives information about compositions and concentration profiles to a depth of about 100 nm. A depth resolution of 0.5 to 1 nm can be obtained with an electrostatic analysing detector with a high energy resolution [24].

Directions parallel to rows of atoms are 'forbidden' to outgoing ions: the atoms nearer to the surface 'block' the ions scattered by deeper atoms. In these directions there is a dip in the back-scattering spectrum. For Si on (001) GaP the [001] blocking directions of film and substrate coincide. The tetragonal distortion, however, shifts the [011] blocking direction of the Si film with respect to the substrate [011] blocking direction, which is at an angle of 45° to the normal to the surface. The measured angular shift $\Delta\theta$ is a measure of the strain in the film.

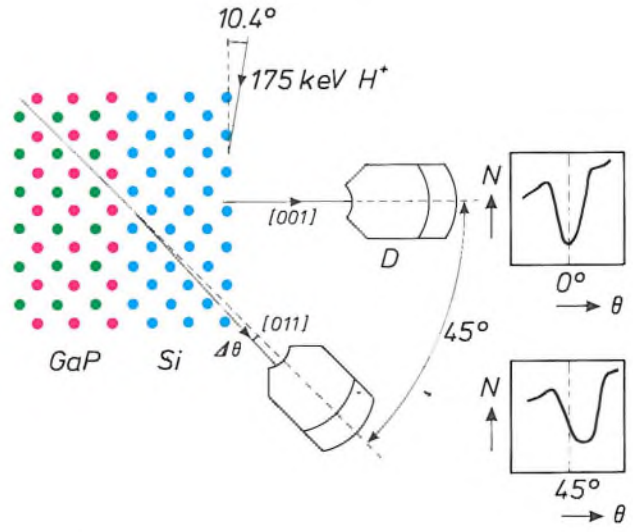

Fig. 15. Schematic view of the ion-blocking experiment, showing the scattering geometry and the measurement procedure. Hydrogen ions with an energy of 175 keV are incident on the Si surface at an angle of 10.4°. The yield of back-scattered ions is measured with a detector D at an angle θ to the normal to the surface. At $\theta = 0°$, the blocking of scattered ions in the [001] direction gives a minimum in the back-scattering intensity yield N. For an undistorted lattice, the blocking in the [011] direction would occur exactly at $\theta = 45°$. A tetragonal distortion with an angular change of $\Delta\theta$ will give a corresponding shift in the intensity minimum.

To ensure a reliable determination of $\Delta\theta$ we first checked that a rotation of the detector through 45° corresponded to the angle between the [001] and [011] blocking directions for an unstrained Si crystal. We made sure that the surface oxide layer and interac-

tions between the ions and the surface atoms did not affect the position of the dip. This was achieved by energy selection of the ions back-scattered from depths of 3 to 11 nm. To be certain that the sample was not misaligned, we checked that the [0$\bar{1}$1] dip, at about 45° in the opposite direction, was shifted by the same amount.

Typical results of ion-scattering measurements are given in *fig. 16*. The back-scattering spectrum of bulk Si has the expected [001] and [011] dips at exactly 0° and 45°. The spectrum of a 30-nm strained Si film on GaP has a shift in the [011] dip: $\Delta\theta = 0.26 \pm 0.04°$. For thicker films (200 and 400 nm) a smaller value of $\Delta\theta$ is found, a clear proof of strain relaxation. The results agree well with those obtained by TEM determinations of the dislocation density. However, the measured shift clearly differs from 0.19°, the theoretical value based on the elasticity constant of bulk Si. This is rather surprising, since X-ray diffraction in films thicker than 0.5 μm always confirms the elasticity-theory predictions exactly. It would appear that this theory does not apply to films as thin as those studied here.

Information about the strain was also obtained by Raman scattering of a monochromatic light beam, e.g. from the 514.5-nm line of an argon laser. The incident photons lose some of their energy by inducing a lattice vibration. The resulting shift in the frequency of the scattered light is related to the stress caused by atomic displacements. The difference from bulk Si is therefore a relative measure of the strain in epitaxial Si.

The results of strain determinations with TEM, ion back-scattering and Raman scattering all agree well; see *fig. 17*. This shows both the parallel elastic strain and the part of the lattice mismatch that is taken up by dislocations, as a function of the film thickness. It is found with all three methods that the strain is approximately equal to the lattice mismatch for films up to about 75 nm thick. This is very different from the equilibrium theory mentioned earlier [18], which gives 14 nm as the critical thickness for dislocation formation.

For Si on GaAs, information about the quality of very thin epitaxial films has been obtained by measuring the back-scattering yield as a function of energy [11]. It was found that a 5-nm Si film grew evenly, with no island formation at first.

Films have also been characterized by the back-scattering of light positive ions (He^+) incident on the surface at high energy (2 MeV) (Rutherford back-scattering, RBS). If the ions are incident in an 'open' crystallographic direction ('channelling'), the scattering yield increases as the number of ions occupying regular lattice sites decreases [25]. The yield ratio for chan-

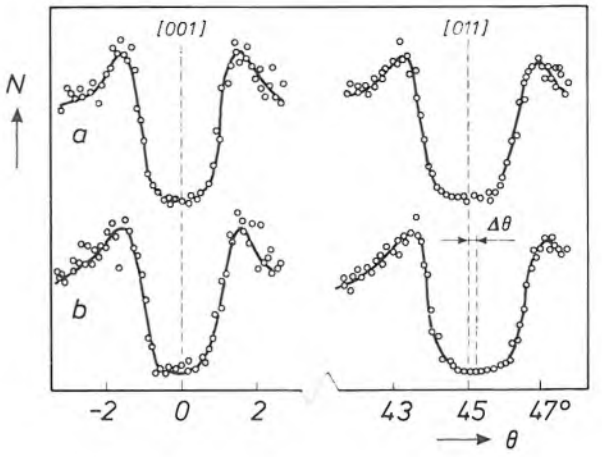

Fig. 16. Measured angular profiles near the [001] and [011] blocking minima for bulk Si (*a*) and for 30-nm MBE-grown Si on (001) GaP (*b*). The measured yield N is given in arbitrary units as a function of the angle θ to the normal to the surface. For bulk Si, the [001] and [011] minima are located at exactly $\theta = 0°$ and $\theta = 45°$, as would be expected in the absence of strain. For Si on GaP, a shift of $\Delta\theta = 0.26°$ is measured for the [011] minimum, as a result of the strain-induced tetragonal distortion.

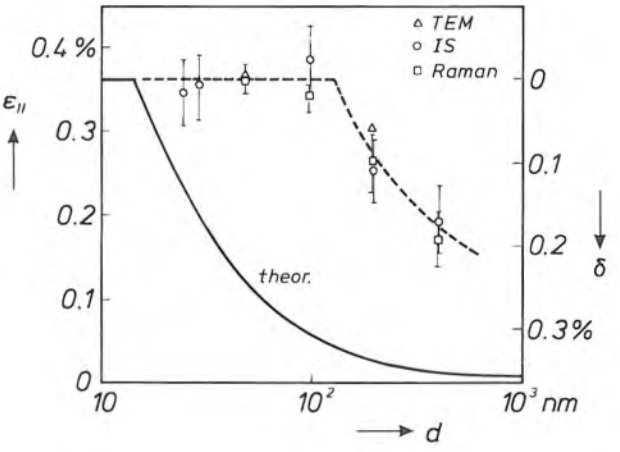

Fig. 17. Results of strain calculations from equilibrium theory and of determinations by transmission electron microscopy (TEM), ion back-scattering (IS) and Raman scattering, for MBE-grown Si on (001) GaP. The elastic strain $\varepsilon_{\parallel}$ and the part of the lattice mismatch that is taken up by dislocations (δ) are plotted against the film thickness d. Ion back-scattering and Raman spectroscopy were used to derive $\varepsilon_{\parallel}$ from the shift in the [011] direction and the frequency shift, and TEM was used to determine δ from the ratio of the parallel Burgers-vector component and the mean separation between the dislocations. The sum of $\varepsilon_{\parallel}$ and δ is equal to the lattice mismatch (0.36%), so that a determination of either also gives the other. The results of the three experimental methods agree well with each other. The critical thickness for dislocation formation (75 nm) is however much larger than predicted by the equilibrium theory (14 nm).

[23] P. M. J. Marée, R. I. J. Olthof, J. W. M. Frenken, J. F. van der Veen, C. W. T. Bulle-Lieuwma, M. P. A. Viegers and P. C. Zalm, Silicon strained layers grown on GaP(001) by molecular beam epitaxy, J. Appl. Phys. **58**, 3097-3103, 1985.

[24] See for example J. F. van der Veen, Ion beam crystallography of surfaces and interfaces, Surf. Sci. Rep. **5**, 199-288, 1985.

[25] See for example W. K. Hofker and J. Politiek, Ion implantation in semiconductors, Philips Tech. Rev. **39**, 1-14, 1980.

nelling and random incidence has a lower value with increasing crystal perfection; the minimum value for pure GaP and GaAs substrates is 3%. For Si on GaP the same value has been derived from the Si contribution to the RBS spectra, which indicates perfect crystalline ordering. With Si on GaAs there is appreciable dechannelling; see *fig. 18*. Near the Si surface the amount of dechannelling is encouragingly low (9%), indicative of good but by no means perfect crystalline ordering. The dechannelling increases considerably (to about 40%) however towards the Si-GaAs interface. The RBS results confirm the information gathered from our TEM investigations.

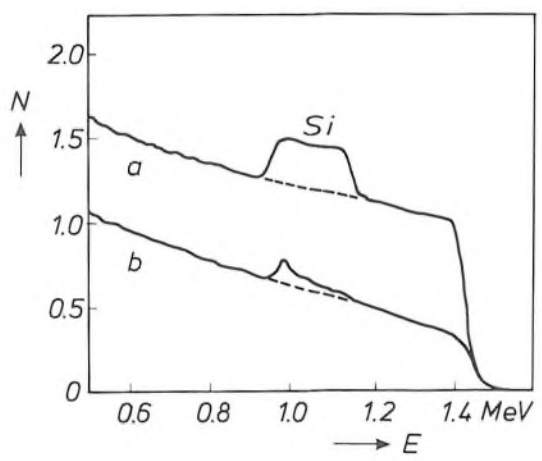

Fig. 18. Rutherford back-scattering spectra of a 500-nm Si film grown by MBE at 600 °C on (001) GaAs. The back-scattering of He^+ ions incident with an energy of 2 MeV on the surface is measured at an angle of 165° to the incident beam. The back-scattering yield N is given in relative units as a function of the energy E of the scattered ions. Curve *a* is obtained with incidence in a random direction, curve *b* with incidence along the 'open' [001] direction. By comparing the Si contribution in the two spectra on the high- and low-energy sides, the amount of dechannelling on the Si surface or the Si-GaAs interface can be estimated.

Information about the doping level in the Si films can be obtained by secondary-ion mass spectroscopy (SIMS) [9]. In this method an ion beam with an energy of a few keV sputters ionized particles from the surface. If the sputtered particles are accelerated to a well-defined energy and subjected to electric and magnetic deflection, they can be analysed by mass. The variation of the composition with depth can now be studied, since the surface is continuously 'peeled off' during the sputtering.

SIMS experiments on Si films on GaP (grown at 550 °C) and on GaAs (grown at 600 °C) reveal not only a surface region containing Ga and P or As, but also a high doping level in the bulk: 10^{18} cm^{-3} Ga and twice as much P or As. When grown on GaP at 400 °C the doping with P was considerably lower. The Ga content, on the other hand, remained the same, confirming an exchange of Ga and Si atoms suggested by LEED and Auger observations.

Prospects

The investigations have provided a better understanding of the formation of dislocations induced by lattice mismatch. We have seen that Si films can be grown on GaP to a thickness of about 75 nm, with no indication of misfit dislocations in TEM images. With GaP grown on Si it would be possible to have even thicker defect-free films, because dislocations are less easily initiated in compressed films. The occurrence of anti-phase disorder (fig. 1) could for example be prevented with a substrate orientation such as (211), offering two significantly different types of bonding sites [26]. The Ga and P atoms will then automatically bond to different sublattices, with the same sublattice pairing over the entire surface.

The tetragonal distortion in strained Si films on GaP has an interesting subsidiary aspect. From band-structure calculations it can be shown that the electron mobility must be twice that in bulk Si at room temperature. This offers possibilities for faster semiconductor switching devices, provided that the accompanying increase in leakage current (by a factor of about ten) poses no additional problems. The positive effect of a tensile stress on the electron mobility has already been demonstrated for thermally treated Si films on SiO_2-coated substrates and on sapphire [27]. In these films, however, the high defect density due to the large lattice mismatch prevents the mobility from exceeding that in bulk Si.

The high level of Ga and P doping in Si films on GaP may have undesirable effects on their electrical properties. Future work must therefore be directed at eliminating this 'background' doping. Some suggestions are:

- Coating the sides and base of the substrate with a material such as Si_3N_4, which acts as a barrier to the surface diffusion.
- A different method of substrate preparation that gives an As-stabilized surface.
- Reducing the temperature to 300-400 °C during growth.

[26] S. L. Wright, H. Kroemer and M. Inada, Molecular beam epitaxial growth of GaP on Si, J. Appl. Phys. **55**, 2916-2927, 1984.

[27] B.-Y. Tsaur, J. C. C. Fan and M. W. Geis, Stress-enhanced carrier mobility in zone melting recrystallized polycrystalline Si films on SiO_2-coated substrates, Appl. Phys. Lett. **40**, 322-324, 1982;
Y. Kobayashi, M. Nakamura and T. Suzuki, Effect of heat treatment on residual stress and electron Hall mobility of laser annealed silicon-on-sapphire, Appl. Phys. Lett. **40**, 1040-1042, 1982.

The crystal quality of Si on (001) GaAs will never be perfect. The dislocation density is enormous, especially near the interface. In thicker films the quality improves considerably towards the surface. Further investigation is required to find out if such defects could affect the operation of devices. A technology-oriented evaluation requires detailed electrical characterization as well as improved growth facilities.

On GaAs, very thin Si films (< 5 nm) can be grown with a complete coverage of the substrate surface. Such thin films are therefore potentially useful for ohmic contacts on GaAs, where a high defect density is no problem and a high background-doping level can even be an advantage.

Many colleagues at Philips Research Laboratories and the FOM Institute for Atomic and Molecular Physics have contributed to the work described here.

Summary. Thin silicon films have been epitaxially grown on GaP and GaAs by molecular beam epitaxy (MBE). Films and interfaces have been investigated by surface analysis and transmission electron microscopy. Both the surface and the bulk of the films are contaminated by atoms from the substrate; this is attributed mainly to surface diffusion and exchange between Si and Ga atoms. On GaP, films thinner than 75 nm are subject to tensile stress because of the lattice mismatch (0.36%), without the appearance of crystal imperfections. Thicker films contain dislocations and stacking faults, related to strain-induced atomic rearrangements. The critical thickness for dislocation formation is significantly larger than is predicted from elasticity theory. On GaAs, the lattice mismatch of 4% gives a greater reduction in crystal quality.

Scientific publications

These publications are contributed by staff from the laboratories and other establishments that form part of or are associated with the Philips group of companies. Many of the articles originate from the research laboratories named below. The publications are listed alphabetically by journal title.

Philips GmbH Forschungslaboratorium Aachen, Weißhausstraße, 5100 Aachen, Germany — *A*

Philips Research Laboratory, Brussels, 2 avenue Van Becelaere, 1170 Brussels, Belgium — *B*

Philips Natuurkundig Laboratorium, Postbus 80 000, 5600 JA Eindhoven, The Netherlands — *E*

Philips GmbH Forschungslaboratorium Hamburg, Vogt-Kölln-Straße 30, 2000 Hamburg 54, Germany — *H*

Laboratoires d'Electronique et de Physique Appliquée, 3 avenue Descartes, 94450 Limeil-Brévannes, France — *L*

Philips Laboratories, N.A.P.C., 345 Scarborough Road, Briarcliff Manor, N.Y. 10510, U.S.A. — *N*

Philips Research Laboratories, Cross Oak Lane, Redhill, Surrey RH1 5HA, England — *R*

C. Ronse	*B*	A strong chord property for 4-connected convex digital sets	Comput. Vision, Graphics & Image Process. **35**	259-269	1986
H. C. de Graaff & W. J. Kloosterman	*E*	New formulation of the current and charge relations in bipolar transistor modeling for CACD purposes	IEEE Trans. **ED-32**	2415-2419	1985
R. L. Maresca	*N*	A general method for designing low-temperature drift, high-bandwidth, variable-reluctance, position sensors	IEEE Trans. **MAG-22**	118-123	1986
E. H. L. Aarts & J. H. M. Korst	*E*	Parallelle netwerken voor het simuleren van leergedrag: Boltzmann-machines	Informatie **28**	632-641	1986
R. Broer*, G. Aissing*, W. C. Nieuwpoort* (* *Univ. Groningen*) & L. F. Feiner	*E*	Hartree-Fock cluster study of interstitial transition metals in silicon	Int. J. Quantum Chem. **29**	1059-1066	1986
A. H. van Ommen, H. J. W. van Houtum & A. M. L. Theunissen	*E*	Diffusion of ion implanted As in $TiSi_2$	J. Appl. Phys. **60**	627-630	1986
H. A. van Sprang & P. A. Breddels	*E*	Numerical calculations of director patterns in highly twisted nematic configurations with nonzero pretilt angles	J. Appl. Phys. **60**	968-972	1986
G. W. 't Hooft & C. van Opdorp	*E*	Determination of bulk minority-carrier lifetime and surface/interface recombination velocity from photoluminescence decay of a semi-infinite semiconductor slab	J. Appl. Phys. **60**	1065-1070	1986
C. van Berkel & M. J. Powell	*R*	Photo-field effect in amorphous silicon thin-film transistors	J. Appl. Phys. **60**	1521-1527	1986
C. W. J. Beenakker	*E*	Ewald sum of the Rotne-Prager tensor	J. Chem. Phys. **85**	1581-1582	1986
H. K. Kuiken, J. J. Kelly & P. H. L. Notten	*E*	Etching profiles at resist edges: I. Mathematical models for diffusion-controlled cases	J. Electrochem. Soc. **133**	1217-1226	1986
P. H. L. Notten, J. J. Kelly & H. K. Kuiken	*E*	Etching profiles at resist edges: II. Experimental confirmation of models using GaAs	J. Electrochem. Soc. **133**	1226-1232	1986
W. A. P. Claassen*, H. A. J. T. van de Pol*, A. H. Goemans* (* *Philips Elcoma Div., Nijmegen*) & A. E. T. Kuiper	*E*	Characterization of silicon-oxynitride films deposited by plasma-enhanced CVD	J. Electrochem. Soc. **133**	1458-1464	1986
J. W. D. Martens & W. L. Peeters	*E*	Anisotropy in cobalt-ferrite thin films	J. Magn. & Magn. Mater. **61**	21-23	1986
R. van Mens	*E*	Ternary phase studies of Nd-Fe-X where X = C, Si, Ge, Pb, Sn	J. Magn. & Magn. Mater. **61**	24-28	1986

J. E. Knowles	*R*	Magnetization reversal by flipping, in acicular particles of γ-Fe_2O_3	J. Magn. & Magn. Mater. **61**	121-128	1986
D. M. Krol (*AT & T Bell Labs, Murray Hill, NJ*), C. A. M. Mulder & J. G. van Lierop	*E*	Raman investigation of autoclave-prepared, monolithic silica gels	J. Non-Cryst. Solids **86**	241-250	1986
M. H. L. M. van den Broek	*E*	Calculation of the radius of the emitting area and the current in triode electron guns	J. Phys. D **19**	1389-1399	1986
M. H. L. M. van den Broek	*E*	Experimental emittance diagrams of triode electron guns	J. Phys. D **19**	1401-1419	1986
E. W. Meijer	E	A model study for coatings containing hexamethoxymethylmelamine	J. Polym. Sci. A: Polym. Chem. **24**	2199-2208	1986
P. J. Courtois & P. Semal	*B*	Block iterative algorithms for stochastic martrices	Linear Algebra & Appl. **76**	59-70	1986
R. B. Helmholdt (*ECN, Petten*), T. T. M. Palstra*, G. J. Nieuwenhuys*, J. A. Mydosh* (* *Univ. Leiden*), A. M. van der Kraan (*IRI, Delft*) & K. H. J. Buschow	*E*	Magnetic properties of $La(Fe_xAl_{1-x})_{13}$ determined via neutron scattering and Mössbauer spectroscopy	Phys. Rev. B **34**	169-173	1986
U. Enz	*E*	The confined breather: quantized states from classical field theory	Physica **21D**	1-6	1986
J. G. Kloosterboer, G. F. C. M. Lijten & F. J. A. M. Greidanus	*E*	Structure and stability of polyacrylate radicals trapped in a network	Polym. Commun. **27**	268-271	1986
R. Brehm, J. C. Driessen, P. v. Grootel & T. G. Gijsbers	*E*	Low thermal expansion materials for high precision measurement equipment	Precision Eng. **7**	157-160	1985
W. J. J. Rey	*E*	Multivariate data analysis, contributions and shortcomings of robustness in practice	Proc. Compstat, Rome 1986	197-204	1986
F. Rausch*, H. Lindeman* (* *Philips Bipolar IC Devel., Nijmegen*), W. Josquin, D. de Lang & P. J. W. Jochems	*E*	An analog BIMOS technology	Proc. Int. Conf. on Solid state devices & materials, Tokyo 1986	65-68	1986
H. C. de Graaff, W. J. Kloosterman & T. N. Jansen	*E*	Compact bipolar transistor model for CACD, with accurate description of collector behaviour	Proc. Int. Conf. on Solid state devices & materials, Tokyo 1986	287-290	1986
J. W. Slotboom, K. Osinski, G. J. T. Davids, H. G. R. Maas, A. Slob, K. E. Kuijk & B. Jansen		High-density CCD video-memories: physics and technology	Proc. Int. Conf. on Solid state devices & materials, Tokyo 1986	315-318	1986
H. L. Peek & D. R. Wolters	*E*	Enhanced tunneling in implanted MOS structures	Proc. Int. Conf. on Solid state devices & materials, Tokyo 1986	487-490	1986
M. P. A. Viegers, B. H. Koek & A. H. van Ommen	*E*	An ordered precipitate structure and the formation of coesite in oxygen implanted silicon	Proc. Int. Conf. on Solid state devices & materials, Tokyo 1986	577-580	1986
C. W. T. Bulle-Lieuwma & P. C. Zalm	*E*	Ion-milling procedures for cross-sectional TEM specimens	Proc. Int. Cong. on Electron Microscopy, Kyoto 1986	351-352	1986
M. P. A. Viegers, B. H. Koek & A. H. van Ommen	*E*	Ordered precipitate structure in oxygen implanted silicon	Proc. Int. Cong. on Electron Microscopy, Kyoto 1986	1507-1508	1986
E. Arnold, U. Landman*, S. Ramesh, W. D. Luedtke*, R. N. Barnett*, C. L. Cleveland* (* *Georgia Inst. Techn., Atlanta, Ga*), A. Martinez, H. Baumgart & B. Kahn	*N*	Formation of facets at the solid-melt interface in silicon	Proc. MRS Conf., Boston, MA, 1986	21-27	1986
S. Ramesh, A. Martinez, J. Petruzzello, H. Baumgart & E. Arnold	*N*	Addressing the problems of agglomeration, surface roughness and crystal imperfection in SOI film	Proc. MRS Conf., Boston, MA, 1986	45-51	1986
L. J. M. Esser, L. G. M. Heldens, L. J. van de Polder, H. C. G. M. van Kuijk, H. L. Peek, G. T. J. van Gaal-Vandormael & C. A. M. Jaspers	*E*	The PAN-imager	Proc. SPIE **591**	61-66	1986

H. Baumgart	*N*	Silicon-on-insulator technology by crystallization on quartz substrates	Proc. SPIE **623**	211-223	1986
A. W. M. van den Enden & G. A. L. Leenknegt	*E*	Design of optimal IIR filters with arbitrary amplitude and phase requirements	Signal processing III, I.T. Young *et al.* (eds), Elsevier Science, Amsterdam	183-186	1986
P. C. W. Sommen	*E*	On the convergence behaviour of a frequency-domain adaptive filter with an efficient window function	Signal processing III, I.T. Young *et al.* (eds), Elsevier Science, Amsterdam	211-214	1986
R. N. J. Veldhuis	*E*	A method for the restoration of burst errors in speech signals	Signal processing III, I.T. Young *et al.* (eds), Elsevier Science, Amsterdam	403-406	1986
F. L. H. M. Stumpers	*E*	Computers of the fifth generation and their role in communications	Software system design methods, J. K. Skwirzynski (ed.), Springer, Berlin	475-489	1986
B. Vitt	*A*	Characterization of a solar selective black cobalt coating	Sol. Energy Mater. **13**	323-350	1986
F. M. Klaassen & W. Hes	*E*	On the temperature coefficient of the MOSFET threshold voltage	Solid-State Electron. **29**	787-789	1986
P. R. Boudewijn, M. R. Leys (*Univ. Lund*) & F. Roozeboom	*E*	SIMS analysis of $Al_xGa_{1-x}As/GaAs$ layered structures grown by metal-organic vapour phase epitaxy	Surf. & Interface Anal. **9**	303-308	1986
B. A. Joyce, P. J. Dobson, J. H. Neave & J. Zhang (*Imp. College, London*)	*R*	The determination of MBE growth mechanisms using dynamic RHEED techniques	Surf. Sci. **174**	1-9	1986

Contents of Philips Telecommunication and Data Systems Review **44**, No. 2, 1986

Contents of Electronic Components & Applications **8**, No. 1, 1987

Contents of Valvo Berichte, November 1986

J. Wolter: Research on layered semiconductor structures,
Philips Tech. Rev. **43**, No. 5/6, 111-117, May 1987.

Research on layered epitaxial structures of semiconductor materials is a field of rapidly growing significance. Structures of special interest are the superlattice consisting of alternate ultra-thin layers of two dissimilar semiconductors, the quantum well formed by a thin semiconductor layer sandwiched between two semiconductor layers with a larger band gap, and the modulation-doped heterojunction. The controlled modification ('tailoring') of the energy-band structure gives some fascinating physical effects. There are also potential new applications, such as quantum-well lasers and high-electron-mobility transistors. Suitable growth technologies are metal-organic vapour-phase epitaxy (MO-VPE) and molecular beam epitaxy (MBE). Various aspects of fundamental physics, growth procedures and device applications are topics of research at several Philips laboratories.

B. A. Joyce and C. T. Foxon: Molecular beam epitaxy of multilayer structures with GaAs and $Al_xGa_{1-x}As$,
Philips Tech. Rev. **43**, No. 5/6, 143-153, May 1987.

The growth of thin films of GaAs and $Al_xGa_{1-x}As$ on GaAs substrates by molecular beam epitaxy (MBE) has been investigated extensively within the Philips Research Laboratories at Redhill. High-quality films and multilayer structures with controlled thickness and composition have been deposited. Detailed information has been obtained on the surface chemistry and the dynamics of growth. It is possible to produce abrupt interfaces between GaAs and $Al_xGa_{1-x}As$ layers, where the compositional changes occur over no more than one monolayer. GaAs layers have been grown with low background impurity concentrations (2×10^{14} cm^{-3}) and this has enabled us to achieve high electron mobilities at low temperatures (3×10^6 cm^{2}V^{-1}s^{-1} at 4 K) in two-dimensional electron-gas structures. Multiple quantum-well structures prepared by growing very thin GaAs wells between $Al_xGa_{1-x}As$ barriers showed laser emission at wavelengths down to 704 nm.

P. M. Frijlink, J. P. André and M. Erman: Metal-organic vapour-phase epitaxy of multilayer structures with III-V semiconductors,
Philips Tech. Rev. **43**, No. 5/6, 118-132, May 1987.

Vapour-phase epitaxy with metal-organic reactants (MO-VPE) is a good method for growing multilayer structures of III-V semiconductor materials such as GaAs and $Al_xGa_{1-x}As$. Precise control of the growth parameters can give interfaces that are abrupt on an atomic scale. The quality of the interfaces and the depth profiling have been assessed by spectroscopic ellipsometry and confirmed by photoluminescence experiments on quantum wells consisting of a thin GaAs layer between two $Al_xGa_{1-x}As$ layers with a larger band gap. The emission wavelength of these wells can be varied in a controlled manner from 800 to 620 nm by decreasing the well width or incorporating aluminium in the well, or both. Laser operation has been obtained for quantum wells with emission wavelengths down to 730 nm. In modulation-doped heterostructures with GaAs and $Al_xGa_{1-x}As$ a two-dimensional electron gas is formed on the GaAs side near the heterojunction. The spatial separation of carriers and donor impurities gives high electron mobilities, particularly at low temperatures. This favours the application of such structures for obtaining transistors with a good high-frequency performance. At low temperatures the presence of a two-dimensional electron gas is responsible for the 'quantized Hall effect'.

P. C. Zalm, C. W. T. Bulle-Lieuwma and P. M. J. Marée: Silicon molecular beam epitaxy on GaP and GaAs,
Philips Tech. Rev. **43**, No. 5/6, 154-165, May 1987.

Thin silicon films have been epitaxially grown on GaP and GaAs by molecular beam epitaxy (MBE). Films and interfaces have been investigated by surface analysis and transmission electron microscopy. Both the surface and the bulk of the films are contaminated by atoms from the substrate; this is attributed mainly to surface diffusion and exchange between Si and Ga atoms. On GaP, films thinner than 75 nm are subject to tensile stress because of the lattice mismatch (0.36%), without the appearance of crystal imperfections. Thicker films contain dislocations and stacking faults, related to strain-induced atomic rearrangements. The critical thickness for dislocation formation is significantly larger than is predicted from elasticity theory. On GaAs, the lattice mismatch of 4% gives a greater reduction in crystal quality.

Supplement to Philips Technical Review
Bijlage van Philips Technisch Tijdschrift
No. 35

May 1987

Recent United States Patents

Abstracts from patents that describe inventions from the following research laboratories, which form part of or cooperate with the Philips group of companies:

Philips GmbH Forschungslaboratorium Aachen, Weißhausstraße, 5100 Aachen, Germany *A*
Philips Research Laboratory Brussels, 2 avenue Van Becelaere, 1170 Brussels, Belgium *B*
Philips Natuurkundig Laboratorium, Postbus 80000, 5600 JA Eindhoven, The Netherlands *E*
Philips GmbH Forschungslaboratorium Hamburg, Vogt-Kölln-Straße 30, 2000 Hamburg 54, Germany *H*
Laboratoires d'Electronique et de Physique Appliquée, 3 avenue Descartes, 94450 Limeil-Brévannes, France *L*
Philips Laboratories, N.A.P.C., 345 Scarborough Road, Briarcliff Manor, N.Y. 10510, U.S.A. *N*
Philips Research Laboratories, Cross Oak Lane, Redhill, Surrey RH1 5HA, England *R*
Philips Research Laboratories Sunnyvale, P.O. Box 9052, Sunnyvale, CA 94086, U.S.A. *S*

4 605 949

Semiconductor device with interdigitated electrodes

M. J. Moore *R*
D. H. Paxman

A semiconductor device, such as a gate turn-off thyristor, has, at a major surface of a semiconductor body a plurality of electrode fingers alternately contacting opposite conductivity type regions (e.g. the cathode and gate) of the semiconductor body. In order to save useful semiconductor area and to allow an improved electrode geometry bonding pads for the electrodes are formed at a level above the electrodes. An insulating layer separates the bonding pads and the electrodes. A first bonding pad contacts a first set of electrode fingers through a first set of windows in the insulating layer and a second bonding pad contacts a second set of electrode fingers through a second set of windows. In operation, the voltage drop along each electrode finger of a set is substantially equal. A third bonding pad may also contact the second electrode set through a third set of windows in the insulating layer.

4 606 017

Optical recording disc

D. J. Broer *E*
L. Vriens

Optical recording disc having successively a transparent substrate plate, a first layer of a formstable synthetic resin comprising an optically readable information track, a second thin layer of a linearly polymerized amorphous synthetic resin and a recording layer in which optically readable information bits are formed by exposure to modulated laser light.

4 606 116

Non-linear resistor and method of manufacturing the same

D. Hennings *A*
A. Schnell
H. Schreinemacher

A non-linear resistor having an operational field strength which optionally is formed as a VDR or as an NTC resistor having a ceramic sintered body on the basis of a polycrystalline alkaline earth metal titanate doped with a small quantity of a metal oxide so as to produce an n-type conductivity, in which the sintered body comprises at its grain boundaries insulating layers formed by re-oxidation of the sintered body and consists of an alkaline earth metal titanate having a Perowskite structure of the general formula $(A_{1-x}Ln_x)TiO_{3-y}TiO_2$ or $A(Ti_{1-x}Me_x)O_{3-y}TiO_2$, wherein: A = alkaline earth metal; Ln = rare earth metal; Me = metal having a valency of 5 or more; $0.0005 < x <$ solubility limit in the Perowskite phase; $y = 0.001$ to 0.02. The sintered body becomes adjustable in its non-linear resistance variation by selection of the re-oxidation temperature and of the re-oxidation duration in such a manner that an initially present NTC-characteristic gradually is observable only at ever increasing temperatures and changes into a VDR-characteristic in the range of the operating temperature of the resistor.

4 606 121

Drive mechanism for a vibration-type dry-shaver

G. Diefenbach *A*
H. Schemmann
R. L. Bukoschek

A drive mechanism for a dry-shaver comprising a shear foil and a cutter reciprocatory relative to the shear foil includes a single-phase synchronous motor having a drive shaft. A cam is mounted on the drive shaft, and a transmission roller is constantly in contact with the cam. The surface of at least one of the cam and the transmission roller is provided with a layer approximately 1 mm in thickness of an elastic material.

4 606 803

Method of manufacturing a mask for the production of patterns in lacquer layers by means of X-ray lithography

H. K. Lüthje *H*
A. M. Brüns
M. Harms
B. R. G. Matthiessen

A method of manufacturing a mask for producing patterns in lacquer layers by means of X-ray lithography comprising a diaphragm

which is very transparent to the X-ray radiation, is stretched on a frame in a self-supporting manner and which is applied as a thin layer to a substrate in a manner such that it is subjected to tensile stress, while the substrate is then removed as far as a part constituting a frame for the then self-supporting diaphragm.

---

4 607 236

Linearized phase comparator and phase-locked loop comprising such a phase comparator

M. LeQuéau *L*

A phase comparator for receiving an input signal and a signal to be compared with this input signal, comprising an auxiliary stage. The auxiliary or dynamic reducing stage includes a circuit for reducing a predetermined value of the phase difference between the two inputs of the comparator and a circuit for recovering said value at the output of the comparator via a circuit delaying the information expressing this value. The phase comparator may be used in a phase-locked loop.

---

4 607 282

Television circuit for the reduction of flicker on a display

L. J. van de Polder *E*

The television circuit is suitable for use with a television picture signal originating from a tele-cine converter which operates at a cine film display rate of 24 frames per second and a 60 Hz field frequency. The picture signal has cycles of alternately two and three field periods with the same picture information which, on display, results in flicker phenomena. To reduce flicker on display of the picture signal on a display screen, the picture signal is applied directly and by a delay device producing a time delay of at least two or more whole field periods to a signal combining circuit which is in the form of a matrix circuit and is followed by a changeover circuit. The matrix circuit produces signal combinations in the output picture signal which on display result in flicker reduction.

---

4 607 284

Movement-adaptive transversal-recursive noise suppression circuit for a television signal

J. G. Raven *E*
M. J. J. C. Annegarn

A movement-adaptive transversal-recursive noise suppression circuit for a television signal can be provided in a simple way with only a single control system for changing from transversal to recursive filtering while maintaining optimum noise suppression. The circuit includes a first combining circuit having a first input for receiving the television signal, a delay circuit coupled to an output of the first combining circuit and a second combining circuit having a first input coupled to an output of the delay circuit and a second input coupled to the output of the first combining circuit, the output of the delay circuit being also coupled to a second input of the first combining circuit, and an output of the second combining circuit being the output of the noise suppression circuit.

---

4 607 382

Electroacoustic transducer unit with reduced resonant frequency and mechanical spring with negative spring stiffness, preferably used in such a transducer unit

K. Dijkstra *E*
B. P. Videc
J. Huizinga

An electroacoustic transducer unit comprises an electroacoustic transducer with a diaphragm, a magnet system with an air gap, and a voice-coil former with a voice-coil arranged in the air gap of the magnet system. The transducer unit comprises means for reducing the transducer resonant frequency including mechanical springs with negative spring stiffness each coupled between a stationary part of the transducer unit and a movable part, for example the voice-coil former or the diaphragm of the transducer. The transducer unit further comprises a control device which generates a control signal for correcting the position of the diaphragm. The mechanical spring with negative spring stiffness comprises two blade springs with both ends coupled to each other and which, under the influence of a compressive force which acts in a direction along an imaginary line through both ends of the mechanical spring, are each bent in on of two opposite directions.

---

4 608 332

Electron lithography mask manufacture

R. Ward *R*

A layer of electron sensitive resist on a semiconductor substrate is exposed to a patterned electron beam emitted from an erasable photocathode mask in an electron image projector. The mask is formed from a transparent plate, such as quartz, on which a layer of caesium iodide or other photoemissive material is provided. A photoemissive pattern is defined in this layer by selective direct exposure to a beam of photons, electrons, or ions, preferably in an evacuated environment containing carbon whereby the photoemission of the exposed areas of the layer is lowered. Alternatively, using a beam of charged particles with a relatively high current density, the exposed parts of the layer are actually removed by evaporation. In either case, the patterned layer can be removed by rinsing in water and the transparent plate can be reused with the same or different photoemissive pattern.

---

4 608 461

Subscriber circuit for a telephone network

A. J. Nijman *E*
F. A. C. M. Schoofs

A subscriber circuit for a telephone network which is coupled to earth via a frequency-dependent coupling circuit. As for direct current the coupling circuit has a much lower impedance than for alternating current, the electrolytic corrosion due to leakage current in the subscriber line is counteracted and no severe requirements need to be imposed on the equality of the impedances in the two wires of the subscriber line.

---

4 608 585

Electrically erasable PROM cell

P. Keshtbod *S*

In an EEPROM memory cell of the kind which relies on tunneling action through a thin oxide layer to store charge on a floating gate, the floating gate and the channel regions of the memory cell are provided with additional doping of the same kind as in the substrate in order to raise the virgin state threshold voltage of the memory cell to a high positive value, such as 4 volt. Additionally, the overlap area between the control gate and the floating gate is reduced to the extent that the capacitance between the floating gate and the control gate is substantially equal to the capacitance between the floating gate and the substrate during programming, but the effective capacitance between the floating gate and the substrate is greatly reduced during erase mode. As a result, little or no tunneling occurs during programming and the threshold voltage level is the same as the virgin threshold value of the memory cell. However, during erase, very efficient tunneling occurs from the floating gate to the substrate and the threshold voltage level decreases to a negative value. The difference between positive and negative values of the threshold voltage is comparable to that of conventional memory cells.

---

4 609 425

Cold crucible system and method for the meeting and crystallization of non-metallic inorganic compounds

D. W. Mateika *A*
R. Laurien

A cold crucible system and method for melting and crystallizing non-metallic inorganic compounds having a crucible, the side and the

bottom of which are formed of metal pipes through which a cooling medium flows and independently excitable induction coils surrounding the side wall and the bottom of the crucible for coupling high energy into non-metallic inorganic compound present in said crucible, a member formed of an electrically conductive material and inert to any of said melt present in said crucible positioned at a distance above the bottom of the crucible and a container, opened at the top, lowered so as to project from the melt formed in the crucible, provided with apertures for the flow of the melt, and so positioned so as to contain up to 25% of the contents of the crucible.

---

4 609 437

Method of manufacturing an optical fiber comprising a coating of a metal

J. C. W. Kruishoop *E*
P. E. J. Legierse
J. van Ruler
D. J. Broer

Optical fibres consisting of a synthetic resin at least on their outer circumference are continuously provided with a metal coating by electroplating. For this purpose the synthetic resin coating is made electrically conductive, for example, by continuous electroless metallization.

---

4 609 582

Dielectric glass in multilayer circuits and thick-film circuits comprising same

H. J. M. Joormann *E*
A. J. M. van Gorp

A dielectric glass and a glass ceramic obtained therefrom is provided for separating crossing conductors in multilayer thick-film circuits. The dielectric glass has a composition in mol.% between the limits of 10-25% ZnO, 7.5-25% PbO, 50-60% SiO_2 and 7.5-12.5% Al_2O_3. These compositions are particularly suitable for conductor patterns having silver because they are free from micropores.

---

4 609 816

Position sensor having at least two layer of light conductors

P. J. W. Severin *E*

The force-sensitive position sensor or writing tablet is composed (for each of the two coordinate directions) of two layers of parallel extending light conductors having a spacing of 0.1 mm or less, the distance between the two layers being approximately 5 μm. By locally exerting a force on the carrier material in which the light conductors are embedded, by means of the tip of a stylus, the light conductors are geometrically deformed. These deformations cause a variation of the optical coupling between the two locally deformed conductors, thus causing a detectable transfer of light variation from one conductor to the other. By connection of one layer to a light source and the other layer to a suitable detector, a force-sensitive position sensor can be constructed by means of electro-optical means.

---

4 609 929

Conductivity-enchanged combined lateral MOS/bipolar transistor

R. Jayaraman *N*
B. M. Singer

A combined lateral MOS/bipolar transistor includes an intermediate semiconductor layer of the same conductivity type as the channel region which extends laterally from the channel region to beneath the drain contact region of the device. Additionally, a floating semiconductor layer of opposite conductivity type to that of the channel region is provided between the intermediate layer and the substrate of the device. Both the intermediate layer and the substrate are relatively lightly doped, to effectively isolate the floating layer from above and below. This structure substantially improves the operating characteristics of the device, thus permitting operation in both the source-follower and common-source modes, while also providing a compact structure which features a relatively low normalized 'on' resistance.

---

4 610 143

Long life vibration canceller having a gas spring

F. R. Stolfi *N*
P. J. Shapiro

A vibration balancing arrangement utilizing a counterbalance mass oscillating at a frequency near its resonant frequency. Resonance is obtained by a gas spring, in which the length of the compression region for the gas is variable to vary the resonant frequency by adjusting the center point of the oscillation of the counterbalance mass.

---

4 610 502

Method of manufacturing a geodetic component and integrated optical device comprising said component

A. J. A. Nicia *E*
G. D. Khoe

A method of manufacturing a geodetic-optical component is described in which non-spherical rotationally symmetrical recesses are formed in a surface of a substrate, and the surface with the recesses are covered with a planar waveguide. This technique forms the recesses in a laminated substrate having a number of layers of varying etching rates, and then etching these layers to form cup-shaped recesses.

---

4 610 746

Method of optically connecting a light conductor to an electro-optical device

D. J. Broer *E*
J. C. J. Finck

In the optical connection of telecommunication glass fibres to semiconductors a curable composition is used which comprises a polyester urethane acrylate or a polyether urethane acrylate. The composition furthermore comprises a heat- or light-activatable initiator. The refractive index of the cured connecting material is adjusted by the addition of both a reactive diluent which increases the refractive index and a reactive diluent which decreases the refractive index. Said reactive diluents furthermore serve to establish the desired mechanical properties of the connecting material prior to and after curing. The curable composition is provided on the glass fibres and/or on the semiconductor laser, after which they are contacted with each other and are optically aligned. The composition is then cured by raising the temperature or by exposure to light.

---

4 610 757

Method of manufacturing a grating

G. D. Khoe *E*
A. J. A. Nicia

The invention relates to a method of manufacturing an optical grating from a body having a surface which is provided with equidistant grooves. In order to obtain cheap and deformation-resistant gratings, according to the invention a surface of a substrate is provided with a number of layers of substantially equal thicknesses. The etching rates of the layers (in a given etchant) increase substantially proportionally to the number of the layer. A cross-sectional surface of the layers is then exposed to the etchant to form the surface with the grooves.

---

4 610 759

Etching solution for and method of etching ferrimagnetic garnet compounds

C. P. Klages *H*

An etching solution for etching ferrimagnetic garnet compounds in which the etching solution comprises at least a strong mineral acid,

for example H_3PO_4, and a reducing agent, for example one- or two-electron donors.

---

4 611 114

Photoelectric detection structure having substrate with controlled properties

P. Dolizy *L*
F. Groliere
F. Maniguet

A photoelectric detection structure of the present invention comprises a photosensitive layer deposited on a substrate consisting of a material transparent to radiation of visible light and of the near infrared light. The substrate has a refractive index for this radiation in the order of 2 with the substrate comprising on its surface incident to the radiation a structure to reduce the reflection of the radiation on that surface.

---

4 612 257

Electrical interconnection for semiconductor integrated circuits

E. K. Broadbent *S*

A structure for an electrical interconnection suitable for a semiconductor integrated circuit is made by a process utilizing selective tungsten deposition at low pressure to form an intermediate conductive layer without significantly ablating nearby insulating material.

---

4 612 420

Loudspeaker system for converting a digitized electric signal into an acoustic signal

J. A. M. Nieuwendijk *E*
W. D. A. M. van Gijsel

An electrodynamic transducer for use in a loudspeaker system for converting an n-bit digitized electric signal into an acoustic signal comprises n voice-coil devices which cooperate with a magnet system. The voice-coil devices each comprise a conductor whose length is the same for all the voice-coil devices. The areas of the perpendicular cross-sections of the conductors increase each time by a factor of two starting from the voice-coil device corresponding to the least significant bit and going to voice-coil devices corresponding to consecutive more significant bits. The invention enables the transducer to be constructed in a simple manner if the transducer is a moving-coil loudspeaker or if it is a ribbon-type loudspeaker.

---

4 612 483

Penetron colour display tube with channel plate electron multiplier

D. Washington *R*

A penetron colour display tube including a channel plate electron multiplier disposed between a low energy electron-beam-producing means and a luminescent screen. The screen is formed from repetitive groups of phosphor elements for luminescing in different colours. Each group includes a first phosphor element having a single layer of material for luminescing in a first colour, such as blue, and a second phosphor element having two layers of material for luminescing in second and third colours, such as red and green. The channel plate electron multiplier includes a multiplicity of electron-multiplying channels for emitting individual electron beams when the low energy electron beam is directed into the channel's input. At the output of each channel are electrode means for selectively directing the emitted electron beam toward either the first or the second phosphor element in a group, and accelerating means for selectively accelerating the emitted electron beam to a predefined energy level to excite the selected layer in the group.

4 612 505

Nuclear magnetic resonance apparatus

H. Zijlstra *E*

A nuclear magnetic resonance apparatus comprises an electromagnetic system in which a shield of a magnetic material is arranged about the coil system for the homogeneous magnetic field. By providing the magnetic material, for example soft iron, directly about the coil system, a comparatively compact magnet with an intesified, interference-insensitive homogeneous magnetic field is obtained. Instead of using a closed cylinder, use can alternatively be made of a cylinder which is formed by rods. The latter is notably attractive for shielding at a larger distance, the original field in the coil then being influenced to only a minor extent. A similar shielding can be obtained by means of a Helmholtz coil pair.

---

4 612 637

Multiple-access communications system

C. K. Davis *R*
P. J. Stein
D. M. Ball

A multiple-access communications system for an unlimited user population wherein a system controller continuously transmits Aloha signals on a slot-by-slot basis giving an updated number of time slots available whereby a calling party can select any one of the designated time slots at random. The calling party checks the time slot immediately preceding its selected time slot to ascertain if the current Aloha number is zero (or an equivalent thereof). If it is zero then the calling party reverts to listening for a time slot containing an Aloha number greater than zero. Alternatively if it is not zero the calling party apparatus sends a signal to the system controller in its selected time slot. Multipurpose signalling in each time slot can be carried out by the system controller thereby reducing the overhead on the system and speeding-up the setting-up of calls which may be off-air or non off-air.

---

4 612 689

Method of manufacturing multilayer capacitors

W. R. de Wild *E*
G. de With
H. C. Smulders

A method of manufacturing multilayer ceramic capacitors characterized by the following steps: forming dielectric foils comprising a mixture of an organic binder with an oxidic ceramic powder; stacking these foils alternately with layers of electrically conductive material which function as electrodes; heating the stack to a previously determined temperature below the atmospheric pressure sintering temperature of the oxidic ceramic powder while simultaneously applying a uniaxial pressure in the direction of stacking to form a unit; releasing the pressure and cooling; and severing the unit into individual capacitor bodies.

---

4 612 810

Optical pressure sensor

G. Martens *H*

An optical pressure sensor is used for determining pressures and differential pressures of explosive liquids and gases and comprises a translucent body, having pressure measurement chambers formed as continuous holes. Sealing plates, seal the pressure measurement chambers from the outside environment. The liquid or gaseous medium, introduced through inlet openings into the pressure measurements chambers and subjected to pressure, produces internal stresses in the body so that the condition of polarization of polarized light, by wich the body is irradiated, varies with the pressure in the pressure measurement chambers. An analyzer filters from the light having a pressure-dependent condition of polarization linearly polarized light, whose intensity varies with the pressure of the medium to be determined. The pressure sensor is constructed in a simple manner and reacts with a high degree of sensitivity and accuracy to pressures and differential pressures. By adjustment of the

diameter of the pressure measurement chambers and their relative distance, the sensitivity of the pressure sensor can be varied within wide limits.

---

4 613 295

Molding apparatus with sensor means

R. Hüppe *H*
H. Käufer
H. J. Lemke

An injection molding apparatus having a sensor probe means for determining a condition or property of a molded article when the mold is open.

---

4 613 961

Optical reader with a limiter in the tracking of focus error servo control loop

R. M. Aarts *E*

Faults in servo control systems as a result of, for example, signal spikes caused by defects such as thickness variations, air bubbles, and scratches and dust particles on the substrate of the record carrier in an apparatus for reading an optical record carrier, can be suppressed effectively by arranging a limiter in the servo control system of such an apparatus. Suitably, the limiter has an adaptive nature, i.e. the limiting levels are adapted to the amplitude of the servo signal.

---

4 614 445

Metal-lubricated helical-groove bearing comprising an anti-wetting layer

J. Gerkema *E*
J. B. Pelzer

In order to prevent the escape of metal lubricant in a helical-groove bearing, the helical-groove bearing is provided with an anti-wetting layer on the surfaces which adjoin the helically grooved surfaces and which could act as a creepage path for the metal lubricant. An extremely accurate definition of the bearing portions to be wetted by the lubricant is also obtained by means of these layers. Thus, more complex bearings can also be locally provided with a metal lubricant.

---

4 614 501

Method of manufacturing a colour cathode-ray tube comprising a magnetic quadrupole post-focusing mask and device for carrying out the method

J. Koorneef *E*
R. H. J. Fastenau
P. J. J. M. van der Heijden

In a method of manufacturing a colour cathode-ray tube comprising a magnetic quadrupole post-focusing mask the mask is formed by a plate of permanent magnetizable material in which apertures are provided arranged according to rows. Sections of the plate are successively magnetized by positioning parallel conductors on at least one side of the plate in such a manner that each time two conductors through which an electric current flows in opposite directions are situated between two rows of apertures and a magnetic quadrupole is formed along the circumference of each of the apertures. A number of outermost conductors determines an edge area of the section. In order to prevent the occurrence of disturbing magnetization errors in the edge area, the edge area is made to coincide with a part of a preceding section already magnetized according to the desired strength. A magnetic induction is generated in the edge area according to a pattern corresponding to the existing pattern in the preceding section but having a strength which decreases towards the outermost conductor.

4 614 947

Planar high-frequency antenna having a network of fully suspended-substrate microstrip transmission lines

E. Rammos *L*

A planar high-frequency antenna having radiating elements for high-frequency signals includes at least two facing conductive plates provided with oppositely-arranged openings which cooperate to form respective cavities. Disposed between each pair of facing plates is a thin dialectric sheet supporting an array of strip conductors of coaxial lines forming suspended-substrate microstrip lines with these plates. Ends of the strip conductors extend into the cavities and form radiating elements. Each thin dielectric sheet is held in place between the facing plates by means of positioning spacers provided on the faces of these plates. The spacers are located in areas where there are no conductors on the dielectric sheet and are sufficiently remote from each other such that at least two cavities and/or lines of the network of strip conductors are located between any two spacers.

---

4 615 025

Data transmission system

M. G. Vry *R*

A data transmission system using a transmission code in which one data state corresponds to a zero transmission level, such as the alternate mark inversion (AMI) code, includes at each terminal adaptive signal processing circuits such as an echo canceller and/or an adaptive equalizer. Each terminal includes a decision circuit an output of which controls a switch which is operative to allow updating of the adaption of the echo canceller and adaptive equalizer only when a data state corresponding to a zero transmission level is detected.

---

4 615 847

Method and apparatus for producing a lens having an accurately centered aspherical surface

H. Howden *R*

A lens is produced having one aspherical surface which is accurately axially aligned with a spherical or flat surface on the opposite side of the lens. The aspherical surface is produced with a mold. The mold has a molding surface having an accurate negative profile and the desired finish of the required aspherical surface. The mold is on a rotatable jig. By means of adjustment screws the mold is adjusted to correct misalignment of the axis of the molding surface and the axis of rotation of the jig. Misalignment is detected by directing a collimated light beam onto the molding surface so that it is reflected onto a screen. When the mold is rotated, the light beam moves on the screen until the molding surface is properly aligned with the axis of rotation. A preformed glass substrate has one aspherical surface of approximately the desired profile and finish and on its opposite side a spherical or flat surface. The substrate is then mounted on the jig with its aspherical surface facing and spaced from the molding surface. By means of further adjustment screws, the substrate is adjusted to correct misalignment of the axis of the spherical or flat surface of the substrate and the rotational axis of the jig. This misalignment also is detected with the collimated light beam and the screen. The gap between the substrate and the mold is then filled with a suitable liquid light transmissive polymeric material. The polymer is allowed to harden and form a molded layer bonded on one side to the substrate. The other side forms an aspherical surface of the required profile and optical finish, axially aligned with the sperical or flat surface of the substrate.

---

4 616 165

Single-phase reluctance motor

J. C. Compter *E*

A single-phase reluctance motor in which the excitation pulse timings and lenghts are controlled as a function of the speed by means of, in particular, a microprocessor; mechanical provisions

are made in order to ensure reliable starting of the motor and special starting pulses are generated by means of a simple motor-position sensor which generates two pulses per revolution.

---

4 616 190

Differential amplifier with current steering to enhance slew rate

R. J. van de Plassche S

A steering circuit in a differential amplifier having a pair of differentially arranged input amplifiers steers current from a pair of current sources in such a way as to enhance slew rate without increasing offset voltage. The steering circuit is formed with a pair of steering amplifiers arranged in a differential configuration through a pair of resistors.

---

4 616 192

Phase-locked loop with switchable phase detector

A. H. M. van Roermund E

A phase-locked loop has a phase detector and a clock pulse oscillator. The phase detector multiplies a received reference signal by a comparison signal. It is constituted by a plurality of signal channels each receiving the reference signal and having a cascade arrangement of a switching circuit and a weighting network. The switching circuit is controlled by one or more sequences of main control pulses supplied by a pulse distributor circuit receiving clock pulses. Each signal channel has a constant weighting factor. For the k^{th} signal channel the weighting factor is equal to the signal sample $n(t_o + kT_s)$ of a fundamental signal n(t) which has a fundamental frequency f_o. T_s is the reciprocal of the clock pulse frequency f_s. For each sequence of main control pulses controlling the switching circuit in the k^{th} signal channel, this signal channel produces a main signal z(k,t). The main signals supplied by all the signal channels are added together. To allow locking of the loop on frequencies which are an integral multiple p of the fundamental frequency, the clock pulse oscillator has a frequency f_s which is an integral multiple N of the fundamental frequency. In addition, the pulse distributor circuit has an input for setting the parameter p and at least N distributor outputs to which the several clock pulses are applied. More specifically, the clock pulse having number n is applied to the distributor output having number np modulo N. The sequence of pulses thus occurring at these distributor outputs constitutes the sequence of main control pulses.

---

4 616 339

Integrated circuit with improved programmable read-only memory

R. Cuppens E
C. D. Hartgring

Field effect transistors having a short channel length are desirable for carrying out logic operations at a high speed. However, they are then not capable of withstanding the comparatively high programming and erasing voltage at which an (E)EPROM has to be operated. During the programming cycle the field effect transistors are kept in the current-nonconducting state, while recording the logic information obtained by the logic operations, the 'fast' transistors are nevertheless capable of withstanding the comparatively high voltage.

---

4 617 041

Method for continuously manufacturing elongated bodies starting from unmolten solid starting material

W. C. P. M. Meerman E

A method for continuously melting a glass by means of a high-frequency electromagnetic field in a melting tube is provided. In this technique, the electromagnetic field is coupled in the melt by means of a coil present within a cooling jacket surrounding the melting tube. A grounded screen and a tube of insulating material are present between the wall of the melting tube and the coil. The melt traverses a heating zone and a refining zone, and a solid elongated body is withdrawn from the bottom of the melting tube.

---

4 617 206

Method of manufacturing a layer of an oxide of an element from group IVa

J. Haisma E
P. Heller
J. M. M. Pasmans
U. K. P. Biermann

Providing a transparent layer of an oxide of an element from group IVa of the Periodic Table, notably TiO_2, by providing a substrate with a solution of a compound of the element which upon heating is converted into the relevant oxide, drying the film and heating the dried film so as to form the transparent layer of the oxide. The oxide thus obtained is a form having a comparitively low refractive index. By heating the product, after providing the film, rapidly to a temperature of above 700° C, preferably above 1,000° C, keeping it at this temperature for some time and then rapidly cooling it again, a modification having a higher refractive index (for example, for TiO_2 rutile) is obtained.

---

4 617 448

Electrically releasable locking device

M. P. Goldowsky N

A locking device for holding a movable member of an apparatus rigidly in place during shipment. A locking element is made from a material exhibiting a 'shape memory', and is deformed at a temperature below its transition temperature and installed in the apparatus so as to lock the movable member firmly in place. When it is desired to be able to operate the apparatus in a normal mode, the locking element is heated electrically to a temperature above the transition temperature, so that it resumes the original shape and releases the movable member

---

4 617 600

Magnetic head having a thin strip of magnetoresistive material as a reading element

G. H. J. Somers E

A magnetic head for reading analogue information on a track of a recording medium associated with the magnetic head. The head has a strip of magnetoresistive material serving as a reading element and arranged in a magnetic yoke at a given distance from the pole faces formed by the ends of the limbs of the magnetic yoke, the strip being connected in the magnetic circuit formed by the magnetic yoke. The magnetic yoke comprises three limbs separated by non-magnetic layers. The pole face of one of the outer limbs is located at a greater distance from the recording medium than the pole faces of the central limb and the other outer limb.

---

4 617 936

Flexible surface coil for magnetic resonance imaging

J. A. Malko N

A surface coil for use with magnetic resonance imaging apparatus comprises an electrically-insulating, flexible tube which is filled with a liquid mercury conductor.

4 618 506

Method of providing a metal mirror

J. S. Temple *E*
P. E. J. Legierse
T. H. G. Martens

A method of providing a metal mirror on polycarbonate in which the surface of polycarbonate is pretreated with an aminosilane, preceded by a corona discharge and/or succeeded by a treatment with tannin.

---

4 618 590

Starting mixture for a dielectric composition

H. Baudry *L*

The invention relates to the formulation of a starting mixture for an insulating composition, comprising a vitreous phase and several ceramic phases in the respective ratios by volume for the vitreous phase between 85 and 60% and for the ceramic phases between 15 and 40%, the vitreous phase being a silicate of zinc and alkaline earth. According to an embodiment of the invention the starting mixture is remarkable in that the vitreous phase is constituted by the molar ratios of the following oxides: 30 to 55% of silicon (SiO_2), 15 to 30% of zinc oxide (ZnO), 0 to 20% of boric anhydride (B_2O_3), 0 to 10% of alumina (Al_2O_3), 15 to 40% of barium oxide (BaO), and in that the ceramic phases are constituted by the ratios by volume of the following oxides: 0 to 10% of cobalt oxide (Co_3O_4), 5 to 20% of zinc oxide (ZnO), and 10 to 25% of lead oxide (PbO_2).

---

4 618 789

Linear motor for the high-speed reciprocating movement of a rotor slide possessing mass

P. Flisikowski *H*

A linear motor for the high-speed reciprocating movement of a mass-possessing rotor slide component and particularly of a radiation filter, with parallel flat stator plates with permanent magnets which are fitted to the facing sides of the stator plates and set up a magnetic field across the air gap between them. Fitted to the slide is a coil which can be slid in the permanent magnetic field. The coil consists of an aluminium foil provided at its surface with an insulating layer, which foil is wound to form an air-cored coil, and the slide is supported on gas bearings which extend through the aluminium bridges between the stator plates. To avoid impacts during acceleration and braking linear motors working reciprocally are provided.

---

4 619 039

Method of manufacturing a semiconductor device and device manufactured by the use of the method

H. G. R. Maas *E*
J. W. Slotboom
J. A. Appels
K. Osinski

A method of manufacturing a semiconductor device having narrow, coplanar, silicon electrodes which are separated from each other by grooves or slots having a width in the submicron range. The electrodes are alternatively covered by an oxide and by an oxidation-preventing layer, such as silicon nitride. According to the invention, a first and second electrode which are both covered with one of these layers, and which enclose a third electrode covered by the other of these layers, are first interconnected inside a connection region. Two of the three electrodes are separated from the connection region by etching. By selective etching, overlapping contact windows are provided on all three electrodes, and inside the contact windows etching of the groove is omitted.

4 619 119

Heat pump comprising a thermally driven liquid pump and liquid pump for use in a heat pump

K. Dijkstra *E*
J. Huizinga

A heat pump, in which there is arranged in a circuit between an absorber and a generator a liquid pump comprising a piston which is displaceable in a cylinder and forms the separation between a gas chamber and a liquid chamber in which simultaneously prevails a pressure of comparatively low level during the suction stroke and a pressure of comparatively high level during the delivery stroke. A guide member secured to the cylinder encloses with the piston an auxiliary chamber of variable volume in which liquid of comparatively low pressure at least during the delivery stroke is constantly present. The gas chamber is connected to alternately a lead of low and high gas pressure in the heat pump, while the liquid chamber is connected synchronously therewith alternately to a lead of low and high pressure in the heat pump. The heat pump provides an attractive solution especially for domestic heating for pumping liquid solution between the generator and the absorber because of the low-noise and low-energy liquid pump driven by means of pressure differences in the heat pump itself.

---

4 620 311

Method of transmitting information, encoding device for use in the method, and decoding device for use in the method

K. A. Schouhamer Immink *E*

A method of converting n-bit information words into m-bit code words, and the other way round, is described. The code words have a limited disparity. For every information word, two code words are assigned to a group of information words, which code words can be derived from one another by inversion. A choice between these two code words is made to limit the digital-sum-value so as to obtain a dc free code. In order to obtain a further limitation of the digital-sum-value within the code words, these code words are derived from each other by inversion and reversal.

---

4 621 235

Method of and device for determining a nuclear magnetization distribution in a region of a body

C. M. J. van Uijen *E*
J. H. den Boef

During measurement cycles for generating and sampling FID signals in MR imaging devices, a 180° pulse and subsequently a 90° excitation pulse are added to the pulse sequence. The 180° pulse produces an additional echo signal. During (the maximum of) the echo signal, the 90° pulse is generated. The waiting period occurring before the beginning of a next measurement cycle can thus be substantially reduced without giving rise to a significant signal loss in the echo signals to be generated during said cycle. In addition to a reduction of the measurment time, MR images with different contrasts (other intensity distribution) can be provided.

---

4 621 423

Shear head of a dry-shaver comprising a shear foil which is clamped so as to be curved

H. Schemmann *A*
R. L. Bukoschek

A vibratory dry-shaver comprises a shear foil having two longitudinal edges, and respective means to clamp the two longitudinal edges in place to cause the shear foil to assume a natural curvature, the tangents to such curvature at the two clamping means forming an acute angle with each other. A cutter is reciprocatingly movable along and adjacent to the shear foil, the cutting edge of the cutter having a curvature corresponding to that of the clamped, curved shear foil. The curved shear foil and the

cutting edge of the cutter each have a hyperbolic cosine curvature according to the formula: $y = c \cdot \cosh x/c$, where y indicates the distances of the individual cutting edge points from the x-axis, x is the coordinate in the direction of the width of the cutter, and c is a constant derived from the width of the clamped shear foil and the height of the curvature h of the clamped shear foil.

---

4 622 096

Method of manufacturing a semiconductor device comprising a silicon body, in which a sunken oxide layer is locally provided

J. G. Dil *E*
J. W. Bartsen

The method of the present invention involves the forming of a depression with sidewalls extending below a first oxidation mask provided on a surface af a silicon body. Subsequently, after the sidewalls of the depression have been provided with a second oxidation mask, an oxidation treatment is carried out. According to the invention, the depression is provided in such a manner that the sidewalls of the depression are flat and form an angle of 25 to 45° with the original surface of the silicon body. The second oxidation mask is formed by a 5 to 50 nm thick layer of silicon nitride or silicon oxinitride applied directly or separated from the surface by a layer of silicon having a thickness of less than 5 nm. This leads to a very flat structure.

---

4 622 501

Ultrasonic sector scanner

A. T. Eventoff *N*
F. R. Stolfi

An ultrasonic sector scanner includes first and second magnetizable stators spaced on a longitudinal axis. First and second rotors are provided in the gaps between the end faces of the first and second stators, respectively. The rotors have tapered surfaces spaced from the end faces of the stators to form gaps therebetween. The gaps between the first rotor and the end face of the first stator decrease as the rotor rotates in a first direction. The gaps between the second rotor and the end faces of the second stator decrease as the rotors rotate in a second direction opposite the first direction. An ultrasonic transducer is connected to the rotors and arranged to be rotatable with the rotors. A servo-control system is provided to cause the rotor/transducer assembly to rotate according to a prescribed reference signal. The ultrasonic sector scanner has a cover assembly in which a flexible membrane is provided with ribs which engage grooves in the wall of the housing. A heatshrink tube or other retaining ring is arranged around the flexible membrane in order to press the ribs into the grooves. The ultrasonic sector scanner includes a rigid nose piece inside and spaced from the flexible membrane in order to increase the skin contact area when the flexible membrane of the sector scanner is pressed against the skin of a patient being examined.

---

4 622 567

Integrated fet device having multiple outputs

J. A. Pals *E*
A. J. Klinkhamer

The invention discloses a compact construction of an n-channel surface MOS source follower in a p-pocket in an n-type substrate. The source is connected to the p-pocket in order to avoid feedback. The drain is connected to the substrate which acts as a supply line. This construction permits manufacturing several output amplifiers with a minimum pitch. The invention is of particular importance for CCD sensors.

4 625 131

Attenuator circuit

W. G. Kasperkovitz *E*
D. J. Dullemond

A frequency-to-phase converter comprises an attenuator circuit, a delay circuit and a comparator. The attenuator circuit is provided with two transistors, which are arranged as a differential pair and whose collectors are coupled to the positive supply-voltage terminal. A voltage divider with a tap is arranged between the collectors. If a signal is applied to the input terminal, the attenuated signal is available on the tap and the attenuated signal is available on the collector. The unattenuated signal is applied to an input of the comparator through an emitter-follower and the unattenuated signal is applied to another input of the comparator through an emitter-follower and a delay circuit. A signal, whose different frequencies are delayed by the same time over a wide frequency range appears at the output.

---

4 625 142

Methods of manufacturing a dispenser cathode and dispenser cathode manufactured according to the method

J. van Esdonk *E*
J. Stoffels

A dispenser cathode body is manufactured from a sintered metallic powder. A large scandium oxide concentration is provided beneath an emissive surface of the body, resulting in increased life, increased current density, and decreased sensitivity to ion bombardment.

---

4 625 146

Cathode ray tube

A. A. van Gorkum *E*

A cathode ray tube comprising in an evacuated envelope an electron gun system for generating at least one electron beam which is focused on a target by means of at least one accelerating electron lens. The lens viewed in the direction of propagation of the electron beam, comprises a first and a second electrode separated by a lens gap. In the second electrode an electrically conductive foil or gauze intersects the beam at a distance from the lens gap. When the foil or gauze is flat and is provided at such a location that $0.25 < l/R < 2.0$, where l is the distance from the foil or gauze to the lense gap and R is the radius of the part of the second electrode in which or against which the foil or gauze is provided. The spherical aberration in the electron beam is drastically reduced. Such a flat gauze moreover is easy to manufacture and assemble in an electron gun.

---

4 625 230

Colour television transmission or data storage system with time division multiplex encoding and data generator and receiver suitable therefor

S. L. Tan *E*
L. J. van de Polder
G. de Haan
F. W. P. Vreeswijk

In a television transmission system, an encoding circuit in a data generator transmits (or stores) identification information relating to variable numbers of television lines or variable portions of television lines in which luminance and chrominance information occur, compressed where appropriate. The data receiver includes a simple, properly adaptable decoding circuit which comprises presettable counters for counting portions of television lines and for counting television lines, outputs of these counters being coupled to address inputs of a programmable memory which is coupled to a multiplexer which is switchable by the identification information and is followed by a logic circuit for generating control signals for a chrominance memory having the same write and read rates and for

OTHER PHILIPS PUBLICATIONS

Philips Journal of Research

A publication in English on the research work carried out in the various Philips laboratories. Published in annual volumes of six issues each of about 100 pages, size 15½ × 23½ cm.

Philips Telecommunication and Data Systems Review

A publication in English, dedicated to systems and equipment for business communications, computer systems and networks, telecommunication services, radio communications and dictation. Published in volumes of four issues, about 40 pages per issue, size 21 × 29½ cm.

Electronic Components and Applications

A publication in English, containing articles dealing with the theory and practice of electronic components and materials. Four issues per year, about 60 pages per issue, size 21 × 29½ cm.

Medicamundi

A publication in English on radiology, nuclear medicine and medical electronics. Three issues per volume, about 60 pages per issue, size 21 × 29½ cm.

Forthcoming issues of Philips Technical Review will include articles on:

HD-MAC: a new television system

Selecting quartz for resonators

Looking at interfaces

Philips Tech. Rev. Vol. 43, No. 5/6, May 1987

Contents

PHILIPS TECHNICAL REVIEW
Philips Research Laboratories
P.O. Box 80000
5600 JA Eindhoven
The Netherlands

Subscription rate per volume	fl. 80.00 or U.S. $ 35.00
Student's subscription	fl. 32.00 or U.S. $ 14.00
Binder	fl. 10.00 or U.S. $ 4.00

Payment only after invoicing, please.

Printed in the Netherlands